THE ROLE OF ALUMINUM, COBALT CO-DOPING ON THE BAND GAP TUNING OF TiO_2 THIN FILM DEPOSITED BY SPRAY PYROLYSIS

A Dissertation Submitted to the Department of Physics, Bangladesh University of Engineering and Technology in Partial Fulfilment of the Requirement for the Degree of Master of Science in Physics

by

Md. Nurul Islam

Roll No: 1017142508F

Session: October-2017

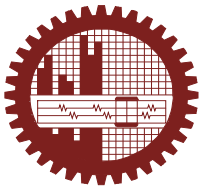

BUET

DEPARTMENT OF PHYSICS

BANGLADESH UNIVERSITY OF ENGINEERING AND TECHNOLOGY,

DHAKA-1000, BANGLADESH.

November, 2019

THE ROLE OF ALUMINUM, COBALT CO-DOPING ON THE BAND GAP TUNING OF TiO_2 THIN FILM DEPOSITED BY SPRAY PYROLYSIS

by

Md. Nurul Islam

Roll No.: 1017142508 F

Session: October-2017

Master of Science

BUET

DEPARTMENT OF PHYSICS

BANGLADESH UNIVERSITY OF ENGINEERING AND TECHNOLOGY

BANGLADESH UNIVERSITY OF ENGINEERING & TECHNOLOGY (BUET), DHAKA

DEPARTMENT OF PHYSICS

Certification of Thesis

The thesis titled **"THE ROLE OF ALUMINUM, COBALT CO-DOPING ON THE BAND GAP TUNING OF TiO_2 THIN FILM DEPOSITED BY SPRAY PYROLYSIS"** submitted by **Md. Nurul Islam,** Roll No. 1017142508F, Session: October/2017, has been accepted as satisfactory in partial fulfillment of the requirement for the degree of **Masters of Science** (M.Sc.) in Physics on 24 November, 2019.

BOARD OF EXAMINERS

1.	**Dr. Jiban Podder** (Supervisor) Professor Department of Physics, BUET, Dhaka	Chairman
2.	**Dr. Md. Forhad Mina** Professor and Head Department of Physics, BUET, Dhaka-1000	Member (Ex-Officio)
3.	**Dr. Md. Mostak Hossain** Professor Department of Physics, BUET, Dhaka-1000	Member
4.	**Dr. Muhammad Rakibul Islam** Assistant Professor Department of Physics, BUET, Dhaka-1000	Member
5.	**Dr. M. Khalilur Rahman Khan** Professor Department of Physics University of Rajshahi, Rajshahi, Bangladesh	Member (External)

DECLARATION

It is thereby declared that this thesis or any part of it has not been submitted elsewhere for the award of any degree or diploma.

Md. Nurul Islam
Roll No. 1017142508F
Session: October, 2017

\

Dedicated

To

My Late father Md. Shefatulla

My mother Rajia

who sacrificed immensely so that their children can grain a fairer share of life.

ACKNOWLEDGEMENTS

Firstly, I express very much gratefulness to the Almighty, who gives me the strength and energy to fulfill this research work. There are lots of people I would like to thank for various reasons.

I would like to express my profound gratefulness to my respectable and honorable supervisor Dr. Jiban Podder, Professor, Department of Physics, Bangladesh University of Engineering and Technology (BUET), Dhaka for his constant support, hand-on instructions, and efforts to establish internal and external cooperation throughout my study. He is a great materials scientist. It is my great honor to be his student. What I learned from him will benefit my whole life.

I would like to express my sincere to my respected teacher Prof. Dr. Md. Forhad Mina, Head, Department of Physics, for allowing me to work in this Department and for his valuable suggestions regarding my thesis.

I am obliged to Prof. Dr. Md. Abu Hashan Bhuiyan, Prof. Dr. Md. Feroz Alam Khan, Prof. Dr. A.K.M. Akther Hossain, Prof. Dr. Md. Mostak Hossain, Prof. Dr. Afia Begum, Prof. Fahima Khanam, Prof. Dr. Md. Rafi Uddin, Prof. Dr. Nasreen Akter, Prof. Dr. Mohammed Abdul Basith, Dr. Muhammad Samir Ullah, Dr. Mohammad Abu Sayem Karal, Dr. Mohammad Khurshed Alam, Dr. Mohammad Jellur Rahman, Dr. Muhammad Rakibul Islam, Mrs. Mehnaz Sharmin, Mr. A.T.M. Shafiul Azam, Dr. Parvin Sultana and Mr. Md. Mehdi Masud, Department of Physics, BUET for their supports and helpful constructive suggestions for this advanced research work.

I would like to give my thanks to Dr. M. A. Matin, Head, Department of Glass and Ceramic Engineering, BUET, Dhaka, for allowing to perform the X-ray Diffractometry, Scanning Electron Microscopy and Energy-dispersive X-ray spectroscopy measurements.

I would like to give my thanks to Dr. Khandker Saadat Hossian, Professor, Department of Physics, University of Dhaka, Dhaka, for help in taking Atomic Force Microscopy data.

I am grateful to the Department of Physics, University of Dhaka, Dhaka for giving me permission for UV-VIS spectroscopy measurements.

I wish to thank Mrs. Muslima Zahan, Ms. Rabeya Rahaman Tofa, Mr. Md. Majibul Haque Babu, Mr. Bidhan Chandra Dev, Dulal Ganguly, Ms. Walia Binte Tarique, Mr. Barik khan, Protima Roy, Tosur saha, S.M. Nazmus Shakib Pias, Sonia, Nila, Hasive, Eashika Mahamud for their sincere help to this work.

I am also thankful to all non-teaching staff, Department of Physics, BUET for their timely help during the work.

I am thankful to the authority of BUET for giving me necessary financial support and ensuring the opportunity to access all sorts of facilities to complete this research work successfully.

I am grateful to my undergrad supervisor Md. Shahajan Ali and other teachers of Department of Physics, Pabna University of Science and Technology for their extensive encouragement. My university life would not have been the same without the guidance and inspiration of them.

The Author

Md. Nurul Islam

CONTENTS

Table of contents

LIST OF FIGURES

LIST OF TABLES

ABSTRACT

Titanium dioxide (TiO_2) thin films were prepared by a spray pyrolysis technique onto a glass substrate. The film properties are characterized by Field-emission scanning electron microscopy, Energy-dispersive X-ray spectroscopy (EDX), Atomic force microscopy (AFM), X-ray diffraction (XRD) technique, and four-probe point method. The Scanning electron microscope and Atomic force microscope images of pristine samples have shown particle shape. The pore diameters are found to be in between 6 nm to 9 nm for Al doped, spherical and slender shaped particles are ranging from 42 nm to 50 nm for co-doped sample observed by field emission scanning electron microscope. The EDX spectra show that all studied samples are stoichiometric. AFM images show that the surface roughness are varying from 34.72 nm to 89.83 nm. The XRD pattern shows that the brookite phase is present in pure, doped and co-doped samples. The cell parameters have been analyzed by FULLPROF package. The lattice parameters are found in good agreements with the experimental and theoretical results. For different compositions of as-deposited studied films, the optical band gap energy varies from 3.52 eV to 3.70 eV for doped and 3.52 eV to 3.57 eV for co-doped samples. The optical properties show that the films are highly transparent in the visible region. The (Al, Co) samples transparency decrease with increasing co-doping as compared to pristine one and reverse phenomena occurred in absorption spectra. The resistivity gradually decreases with an increase of temperature, which confirms that the samples exhibit semiconducting behavior. Experimental studied structural parameters were used in theoretical calculation via Material studio 8.0. The mechanical properties indicated that the optimized sample is ductile and possesses a low bulk modulus. Pristine and Al-doped and (Al, Co) co-doped samples are found to have an indirect electrical band gap, mechanical stability. The electrical band gap of the samples varies from 3.11 eV to 4.39 eV for doped and 2.38 eV to 3.11 eV for co-doped samples. The absorbance edge is shifted to the lower energy region after (Al, Co) co-doped (red shift). The charge density map indicated that the covalent bond is present in all samples. A combined analysis of the structural, morphological, electronic, and optical properties of the compound suggests that the studied sample is a potential candidate for gas sensing and optoelectronic applications.

CHAPTER-1

GENERAL INTRODUCTION

1.1 Introduction

Titanium dioxide (TiO_2) is one of the most familiar semiconductor material, due to it was used in catalysis, gas sensing, photo-voltaic, the chemical industry, energy storage, medicine [1-4]. In the particular case, titanium dioxide is mainly used in the branch of photo-catalysis, because titanium dioxide has a wide band gap (3 to 3.2 eV) and stable nature in ambient temperature. The physical properties of TiO_2 thin film are influenced by their crystal structures, morphological and growth method [7, 8]. Amorphous, anatase, rutile, and brokite are of phase of TiO_2 thin films. The application of TiO_2 thin film strongly depends on proper dopant such as transitions or rare-earth metal, crystal structure, optical and electronic properties [5, 6]. TiO_2 thin films are used in photo-catalysis, a coating on lenses, solar cells, and self-cleaning windows [9, 10]. For this consequence, TiO_2 thin films are broadly studied. In general, anatase and rutile are well-known phases of titanium dioxide but the brookite phase is rare. Brookite is the metastable phase of TiO_2, it is composed of anatase and rutile. Under the laboratory condition, the prepared brookite phase of TiO_2 is more difficult. Recently, there are only a few published papers, dealing with the synthesis of the brookite phase of TiO_2 and have proposed the brookite phase is the potential candidate material for photovoltaic device applications.

The n-type semiconductor TiO_2 donors directly donate electrons into the conduction band (CB), leading to compensate the conduction band states and Moss-Burstein widening optical band gap [11-14]. The Al dopants is controlled the position of the conduction band minimum relative to the electron affinity. A large number of electron affinity identifies that the charge carrier easily incorporated in the system, effectively increasing carrier concentrations. However, the major drawbacks would be that TiO_2 does not absorb the visible sunlight, owing to large electrical band gap and a high number of electron-hole recombination rate [15, 16]. Simultaneously, doping with Al ion is modified the structural, electrical and optical properties of titanium dioxide samples. The Al ions introduce new electronic energy states that reason the conduction band and valance band located on the close of Fermi-level [17]. Recently doping with aluminum decrease the electrical band gap, enhance the thermal stability, modify the conduction band to valance band and enhance the photo-degradation efficiency.

Titanium dioxide thin films have been deposited using various techniques, among these, are sol-gel processes, the ion beam technique, reactive technique, electron beam evaporation, chemical vapor deposition, spray pyrolysis, etc. [18-20]. In our investigation, we used in the thermal spray pyrolysis technique. In our samples Al-doped and (Al, Co) co-doped TiO_2 thin films were deposited onto a glass substrate in the thermal spray pyrolysis technique. In order to theoretical calculation, we used in experimental parameters on the based on density functional theory (DFT). The influence of Al-doped, (Al, Co) co-doped TiO_2, we adopted the plane-wave an ultra-soft pseudo-potential method within the framework of density functional theory to calculate the electronic properties (band structure, the density of states and charge density) of super cell structures, in which a Ti atom was substituted by Al and Co atoms. In addition, the present calculation experimental results were compared with the theoretical results reported in the literature.

1.2 Application of Thin Films

Thin films are extensively used in modern technology, and their applications are expected to be even more widespread in future. It is not possible to given survey over thin film applications, but a listing may, nevertheless, be of some interest. This applications areas for thin films are

A. Optical function

1. Solar absorbing
2. Anti-reflection layers on optical components
3. Coatings for laser optics
4. Display devices (CD)

B. Electrically function

1. Conductors, Insulators (resistors, capacitors)
2. Microelectronic devices
3. Semiconductor, Super-conductors device
4. Solar cells

C. Magnetically function

1. Computer memories
2. Computer logic elements
3. Radio-frequency

D. Chemically function

1. Gas/liquid sensors

E. Decorative

1. Eyeglass frames
2. Costume jewelry

F. Optoelectronic applications:

Thin films are of current interest due to their potential application in light emitting diodes (LED) and laser diodes, solar cells, sensors, photoconductive, telecommunication etc.

1.3 Review of Previous Work

Transparent conducting oxide (TCO) titanium dioxide (TiO_2) thin films were prepared two aspect theoretical and experimental. Experimentally deposited process are sputtering, spin coating, spray pyrolysis technique, chemical vapor deposition, and atomic layer deposition, etc. and theoretically investigated process is Density Functional Theory [21-23]. Titanium dioxide thin films were deposited by spray pyrolysis, they were investigated X-ray diffraction (XRD), atomic force microscopy (AFM) and scanning electron microscopy (SEM), reflection and transmission spectroscopies. From X-RD patterns study was observed that at deposited temperature 500^0C (111) plane associated rutile structure and AFM analyzed indicated that the surface roughness is increased with variation on sample, at silicon substrate, deposited temperature at 500^0C surface roughness 22.50 nm. Spectroscopy transmission was observed the band gap values change according to the crystalline state of the thin films and they are slightly higher than those reported for single crystals of TiO_2-anatase phase. Al doped TiO_2 thin films was prepared by pulse laser deposition, they were investigated at deposited temperature 450 ^{0} C. The X-rays diffraction spectra showed that the obtained films are polycrystalline of anatase structure with preferential of (101) plane direction. The atomic Force Microscopy (AFM) image showed that nanoparticle size and surface roughness mean square values and the surface of Al doped TiO_2 thin films are smoother than of pristine TiO_2 films. Al concentration increased, the band gap energy shifted towards the higher energy region (blue shift) compared to the pristine one. The determined band gap of pristine and doped samples varies from 3.43 to 3.61 eV, which is in accordance to Burstein-Moss shift [24, 25]. The grain size is increased,

the surface roughness goes to smooth. When the resistivity is low, then current would increase. Substitution of Ti^{+4} (0.54 Å) with Al^{+3} (0.61 Å) would create oxygen vacancies and donate electrons, causing an increase in charge carrier concentration, therefore the higher electrical conductivity of TiO_2 thin films [26]. Cobalt doped TiO_2 thin films was prepared by sol-gel process onto a glass substrate at room temperature. The calculated optical band gap decreases from 3.03 eV to 2.96 eV with increasing Co doping [27]. X-ray diffraction (XRD) peaks revealed that the films exhibit showed that Co: TiO_2 films are anatase crystalline structure at orientation (101). The optical properties were studied by using UV-visible (UV-Vis) with a wavelength range of 300 nm to 1000 nm. The investigated optical band gap decreasing with increasing Co concentration. Cobalt changes the absorption edge and the band gap of TiO_2 thin films.

1.4 Aim of the Present Work

In the recent years, titanium dioxide semiconductor nanomaterial has attracted much attention due to their potential technological applications such as waste remediation, biocompatible material, antibacterial, optoelectronic and solar cells device. TiO_2 is potentially useful, because of attractive properties like non-toxicity, good electrical, optical and piezoelectric behavior. However, TiO_2 is a wide band gap semiconductor (3 to 3.2 eV) due to TiO_2 can just be excited under Ultraviolet light with wavelength of less than 387 nm, which restrict the applications. To remove this problem, researchers have used variety of effective methods to modify TiO_2, including dye-sensitizing, noble metal loading, semiconductor mixing and ion doping. Among them, ion doping is a familiar method. Amorphous, anatase, rutile and brookite are of the phase of TiO_2 thin films. The crystal structure of TiO_2 is a tetragonal (a= 9.87 Å, c= 3.97 Å) and orthorhombic (a= 5.23 Å, b=10.14 Å and c=5.50 Å). However, the main drawbacks would be that TiO_2 does not absorb the visible sunlight, because of a large electrical band gap and high number of electron hole recombination rate. Recent reports show that physical properties of material are controlled by mono-doping. But several researchers have revealed that mono-doping of material introduces a series of problems such as instability, recombination of photon-excited electron-hole pairs, reducing the photo-excited current, declines the photo-catalysis efficiency, etc. and that could be solved by co-doping.

It is generally believed that Al doped TiO_2 can induce a lattice defects, make the absorption edges exhibits a red shift, which further improve the photo-catalytic efficiency of material. In additional, (Al, Co) co-doped TiO_2 thin films reduce the optical band gap (red shift) compared to pristine one. This has motivated to investigate the influence of transition metals (Al, Co) co-doped TiO_2 thin films on the tuning the band gap in the present study. Although much work has been done on the electronic and optical properties of TiO_2 thin films but sufficiently information is not available on the $Ti_{1-x}Al_{0.06}Co_xO_2$ thin films synthesized by spray pyrolysis deposition technique. Spray pyrolysis deposition technique is a sample, economical, viable technique and capable of producing good quality films for device application.

From practical point of view, Al doped and (Al, Co) co-doped TiO_2 thin film samples semiconductor to be deposited on the glass substrate and to be studied as follows:

- Synthesis of Al doped and (Al, Co) co-doped TiO_2 by spray pyrolysis technique.
- The crystal structure of the deposited films to be analyzed by XRD.
- The surface morphology of thin films sample.
- The surface roughness to be analyzed by AFM.
- The optical constants e.g. absorption, optical band gap, refractive index etc. to be determined by UV visible spectrophotometer.
- Electrical conductivity and resistivity are measurement by four probes method.
- The Electrical band structure, Mechanical properties, Charge density to be determined by density functional theory based theoretical method.

1.5 Outline of the Thesis

The rest of the thesis is organized as follow:

- Chapter one provides a brief overview of introduction, aim of present work, review work of TiO_2 thin films and applications.
- Chapter two provides a technique of thin films deposition.
- The samples preparation experimental details are described in chapter three.
- Chapter four provides a characterization techniques employed in this thesis work.
- The theoretical methodologies which are used to study the co-doped profile of TiO_2 are described in chapter five.

- The results associated with different properties investigated in this research are presented and discussed in chapter six.
- Chapter seven contains the concluding remarks and the scope of future work.

Reference

[1] Roy, S. C., Varghese, O. K., Paulose, M., and Grimes, C. A. "Toward solar fuels: Photo-catalytic conversion of carbon dioxide to hydrocarbons", *ACS Nano*, vol. 4 pp.1259–1278, 2010.

[2] Gratzel, M., "Photoelectrochemical cell" *Nature,* vol. 414, pp. 338–344, 2001.

[3] Hanaor, D. A. H., Sorrell, C. C., "Review of the anatase to rutile phase transformation" *J. Mater. Sci.,* vol. 46, pp. 855– 874, 2011.

[4] Asahi, R., Morikawa, T., Ohwaki, T., Aoki, K., and Taga, Y., "Visible-light photo-catalysis in nitrogen titanium dioxides" *Science*, vol. 293, pp. 269–271, 2001.

[5] Manil, K., Sok, K. W., and Hyo, P. Y., "Optical properties of TiO_2 thin films with crystal structure" *J. Phys. Chem. Solids*, vol. 123, pp. 266-270, 2018.

[6] Shaoyou, L., Guocong, L., and Qingge, F., "Al-doped TiO_2 mesoporous materials: synthesis and photodegradation properties" *J. porous mater*, vol. 17, pp. 197-206, 2010.

[7] Gao, Y., Masuda, Y., Peng, Z., Yonrezawa, T., and Koumoto, K., "Room temperature deposition of a TiO_2 thin film from aqueous peroxotitanate solution" *J. Mater. Chem*., Vol. 13, pp. 608, 2003.

[8] Mohama, M. R., Garzella, C., Comini, E., Tempesti, E., Frigeri, C., and Sberveglier, G., "Sensor, TiO_2 thin films by a novel sol-gel processing for gas sensor applications" *Actuator*, vol. 68, pp. 189-196, 2000.

[9] Vasquez, G. C., Peche-Herrero, M. A., Maestre, D., Cremades, A., Ram´ı rez-Castellanos, J., Gonz´alez-Calbet, J. M., and Piqueras, J., "Effect of transition metal doping on the growth properties of rutile TiO_2 nanoparticles" *J. Phys. Chem. C*, vol. 117, pp. 1941-1947, 2013.

[10] Setiawati, E. , and Kawano, K., "Stabilization of anatase phase in the rare earth; Eu and Sm ion doped nanoparticle TiO_2", *J. Alloys Compd*., vol. 451, pp.293-296, 2008.

[11] Ganose, A. M., and Scanlon, D. O., "Band gap and work function tailoring of SnO_2 for improved transparent conducting ability in photovoltaics" *Mater. Chem. C,* vol. 4 pp. 1467-1475, 2016.

[12] Burstein, E., "Anomalous optical absorption limit in lnSb" *Phys. Rev*, vol. 93, pp. 632-633, 1954.

[13] Zhang, S., and Zunger, A., "Over-comong doping bottlenecks in semiconductors and wide-gap materials" *Phys. B*, vol. 273, pp. 976-980, 1999.

[14] Ohno, T., Tokieda, K., Higashida, S., and Matsumura, M., "Synergism between of rutile and anatase TiO_2 particles in photocatalytic oxidation of naphthalene" *Appl. Catal., A*, vol. 244, pp. 383–391, 2003.

[15] Deepa, M., Joshi, A.G., Srivastava, A.K., Shivaprased, S. M., and Agnihotry, S. A., "Electrochromic nanostructured tungsten oxide films by sol-gel: structure and intercalation properties" *J. Electrochem. Soc.*, vol. 153, pp. 365-376, 2006.

[16] Mor, G. K., Shankar, K., Paulose, M., Varghese, O. K., and Grimes, C. A., "Use of highly-ordered TiO_2 nanotube arrays in dye-sensitized solar cells", *Nano Lett.* Vol. 6, pp. 215–218, 2006.

[17] Bouras, P., Stathatos, E., and Lianos, P., "Pure versus metal–ion-doped nanocrystalline titania for photocatalysis" *Appl. Catal. B Environ.*, vol. 73,pp. 51–59, 2007.

[18] Macwan, D. P., Dave, P. N., and Chaturvedi, S., "A review on nano-TiO_2 sol-gel type syntheses and its applications" *J. Mater. Sci.*, vol. 46, pp. 3669-3686, 2011.

[19] Mingzheng, G., Chunyan, C., Huang, J., Shuhui, L., and Zhong, C., "A review of one dimensional TiO_2 nanostructured materials for environmental and energy applications" *J. Mater. Chem. A*,, vol. 4, pp. 6772-6801, 2016.

[20] Babu, M., Dev, C. B. , Podder, J., and Islam, N., " Influence of Fe^{2+}/Fe^{3+} ions in tuning the optical band gap of SnO_2 nanoparticle synthesized by TSP method: Surface morphology, structural and optical studies" *Matt. Sci. proc.,* vol. 89, pp. 223-233, 2018.

[21] Anna, A., Murashkina., Murxin, P.D., Rudakova, A.V., Ryabchuk, V.K., Emeline, A.V., and Bahnemann, D.W., "Influence of the dopant concentration on the photo-catalytic activity: Al-doped TiO_2." *J. phys. chem. C*, vol. 119, pp. 24695-24703, 2015.

[22] Masayuki, O., Shiozaki, K., Horikawa, N., Tsuyoshi, K., Kumara, G.R.A., Madarasz, J., Kaneko, S., and Gyorgy, P. "Porous TiO_2 thin films prepared by spray pyrolysis deposition (SPD) technique and their application to UV sensors" *Solid state ionics*, vol. 172, pp. 527-531, 2004.

[23] Wang, Y., Zhang, R., Jianbao, L., Liangliang, L., and Shiwel, L., "First-principle study on transition mrtal-doped anatase TiO_2" *Nano. Scale res. Let*. vol. 9, pp. 46, 2014.

[24] Bouachiba, Y., Hanini, F., Bouabellou, F., and Taabouche, A., "TiO_2 thin films studied by FTIR, AFM and Spectroscopic ellipsometry" *Int.J. Nanoparticles*, vol. 6, pp. 2-3, 2013.

[25] Song, Y.S., Kim, B.Y., Cho, N.L., and Lee, D.Y., "Effect of Al doping on optical band gap energy of Al-TiO_2 thin films" *J. nano. Sci.,* vol. 15, pp. 5228-5231, 2015.

[26] Khan, M.I., "Synthesis, characterization and application of Co doped TiO_2 multilayer thin films" *Res. in Phys.* vol. 9, pp. 359-363, 2018.

[27] Hanini, F., Bouachiba, Y., Kermiche, F., Taabouche, A., Bouabellou, A., Kerdja, T., and Boukheddaden, K., "Characteristics of Al-doped TiO_2 thin films grown by pulsed laser deposition", *Inter. J. Nano.,* vol.. 11, pp. 132-142, 2013.

CHAPTER-2
TECHNIQUES OF THIN FILM DEPOSITION

2.1 Introduction

Thin film can be prepared by various deposition techniques, which are greatly influencing the several parameters substrate materials, substrate temperature, rate of deposition, background pressure etc. To know the property of metals, semiconductors and insulators create thin film on a substrate and measuring different properties. Specific applications in modern technology demand film properties such as high optical reflection, transmission, hardness, adhesion, non-porosity, high mobility of charge carriers, chemical inertness towards corrosive environments, and stability with respect to temperature. The need for the new and improved optical and electronic devices stimulated the study of thin solid films of single elements, binary and ternary system, with controlled composition and specific properties. Thin film is prepared by deposition of the film materials (metals, semiconductors, insulator, dielectric etc.) atom by atom on a substrate through a phase transformation. Sufficiently time interval between the two successive deposition of atoms and also layers are required so that these can occupy the minimum potential energy configuration. In thermodynamically stable films, all atoms or molecules should be in their minimum potential energy sites and incoming atoms or molecules will take up positions and orientations energetically compatible with the neighboring atoms of the substrate or to the previously deposited layers, the effects of substrate or the initial layer will diminish gradually.

2.2 Classification of Deposition Techniques

In order to obtain thin films with good quality, there are two common deposition techniques:

1. Physical deposition techniques and
2. Chemical deposition techniques.

The different technique for producing thin film is given below:

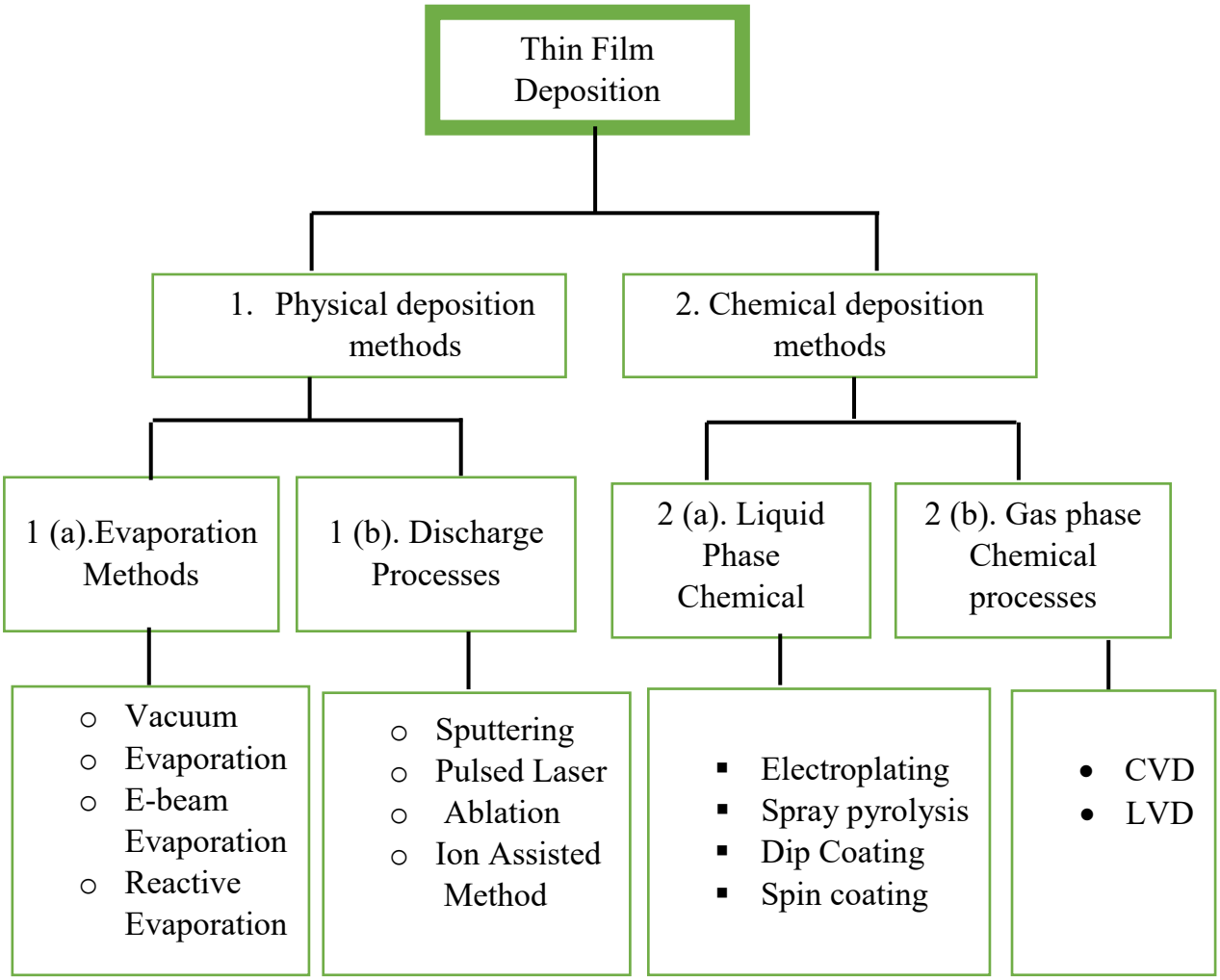

Fig. 2.1: The schematic diagram of different deposition technique.

2.3 Spray Pyrolysis Method

Spray pyrolysis is a powerful technique to synthesize a wide variety of high purity chemically homo-genous ceramic powders. Large quantities of oxide powders with homogenous particle sixes and crystalline sizes less than 100 nanometers may be produced by this method. This is one of the best methods for the deposition of thin films. The method involves spraying a solution usually in aqueous, containing soluble of the constituent atoms of the desired compound on to heated substrate [1-2]. Every sprayed droplet reaching the substrate undergoes pyrolysis decomposition and forms a single crystallite or a cluster of crystallites of the products. Different parameters like volume of solution distance between the substrate and the spray nozzle have to be

optimized to get–a homogenous uniform thickness and good quality of the film. Hydrolysis and pyrolysis are the main chemical reactions involved in this process [3].

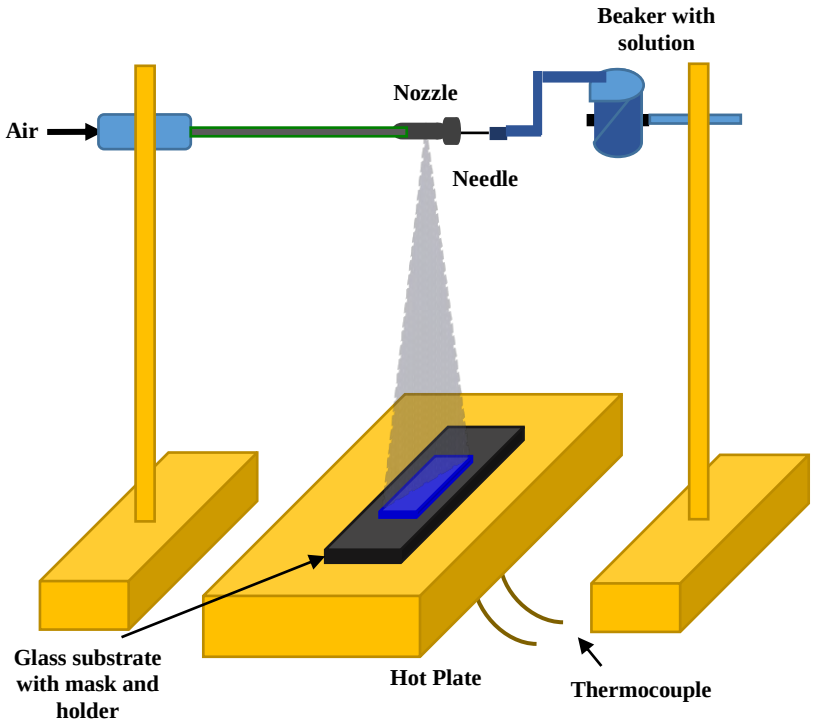

Fig. 2.2: Schematic diagram of the spray pyrolysis deposition method.

In this technique, the chemicals vaporized and react on the substrate surface after reaching on it. In principle spray pyrolysis technique is very simple, cost effective and suitable for industrial applications [4]. The apparatus, needed to carry out the chemical spray process, consists of an atomizer the spray solution and a substrate heater. The spray deposition has been used to prepare coatings for the cover glass, required for flat plate collectors and cutter tubes used in the focusing type cylindrical collectors.

The following advantages of spray pyrolysis method are listed below:

1. Operates at atmospheric pressure, well controlled stoichiometry, homogeneity.
2. Film deposit over large surface area, low operational cost, purity of product
3. Coating are more durable than vacuum deposited coatings
4. Variety of precursors could be used
5. Multi-layer fabrication capability which is very attractive for making functionally graded films.
6. Low processing temperature

2.4 Different Stages of Film Formation

2.4.1 Films Growth Mechanism

There are three mechanism of thin films condensation which can be distinguished, depending on the strength of interaction between the atoms of the growing film and between the atom of the film and substrate. There are

i. In the Frank-van der Merwe Or layer by layer growth mode, the adsorbate substrate interaction with each other and thus a new layer beings to grow only when the previous layer is completed.

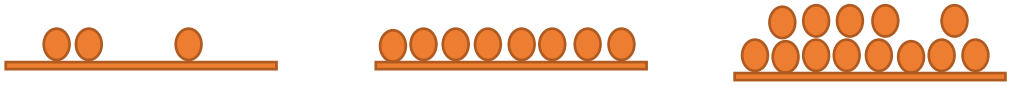

ii. In the Vollmer-Weber or Island growth mode, the adsorbate-adsorbate interaction dominates and thus deposition produces multilayer islands.

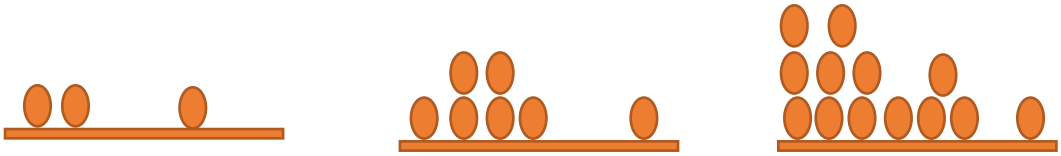

iii. The **Stranski-Krastanov** or layer+island growth mode is a particularly interesting case that has recently exploited in the production of nanometer scale islands. After the formation of I or more complete monolayer, three dimensional island nucleate and grow on top of the complete latyer.

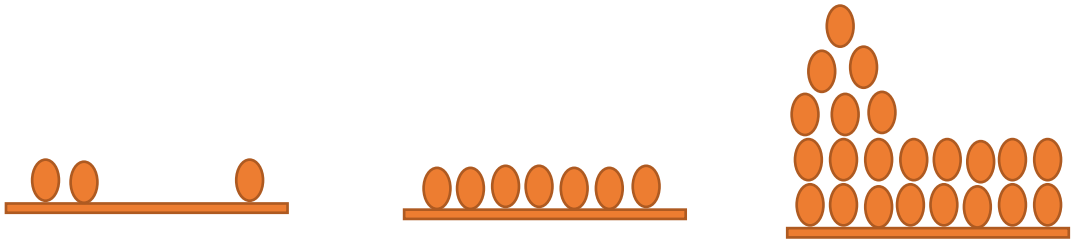

2.4.2 Condensation

Thin films are most commonly prepared by the condensation of atoms on a substrate from the vapor phase of the material. Condensation means the transformation of a gas in to a liquid or solid. Thermodynamically, the only requirement for condensation to occur is that partial pressure of the film material in the gas phase be equal or larger than its vapor pressure in the condensed phase at that temperature. Condensation of a vapor atom is determined by its interaction with the impinged surface. The impinging atom is

attracted to the surface by the instantaneous dipole and quadruple moments of the surface atoms. Consequently the atoms losses its velocity component normal to its surface in a short time, provided the incident kinetic energy is not too high. The vapor atom is then physically absorbed (called atom) but it may or not be completely thermally equilibrated [5-6]. It may move over the surface by jumping from one potential to other because of the thermal activation from the surface and its own kinetic energy parallel to the surface. The ad atom has a finite stay or residence time on the substrate during which it may interact with other ad atoms to form stable cluster and be chemically absorbed with the release of heat of condensation. If is not absorbed the ad atom re-evaporates or desorbs into the vapor phase. Therefore, condensation is the net result of equilibrium between the absorption and desertion process. The probability that an impinging atom will be incorporated into the substrate is called the "condensation" or "striking coefficient". It is measured by the ratio of the amount of material condensed on a surface to the total amount impinged. In fact, often the striking coefficient is so small that condensation is not observable by ordinary techniques. On the other hand, the striking coefficient is found to be strongly dependent on the total time during which the substrate was subjected to the impingement and also on the substrate temperature. A non-unity striking coefficient is usually explained in terms of monomer re-evaporation from the areas on the substrates, which are outside, the capture zones around each stable nucleus [7].

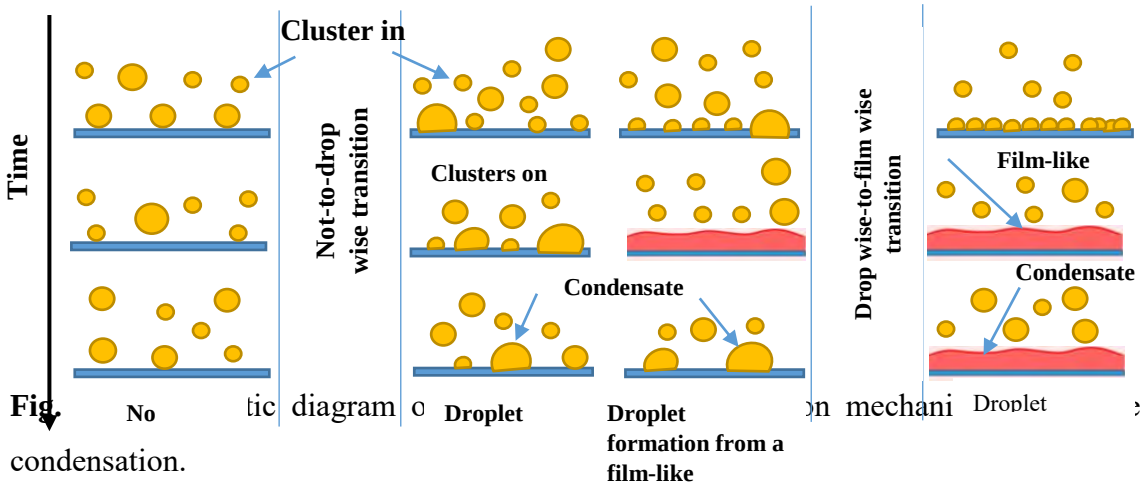

Fig. tic diagram o n mechani ;
condensation.

2.4.3 Nucleation

Nucleation is the birth stage of a film. Condensation is initiated by the formation of small cluster through the combination of several absorbed atoms. These clusters are called nuclei and the process of formation is called nucleation.

There are two types of nucleation occur during the formation of a film. They are

a) **Homogenous nucleation:** The total free energy is used in the formation of a cluster of ad-atoms.
b) **Heterogeneous nucleation:** Particular shapes of clusters are formed by collisions of atoms on the substrate surface, and in the vapor phase its super saturation is sufficiently high. They initially developed within increase in free energy until a critical size is reaches above which growth continuous with a decrease in free energy. In atomistic theory, in low substrate temperature or very high super saturations, the critical nucleus may be a single atom which will form a pair with another atom by random occurrence to become a stable cluster and grow spontaneously.

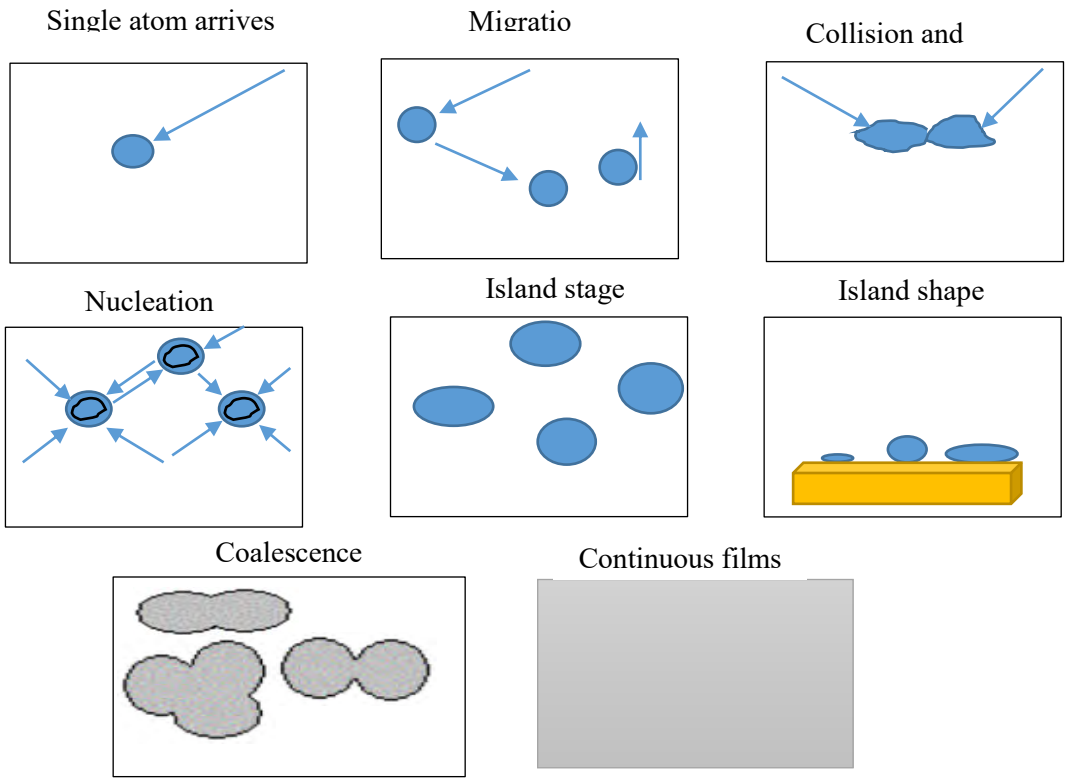

Fig. 2.4: The growth mechanism of films.

2.4.4 The Island Stage

When atoms are deposited slowly onto a flat surface, the first one undergoes a random walk on that surface. Eventually a second atom is deposited; in all likelihood it will eventually meet the first. Once the two atoms meet they may bond to form a particle with a higher mass and a lower random walk velocity. Because the bonded particles are now more stable and less mobile than before, they are called an island. Subsequent atoms deposited on the substrate eventually meet and bond with the island, further increasing its size and stability. Eventually the island can grow to fill the entire substrate with a sngle large grain. The faster the atom are deposited, the greater amount of atoms on the substrate before any large stable island form. As these atoms meet, they will bond to their local neighbors before having the change to migrate to a distant island. In this way a large number of separate islands are formed and can grow independently. Eventually the separate island will grow to become separate grains in the final film [8-10].

2.4.4 The Coalescence Stage

In this stage of thin film growth, the islands are combined with the neighbouring ones to form large island. The phenomenon of formation of larger island from the smaller ones is called agglomeration or coalescence. This coalescence stage involves the transfer of mass between islands by diffusion and hence small islands disappear rapidly. The time of coalescence is very short, of the order of about 0.6 seconds. In addition, nuclei having well-defined crystallographic shapes before coalescence become rounded during the event.

2.4.5 Channel, Hole and Continuous Film Stages

As a consequence of the arrival of more and more species on the substrate, the coalescence continues, resulting in a network of the deposited areas with channels in between. The channels last only for small time, as some secondary nuclei begin to grow within these void space. Further deposition of the material leads to the diminishing or even vanishing of these voids resulting in an eventually continuous film, even though some pores may be present in some cases. To obtain a perfectly continuous film, a minimum thickness is need which depends upon the nature of the deposited material, method of deposition and the deposition parameters involved in that particular deposition technique.

References

[1] Haque. B.M., Chandra. D.B., Jiban. P., and Nurul. I., Abdullah. Z., "Influence of Fe $^{2+/}$Fe $^{3+}$ ions in tuning the optical band gap of SnO_2 nanoparticles synthesized by TSP method: Surface morphology, structural and optical studies" *Mat. Sci. semi. Proc.,* vol. 89, pp. 223-233, 2019.

[2] Chandra. D.B., Haque. B.M., Jiban. P., Sagadevan, S., and Abdullah. Z., "Low temperature synthesis of $\alpha -$ and $\beta -$phase Bi_2O_3 thin films via B doping: tailoring optical band gap and n- to p-type Bi_2O_3" *J. Mat. Sci. Mat. Electro*. 2019.

[3] Sharmin. M., and Jiban. P., "Influence of Al doping on the structure and properties of Fe_2O_3 thin films: High transparency, wide band gap, ferroelectric behavior" *Semi. Sci. and tech.*, vol. 30, pp. 075033, 2019.

[4] Reddy. T. S., and Kumar. M. C. S., "Co-evaporated SnS thin films for visible light photo-detector applications" *RSC Adv.,* vol. 6, pp. 95680, 2016.

[5] Sheng. Q., Sun. J., Wang. Q., Wang. W., and Wang. H.S., "On the onset of surface condensation: formation and transition mechanism of condensation mode" *Sci. Reports.* vol. 6, pp. 30764, 2016.

[6] Pavlo. I., Stakhira., L., and Georgij, "Photovoltaic cell based on nickel phthalocyanine and zinc oxide formed by atomic layer deposition" *Cent. Eur. J. Phys.,* vol. 8, pp. 798-803, 2010.

[7] Chorpa., K.L., "Nucleation Growth and Structure of Films" Thin film Phenomena, McGraw-Hill book Company, New York, pp. 110-137, 1969.

[8] https://en.wikipedia.org/wiki/Island_growth.

[9] Suri., A. K., Krishnamurthy., N., and Batra., I. S., "Materials issues in fusion reactors" J. Phys. conf. Ser. P. 012001, 2010.

[10] Ratsch, C., and Venables, J.A., "Nucleation theory and the early stage of thin film growth" *J. Vacuum. Sci. Techn*., vol. 21, pp. 0734-2101, 2003.

CHAPTER-3
SAMPLE PREPARATION

3. 1 Introduction

This chapter deals with mainly the design and construction of different experimental apparatuses and preparation of Al doped and (Al, Co) co-doped TiO_2 thin films on glass substrate. Various steps taken for the film on glass substrate by spray pyrolysis deposition process will be discussed in the later part of this chapter. Spray pyrolysis is the most common used technique adopted for deposition of metals, alloys and many compounds [1]. Processes involved in spray pyrolysis technique, such as atomization of the precursor solution, aerosol transport and decomposition of the precursor are discussed in this chapter.

3.2.Experimental Equipment

3.2.1 Preparation of mask

In order to study the various properties of thin film, it is necessary that the film must be properly patterned. The most commonly used method of patterning thin film is the physical masking, which is accomplished by placing the mask of desired shape on the substrate. We found mica and stainless steel as suitable masking material. Since the thickness of the films deposited is of order the mask should be as thin as possible so as to obtain uniformity of thickness throughout the film pattern.

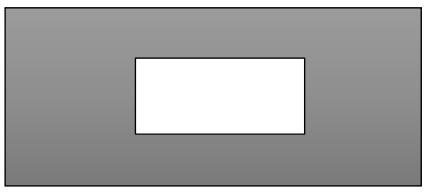

Fig. 3.1: Mask used for the preparation of films.

3.2.2 Experimental set up for spray pyrolysis technique

The design of a typical reactor is shown in fig. 2.2 (Chapter-2). It is a vertical batch type reactor composed of a galvanized iron enclosure, heater, and heat susceptor. For the rapid expulsion of the byproduct gasses there are opening at the side and at the top of the–reactor. It helps focusing aerosol towards the substrate and also provides a chimney action to the exhaust gas upwards.

3.2.3 Heater

The heater “H” is an ordinary hot plate 2-kilowatt nichrome wire heater. The top of the place is covered with a thick sheet of stainless steel plate. Substrate is placed on this plate to have a uniform temperature throughout the substrate surface. A mica sheet with the same design of mask is placed in between the substrate and the mask to prevent spreading in solution beyond the opening of the mask. An electrical voltage variac controls the heater power. The temperature of the heater was measured by copper constantan thermocouple tightly attached to the substrate surface placed on the heater susceptor.

3.2.4 Air compressor

It is a reservoir type electrical air compressor. A rotary pump in this section mode draws atmospheric air and keeps it reverse in a large capacity air tank. At the outlet of the tank a pressure gauge is attached which records the pressure of the air at the time of supplying it form the tank. There is a bypass control valve which can keep the output pressure constant.

3.2.5 Head/Nozzle

The single spray nozzle consists of capillary tubes fitted at perpendicular to the other tube as shown in fig. 2.2.when compressed air is placed rapidly through the upper tube “p” in direction tangential to the mouth of the lower tube “A” whose other end is kept deep in the spray liquid. Due to this partial vacuum the liquid rises up through the tube “A” and the compressed air drives it away in the form of the fine spray particles (aerosol). The thinner the spray nozzle the finer would be the spray particles. A very fine needle shaped capillary tube was used for the spray nozzle.

3.2.6 The Fume Chamber

It is a large box type chamber with a slanting top and is provided with a chimney. There is an exhaust fan with regulated power supply fitted at the top of the chimney [2]. The slanting top and the sidewalls are made of glass. There are air tight doors in the front side. The chamber has purging facilities. The whole spray is kept inside the fume chamber at the time of film deposition because of safety grounds and to check air current disturbances at the deposition site. These two points just stated are very important for the pyrosol process when deposition is carried out in open air atmosphere.

3.2.7 Film Thickness and Control

Thickness play an important role in the film properties unlike a bulk material and almost all film properties are thickness dependent at least for thin films. Reproducible properties are achieved only when the film thickness and the deposition parameters are kept constant [3-5].

In the present spray deposition process, the deposition time is the main thickness controlling factor, provided the other parameters remain constant. Since the deposition is carried ot in normal atmosphere a direct control of thickness is not so easy. To control the thickness therefore calibration chart may be used. The charts are generally plots of deposition time versus thickness, and can be prepared at different constant substrate temperature prior to the preparation of particular experimental samples using the different solution and deposition variables. Since the rate of deposition in present set up to rather small, the thickness control is therefore not difficult.

3.3 Solution Preparation

The solution was prepared by taking titanium butoxide Ti $(OCH_2CH_2CH_3)_4$ as source compound. The most commonly used solvent are water. As Aluminum Chloride ($AlCl_3.6H_2O$) dissolves in water at room temperature, water was taken as solvent. Since the spray system used in the present experiments operates via a partial path at the mouth of the spray nozzle, the concentration of the solution prepared by the solvent should be such that the nozzle could at least draw it. The higher the solution concentration, the lower the spray rates. The spray solution will be prepared from a mixture of 3.4032 ml of titanium butoxide [$Ti(OCH_2CH_2CH_3)_4$] mixed with 1.8 ml of 0.5 M HCl, followed by dilution with 100 ml of distilled water, to prepare of 0.1 M Aluminum Chloride ($AlCl_3.6H_2O$) and Cobalt acetate [$(Co(CH_3COO)_2$] will be added to the starting solution as dopants. In the case of Al doped TiO_2 samples Al concentrations are varied from 0, 2, 4, 6 and 8 at %. The co-doping of (Al, Co), the atomic ratio of Al was fixed 6% and Cobalt concentration are varied from 1, 2, 3 and 4 at. %. Before the deposition, the substrates will be well cleaned by acetone and distilled water. The flow rate of the solution during spraying will be adjusted to about 2.5 mL/min and kept constant throughout the experiment. The distance between the spray nozzle and the substrate will

be maintained about 25 cm. The temperature of the substrate will be measured by an optical pyrometer. Substrate temperature will be maintained 450 ^{0}C.

3.4 Steps of Thin Film Processes

There are four sequential steps are followed when a thin film is growth on a substrate. A source of film material is provided, the material is transported to the substrate, deposition take place, so the film is subsequently annealed, and finally it is analyzed to evaluate the process. The results of the analysis are then used to adjust the condition of the steps for film property modification.

Process steps:

a. Source: solid, liquid, vapor or gas; (flux)
b. Transport: in vacuum or in gas phase (uniformity)
c. Deposition: absorption, surface migration and reaction (morphology)
d. Analysis

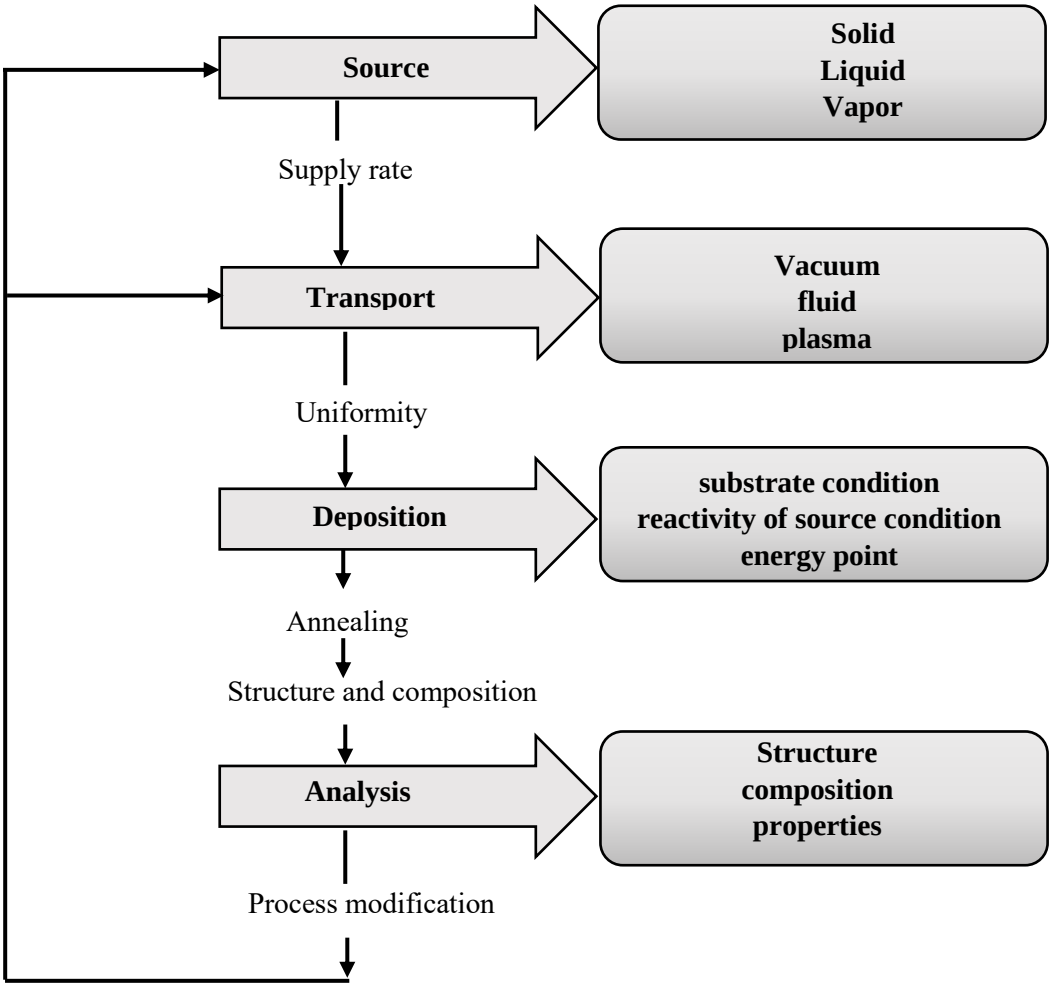

Fig. 3.2: Thin films process

3.5 Sample Deposition

It has been declared earlier that spray pyrolysis method for preparing thin films is an economically attractive method [6-8], which consist basically of spraying solution on a heated glass substrate. The apparatus needed to carry out the chemical spray process consist of a device to atomize the spray solution and a substrate heater. Fig. 2.2 (chapter-2) shows a typical experimental setup of spray pyrolysis. A considerable amount of 100 ml solution taken in the container "F" fitted with the spray nozzle "A". The clean substrate with suitable mask was put on the heater "H". The distance between the tip of the nozzle and the surface of the glass substrate was kept 25 cm. before supplying the compressed air the substrate temperature "T_s" was to be kept at a level slightly higher than the required substrate temperature because at the onset of spraying a slight fall of temperature is likely. The temperature of a substrate was controlled air is passed through "P" at constant pressure (0.5 bar), a fine Al doped and (Al, Co) co-doped TiO_2 was produced and was automatically carried to the reactor zone where film was deposited on the heated substrate [9, 10].

Reference

[1] Antonaia P., Menna, M. L., Addonzio, and Crocchilo, "Transparent properties of polycrystalline tin oxide films" *Sol. Energy Mater,* vol. 28, pp. 167-173, 2009.

[2] Patil P. S., Kadam L. D., and Lokhande C. D., "Preparation and chacterization of spray pyrolysis cobalt oxide thin films" *Thin solid Films*, vol. 272, pp. 29-32, 1996.

[3] Kadam L. D., and Patil P. S., "Thickness-dependent properties of sprayed cobalt oxide thin films" *Mater, chem, and Phys*., vol. 68, pp. 225-232, 2001.

[4] Kadam L. D., Pawar S. H., and Patil P. S., " studies on ionic intercalation properties of cobalt oxide thin films prepared by spray pyrolysis technique" *Materials science communication, Mater. Chem. And phys*. vol. 68, pp. 280-282, 2001.

[5] Korotecenkov G., Brinzari V., and Boris I., "(Cu, Fe, Co, or Ni)-doped tin dioxide films deposited by spray pyrolysis: doping influence on film morphology" *J. Mater. Sci.,* vol. 43, pp. 2761-2770, 2008.

[6] Jachon J., Varghes M., and Abraham K. E., "Studies on Cu, Fe, and Mn doped SnO_2 sem. Conducting Transparent Films Prepared by a Vapor Deposition Technique" *Chines. J. of Phys.,* vol. 45, pp. 84-97, 2007.

[7] Hong N. H., Sakai J., Prellier W., and Hassini A., " Transparent Cr-doped SnO_2 thin films ferromagnetism beyond room temperature with a giant magnetic moment" *J. Phys. Condens. Matter.,*vol. 17, pp. 1697-1702, 2005.

[8] Korotcenkov G., Macsanov V., Tolstoy V., Brinzai V., Schwank J. and Faglia G., " Structural and gas response characterization of nano-size SnO_2 films deposited by SILD method." *Sensor. And Actu. B: Chem*., vol. 96, 3, pp. 602-609, 2003.

[9] Anuar K., Ho S. N., Tan W. T., Atan M. S., Kuang D., Jelas H. M., and Saravanan N., " Effect of Solution concentration on the properties of Cu_4SnS_4 thin films" *Mater. Sci.* Vol. 14. P. 2, 2008.

[10] Elangovan E., and Ramamurthi K, "Studies on Optical properties of polycrystalline SnO_2: Sb thin films prepared using $SnCl_2$ Precursor" *Cryst. Res. Technol*., vol. 38, pp. 779-784, 2003.

CHAPTER-4
CHARACTERIZATION TECHNIQUE

4.1 Introduction

This chapter deals with mainly the experimental characterization techniques will be discussed in this chapter. The effect of (Al, Co) co-doping on the structural, morphological, optical and electrical properties of TiO_2 thin films were studied, in the case of used techniques are detailed discussed in the chapter.

4.2 Scanning Electron Microscopy (SEM)

The surface morphology of the thin films was taken by scanning electron microscope (SEM). The scanning electron microscope is a type of electronic microscope that images the sample surface by scanning it with a high-energy beam of electrons in a raster scan pattern [1]. There are many advantage to using the SEM instead of a light microscope. The SEM has a large depth of field, which allows a large amount of the sample to be in focus at one time. The SEM also produces images of high resolution, which means that closely spaced features can be examined at a high magnification [2]. A beam of electron is generated in the electron gun, located at the top of the column, which is pictured to the left. This beam is attracted through the anode, condensed by a condenser lens, and focused as a very fine point on the sample by the objective lens. The scan coils are energized (by varying the voltage produced by the scan generator) and create a magnetic field which deflects the beam back and forth in a controlled pattern. The varying voltage is also applied to the coils around the neck of the cathode-ray tube (CRT).

This produces a pattern of light deflected back and forth on the surface of the CRT. The pattern of deflection of the electron beam is the same as the pattern of deflection of the spot of light on the CRT. The electron beam hits the sample, producing secondary electrons from the sample. These electrons are collected by a secondary detector or a backscatter detector, converted to a voltage and amplified. The amplified voltage is applied to the grid of CRT and causes the intensity of the spot of light to change. The image consists of thousands of spots of varying intensity on the face of a CRT that correspond to the topography of the sample.

Fig. 4.1: Scanning electron microscopy.

The SEM column can be broken down into several component parts:

- An electron gun which provides a source of electrons.
- A pair of electromagnetic condenser lenses which produce a beam with a very small diameter.
- An objective lens to focus the beam on the specimen surface and scan coils to cause the beam to traverse across the specimen.
- The specimen chamber containing s manipulative stage and secondary electron detector.
- A vacuum system to remove the air from the electron optical column thus providing a free path for the beam electrons.

4.3 Compositional Study

EDX analysis stands for Energy Dispersive X-ray analysis. It is sometimes referred to also as EDS of EDAX analysis. It is a technique used for identifying the elemental composition of the specimen. The EDX analysis system works as an integrated feature of a scanning electron microscope (SEM), and cannot operate on its own without the latter. During EDX analysis, the specimen is bombarded with an electron beam inside the scanning electron microscope. The bombarding electron collide with the specimen atom‟s own electrons, knocking some of them off in the process. A position vacated by

an ejected inner shell [3]. To able to do so, however, the transferring outer electron must give up some of its energy emitting an X-ray. The amount of energy released by the transferring electron depends on which shell it is transferring from, as well as which shell it is transferring to. Furthermore, the atom of every element released X-rays with unique amounts of energy during the transferring process. Thus, by measuring the amounts of energy present in the X-rays being released by a specimen during electron beam bombardment, the identity of the atom from which the X-ray was emitted can be established.

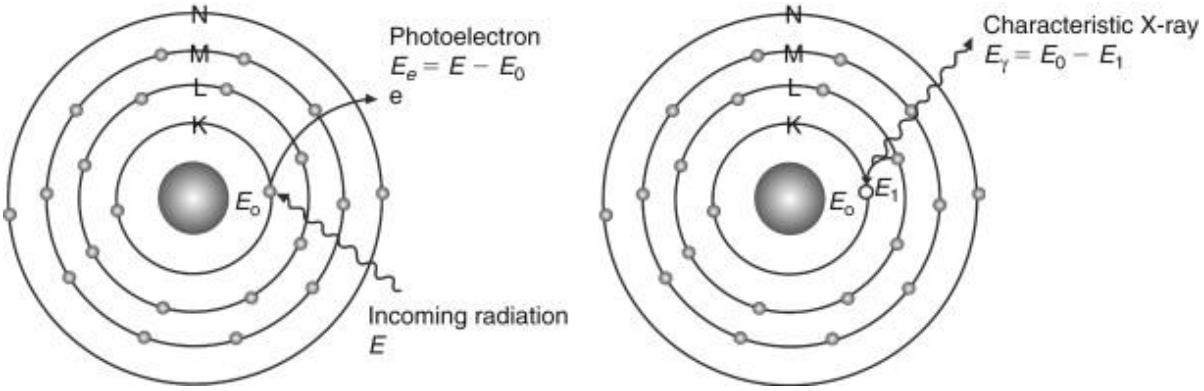

Fig. 4.2: Schematic diagram of Energy Dispersive X-ray spectra.

The output of an EDX analysis is an EDX spectrum. The EDX spectrum is just a plot of how frequently an X-ray is received for each energy level. An EDX spectrum normally displays peaks corresponding to the energy level for which the most X-rays had been received [4]. Each of the peaks are unique to an atom, and therefore corresponds to a single element. The higher a peak in a spectrum, the more concentrated the element is in the specimen.

An EDX spectrum plot not only identifies the element corresponding to each of its peaks, but the type of X-ray to which it corresponds as well. For example, a peak corresponding to the amount of energy processed by X-rays emitted by an electron in the L-shell going down to the K-shell is identified as a K-Alpha peak. The peak corresponding to X-rays emitted by M-shell electrons going to the K-shell is identified as a K-Beta peak.

4.4 Atomic Force Microscopy

Atomic force microscopy (AFM) or Scanning force microscopy (SPM) is a very high resolution type of scanning probe of microscopy with demonstrated resolution on the

order of fraction of a nanometer, more than 1000 times better than the optical diffraction limit. An AFM has three major abilities: force measurement, imaging and manipulation. In force measurement, AFMs, can be used to measure the force between the probe and the sample as function of their mutual separation. This can be applied to perform force spectroscopy, to measure the mechanical properties of the sample, such as the samples young modulus, a measure of stifiness [5].

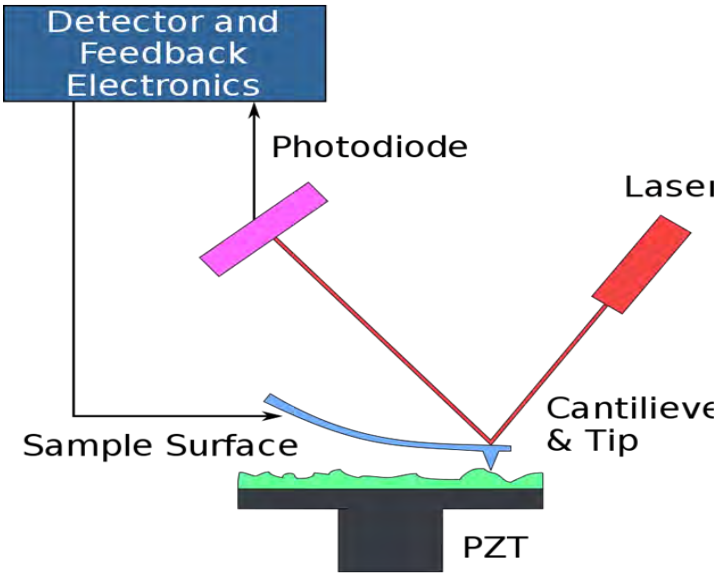

Fig. 4.3: Block diagram of atomic force microscope using beam deflection detection [5].

4.5 X-ray Diffraction Studies

X-ray diffraction (XRD) is a powerful tool in the solid state materials. The uniqueness of this technique is that it is a non-destructive technique and furnishes multiple results including crystal lattice details down to the atomic level. As the wavelength of X-ray is on the atomic scale, X-ray diffraction is also a primary tool for probing structure of nano-materials. When monochromatic rays pass through a crystal, the crystal acts as a diffracting net: diffracts the X-rays with a concrete direction and intensity and a pattern of peaks is obtained [6]. X-ray diffraction is a tool for the investigation of the structure of the mater and is a versatile technique that reveals details information about the chemical composition and crystallographic structure of nature and manufacture materials [7]. Using X-ray diffraction, a wealth of structure, physical and chemical information about the investigated material can be obtained. Crystalline materials give rise to the most obvious applications, but there is also important information to be obtained from semi crystalline and even amorphous materials. Crystalline size is the

fundamental characteristic of nano-materials and microstructure is often a key to understanding and controlling bulk properties. Small size results in broadened diffraction patterns. Analysis of peak shapes cans distortions (due to variations in composition or micro-strain) and faulting. A string of parameters can be obtained from XRD such as phase identification and quantification, crystal structure variations (e.g. lattice parameters), crystalline size and shape and lattice distortion, crystalline, non-crystalline periodicity and size, orientation (crystalline and amorphous) dynamic studies, in situ studies at process temperature and in reactive atmosphere [8]. A host of applications techniques for various material classes is available; each revealing its own specific details of the sample studied applying in chemical analysis, stress and strain measurement, the study of phase equilibrium, measurement of particle size, as well as crystal structure [7]. Determination of the equilibrium phase diagram of the alloys in metallurgy, the residual stress measurements in mechanical engineering, the surface coating/electro-deposits and electrochemical reaction studies in chemistry, study of the structure of nucleic acids in biological sciences, crystal structure analysis in solid state physics/material science etc., are some of the fields that have used the vast potentials of this technique. Thus XRD is a sample technique and does not require elaborate sample preparation, which partly explain the wide usage of XRD method in material characterization. Diffraction peak positions are accurately measured with XRD, which makes it the best method for characterizing homogenous and inhomogeneous strain [9].

One of the disadvantage of the XRD, compared to electron diffraction, is the low intensity of diffracted X-rays, particularly for low-Z materials. XRD is more sensitive to high Z-materials, and for low Z-materials neutron or electron diffraction is more suitable. Typical intensities for electron diffraction are ~ 108 times larger than for XRD. Because of small diffraction intensities, XRD generally requires large specimens and the information acquired is an average over a large amount of material [10]. In crystalline solids, atoms (and molecules) are arranged in periodic and regular fashion conforming to a standard geometry called crystal lattice. In this crystal lattice, the atoms can be arranged in different planes taking part in the coherent scattering process. When X-ray beam is incident on a set of parallel planes (within each crystal) of the crystalline bulk, the electron clouds of these atoms diffract the X-ray beam in a rational approach as shown in fig. 4.4.

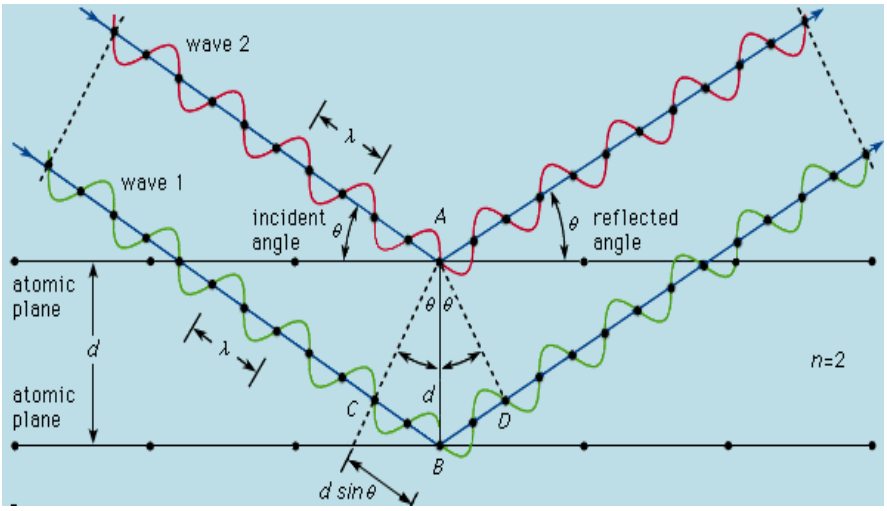

Fig. 4.4: Reflection of X-rays from two planes atoms in a solid [12].

From the geometrical consideration, the basic Bragg equation is formed 2d sin θ = nλ, where d is the inter-planar distance (or lattice constant), λ is the wavelength of the characteristic X-ray, and 2θ are incident and diffracted angles and n is the order of the scattered beam. The famous Bragg‟s law provides the basic platform for the XRD methods. By varying the angle theta, the Bragg‟s law conditions are satisfied for different d- spacings in polycrystalline materials. Plotting the angular positions and intensities of the resultant diffracted peak of radiation produces a pattern which is characteristic of the sample. Where a mixture of different phases is present, the resultant diffracto-gram is formed by addition of the individual patterns. Based on the principle of X-ray diffraction, a wealth of structure, physical and chemical information about the material investigation can be obtained [11]. The average crystalline size was estimated by Debye-Scherrer formula [12, 13] as follows

$$<D>= \frac{0.9\,\lambda}{\beta \cos\theta} \tag{4.1}$$

Where D is the average crystalline size in (Å), shape factor taken as 0.9, λ is the wavelength of X-ray radiation, β is the full width half maximum (FWHM) after making appropriate base correction and θ is the diffraction angle at the position of the peak maximum. Strain is defined as the fractional change in length and the dislocation density as the length of dislocation lines per unit volume of the crystal, and it is measured from the following equation [14-16]

$$\varepsilon = \frac{\beta \cos \theta}{4} \tag{4.2}$$

$$\delta = \frac{1}{D^2} \tag{4.3}$$

4.6 Ultraviolet-Visible (UV-Vis) Near Spectroscopy

To understand why some compounds are colored and others are not, and to determine the relationship of conjugation to color, we must take accurate measurements of light absorption at different wavelengths in and near the visible part of the spectrum. Ultraviolet-visible spectroscopy or spectrophotometry refers to absorption spectroscopy or reflectance spectroscopy in the ultraviolet-visible spectral region. This is means it uses light in the visible and adjacent (near-UV and near-infrared (NIR) ranges. The absorption or reflectance in the visible range directly affects the perceived color of the chemical involved. In the region of the electromagnetic spectrum, molecules undergo electronic transitions. This technique is the complementary to fluorescence spectroscopy, in that fluorescence deals with transition from the ground state, while absorption measures transition from the ground state to the excited state [17]. UV-vis spectroscopy is routinely used in analytical chemistry for the quantitative determination of different analysis, such as transition ions, highly conjugated organic compounds and biological macromolecules.

4.6.1 Principle

Molecules containing π-electrons or non-bonding electrons (n-electrons) can absorb the energy in the form of ultraviolet or visible light excite these electrons to higher anti-bonding molecular orbitals. The more easily excited the electrons (i.e. lower energy gap between the HOMO and the LUMO) the higher the wavelength of light absorb. When white light falls upon a sample the light may be totally reflected, in which case the substance appears white/or the light may be totally absorbed in which case the appear black. If however, only a portion of the light is absorbed and the balance is reflected, the color of the sample is determined by the reflected light. Thus if violet is absorbed, the sample appears yellow-green and if yellow is absorbed the sample will appear blue. The color is described as being complementary. However, many substances which appear–colorless do have absorption spectra. On such, occasions, the absorption will

take place in the infrared or ultraviolet and not in the visible region. A close relationship exists between the color of the substance and its electronic structure. A molecules or ion will exhibits absorption in the visible or the UV region when radiation causes an electronic transition within its structure. Thus the absorption of light by a sample in the UV or visible is accompanied by change in electronic state of the molecules in the sample. The light energy supplied will promote electrons from their ground state orbitals to higher energy excited state orbitals or anti-bonding orbitals. Potentially three types of ground state orbitals may be involved;

1. σ (bonding) molecular orbital
2. π (bonding) atomic orbital

In additional, two types of anti-bonding orbitals may be involved in the transitions

1. σ^* (sigma star) orbital
2. π^* (pi star) orbital

(There is no such as an n* anti-bonding orbit as the n electron do not form bonds)

A transition in which a bonding σ electron is excited to an anti-bonding σ electrons is referred to as an σ-σ^* Transition. In the same way π- π^* represents the transition one electron of a lone pair (non-bonding electron pair) to an anti-bonding π orbital. Thus the following electronic transitions can occur by the absorption of ultraviolet and visible light. σ-σ^*, n-σ^*, n- π and π- π^*. Both σ-σ^* and n-σ^* transitions require a great deal of energy and therefore occur in the far ultraviolet region in the region 180-240 nm. Consequently, saturated groups do not exhibits strong absorption in the ordinary ultraviolet region. Transition of the n- $\pi^*$and π- π^* types occur in molecules with unsaturated centres; they require less energy and occur at longer wavelengths than transitions to σ^* anti-bonding orbitals. The wavelength of maximum absorption and the intensity of absorption are determined by molecules structures. Transition to σ^* anti-bonding orbitals which occur in the ultraviolet region for a particular molecules may well–take place in the visible region if the molecular structure is modified [18]. The reference beam intensity in the spectrophotometer travels from the light source to the detector without interacting with the sample. The sample beam interacts with the sample exposing it to ultraviolet light of continuously changing wavelength. When the

emitted wavelength corresponding to the energy level which promotes an electron to a higher molecular orbital, energy is absorbed.

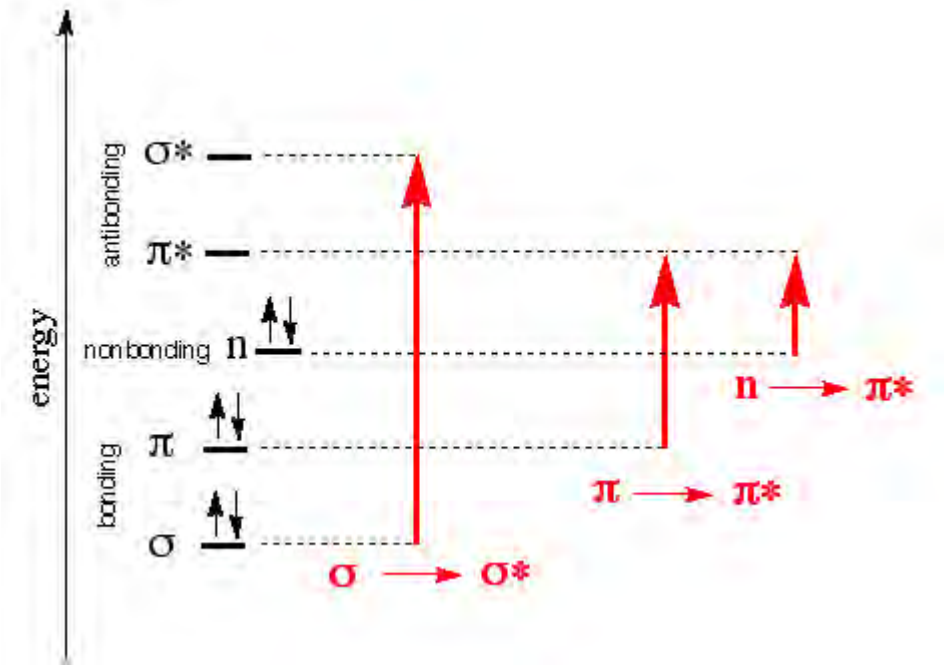

Fig. 4.5: Uv-visible absorption spectra [14].

The detector records the ratio between reference and sample beam intensities (I_0/I). The computer determines at what wavelength the sample absorbed a large amount of ultraviolet light by scanning for the largest gap between the two beams. When a large gap between intensities is found, where the sample beam intensity is significantly weaker than the reference beam, the computer plots in this wavelength having the highest ultraviolet light absorbance when it prepares the ultraviolet absorbance spectrum.

4.7 Optical Properties of Thin Films

Optical properties of films have been studied extensively primarily because of their applications in various optical and electro-optical device. The optical study of a solid concerns not only with the physical phenomena such as reflection, refraction, transmission, absorption, polarization, interference of light but also the interactions of photon energy with matter and the consequent changes in the electronic states [19].

4.7. 1 Absorption and Transmittance of Thin Films

When a semiconductor is illustrated by light, photon strikes the surface a function of photons is reflected and the remaining photon enters the semiconductor, some of these are absorbed within the semiconductor and the reminder transmitted into the semiconductor. The absorption of radiation by any medium occurs through the excitation of electrons and photons. For semiconductor, it is convenient to consider several types of absorption arising form

1. Electronic transition between different energy bands
2. Electronic transitions within any energy band
3. Electronic transition to localized states of impurity atoms
4. Lattice vibrations
5. Vibration of impurity atoms

The fundamental absorption region the transmission T is given by

$$T = \text{A exp } (\frac{4\,\pi kt}{\lambda}) \tag{4.4}$$

Where A is constant, k is the excitation co-efficient and t is the thickness. For $k^2 << n^2$, the principle variation of T occurs in the exponential term and pre-exponential term A. Therefore

$$T \approx \text{exp } (-\alpha t) \tag{4.5}$$

Where $\alpha = -\frac{4\pi k}{\lambda}$ is the absorption coefficient of the film. Thus the value of absorption coefficient may be calculated from the relation [21]

$$\alpha = \frac{\ln\frac{1}{T}}{t} \tag{4.6}$$

4.7.2 Direct and Indirect Optical Band Gap Semiconductor

If the maximum of the valance band and the minimum of conduction band energy exist for the same value of crystal momentum P in a semiconductor, then the semiconductor is called direct band gap semiconductor.

The form of the absorption process for a direct for a band gap semiconductor is shown in energy momentum of fig. 4.8. Since the momentum of photon small compared to the crystal momentum, the later essentially is converted in the transition. The energy difference between the initial and final state equal to the energy of the original photon.

$$\text{i.e. } E_f - E_i = h\vartheta \tag{4.7}$$

interms of parabolic band

$$\text{i.e. } E_f - E_c = \frac{P^2}{2m_c^*} \tag{4.8}$$

Therefore the specific value of crystal momentum at which the transition occur is given by

$$(E_f - E_i) - (E_c - E_v) = \frac{P^2}{2}\left[\frac{1}{m_c^*} + \frac{1}{m_n^*}\right] \tag{4.9}$$

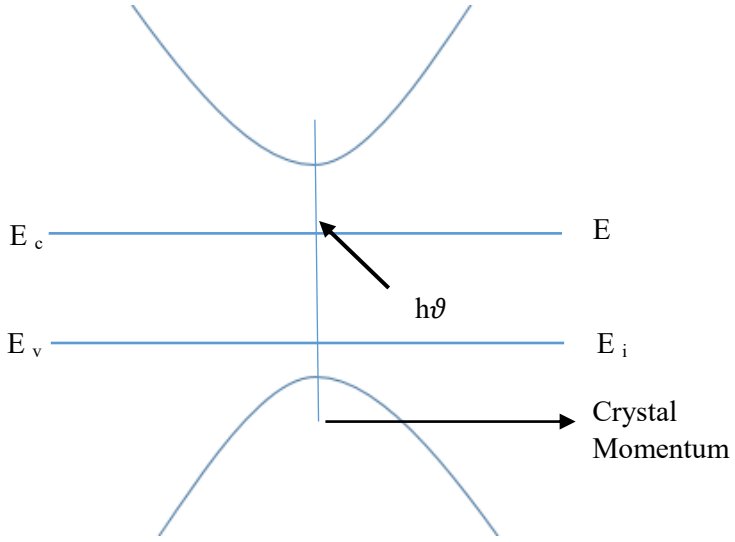

Fig. 4.6: Energy-crystal momentum of a direct band gap semiconductor.

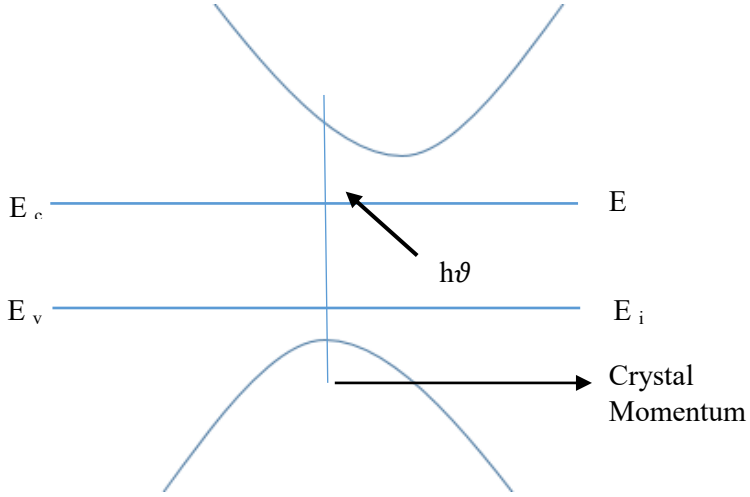

Fig. 4.7: Energy-crystal momentum of a indirect band gap semiconductor.

As the photon energy, hϑ increases, so does the value of the crystal momentum at which the transition occurs fig. 4.8. The energy from the band edge of both the initial

and the final states of also increases. The probability of absorption depends on the density of empty states at the final energy. Since both of these quantities increase with energy away from the band edges the absorption co-efficient increase rapidly with increasing photon energy above E_g. A simple theoretical treatment gives the results, as

$$\alpha\,(h\vartheta) \approx A^{*}\,(h\vartheta - E_g)^{2} \tag{4.10}$$

Where A^{*} is a constant having the numerical value of 2×10^{4} when α is expressed in cm $^{-1}$, $h\vartheta$ and E_g in electron volts (eV) [22].

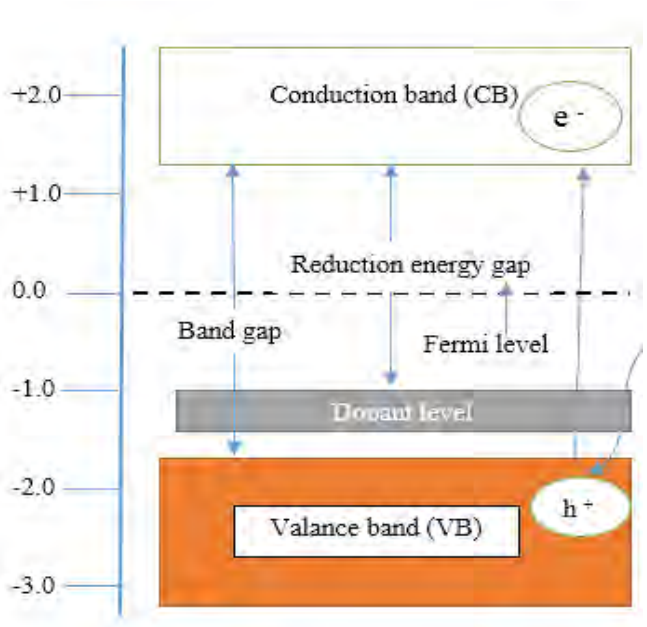

Fig. 4.8: Schematic plot of the theoretical band energy tuning alignment of the dopants level.

4.8 Fizeau Fringes Method

Weiner was the first to use interference fringes to measure film thickness. When two reflecting surfaces are brought into close proximity, interference fringes are produced, the measurement of which make possible a direct determination of film thickness and surface topography with high accuracy. In this method, two types of fringes are utilized for thickness measurement.

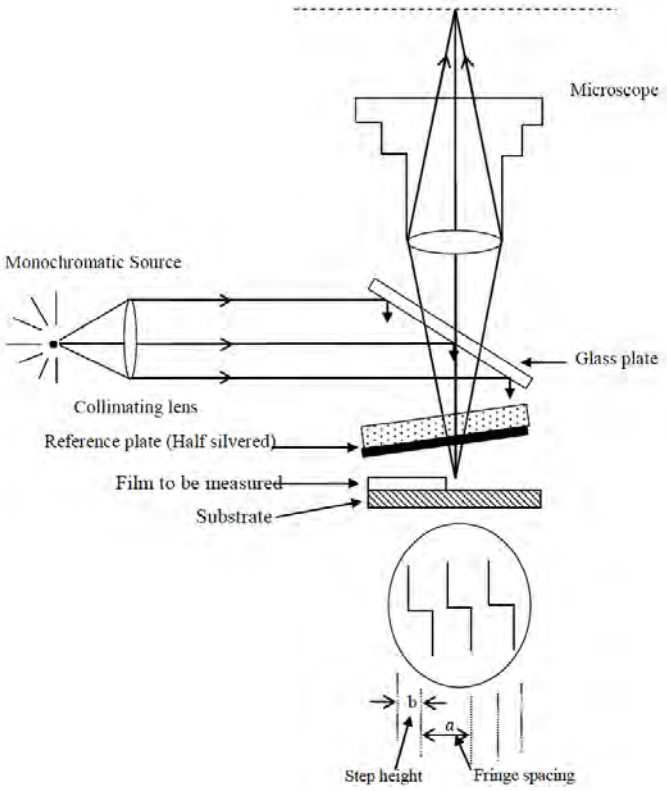

Fig. 4.9: Interferometer arrangement for producing reflection Fizeau fringes of equal thickness. [23].

The first produces Frzeu fringes of equal thickness, using a monochromatic light source. The second uses a white light source and produces fringes of equal chromatic order. To make the Fizeau fringes of equal thickness visible in a multiple beam interferometer formed by a thin absorbing film on a glass substrate. But if the experimental sample is transparent with a very smooth surface no such auxiliary coating is necessary.

This illuminated with a parallel monochromatic beam of light a fringes system as shown in fig. 4.9 is produced. The displacement „h" of the fringe system across the film substrate step is then measured to calculated the film thickness„t" usingthe relation

$$t = \frac{h}{frings-pacing} \times \frac{\lambda}{2} \tag{4.11}$$

Where λ be the wavelength of the monochromatic light employed. If the fringe spacing is „I" then we can written as

$$t = \frac{h\lambda}{2\,l} \tag{4.12}$$

4.9 Four-Probe Technique

Four- probe method is usually used for the determination of low resistivity. For this purpose four metal pins at equal distance D are pressed by springs against the semiconductor sample as shown in fig. 4.10. If the outside pins carry a current of intensity, I a voltage drop is measured between the inner probes of magnitude V.

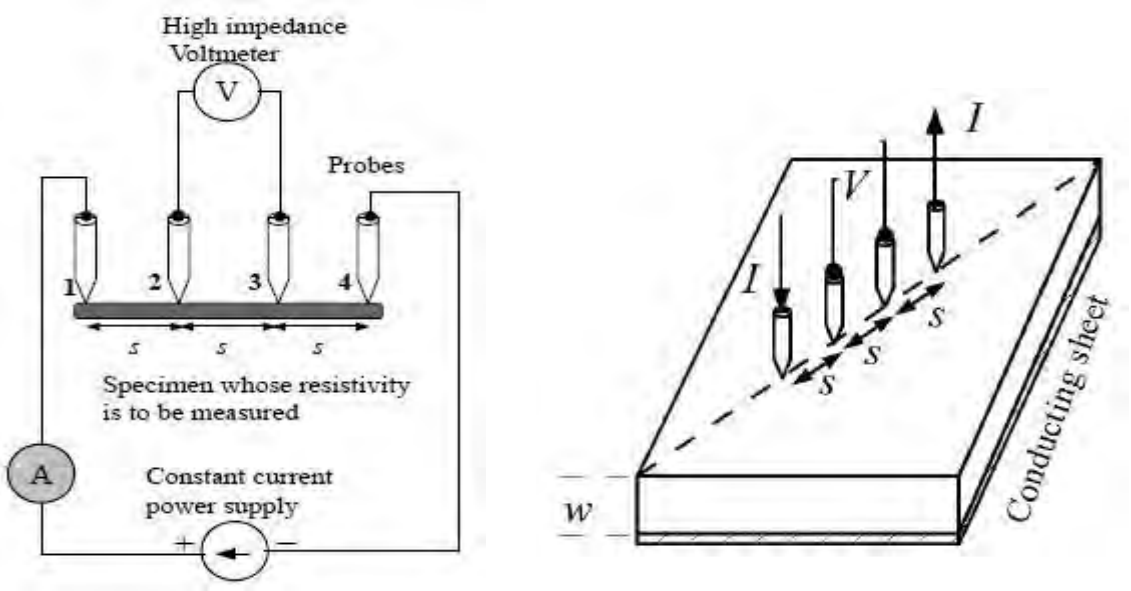

Fig. 4.10: Schematic diagram of four-point probe method [24].

At a constant temperature, the resistance, R of a conductor is proportional to the length L and inversely proportional to its area of cross-section A.

$$R = \rho \frac{L}{A} \tag{4.13}$$

A semiconductor has electrical conductivity intermediate in magnitude between that of a conductor and insulator. Semiconductor differs from metals in their characteristic property of decreasing electrical resistivity with increasing temperature. According to the band theory, the energy levels of semiconductors can be grouped into two band valance band and the conduction band. In the presence of an external electrical field it is electronic in the valance band that move freely, thereby by responsible for the electrical conductivity of semiconductors. In case of intrinsic semiconductor, the Fermi-level lies in between the conduction band minimum and valance band maximum. Since conduction band lies above the Fermi-level at 0k, when no thermal excitations are available, the conduction band remains unoccupied. So conduction is not possible at 0k,

and resistance is infinity. At temperature increase, the occupancy of conduction band goes up, thereby resulting in decrease of electrical resistivity of semiconductor [25].

Resistivity of semiconductor by four probe method

1. The resistivity of material is uniform in the area of measurement.
2. If there is a minority carrier injection into the semiconductor by the current-carrying electrodes most of the carriers recombine near electrodes so that their effect on conductivity is negligible.
3. The surface on which the probes rest is flat with no surface leakage.
4. The four probes used for resistivity measurement contact surface at points that lie in a straight line.
5. The diameter of the contact between metallic probes and the semiconductor should be small compared to the distance between the probes.
6. The boundary between the current carrying electrodes and the bulk material is hemispherical and small in diameter.
7. The surface of semiconductor material may be either conducting and non-conducting. A conducting boundary is one on which material of much lower resistivity than semiconductor has been plated. A non-conducting boundary produced when the surface of the semiconductor is in contact with insulator.

Fig. 4.10 shows the resistivity probes on a die of material. If the side boundaries are adequately far from the probes, the die may be considered to be identical to a slice. For this case of slice of thickness W and the resistivity is computed as

$$\rho = \frac{\rho_0}{f(\frac{W}{S})} \tag{4.14}$$

The function, f $(\frac{W}{S})$ is a divisor for computing resistivity which depends on the value of W and S. we assume the size of metal tip is infinitesimal and sample thickness is greater than the distance between the probes,

$$\rho_0 = \frac{V}{I} \times 2\pi S \tag{4.15}$$

References

[1] Huang, X., Guanghai, Li., Cao, B., Wang, M., and Hao, C., " Morphology Evolution and CL property of Ni-doped Zinc oxide nanostructures with Room-Temperature Ferromagnetism" *J. Phys. Chem. C*., vol. 113, pp. 4381-4385, 2009.

[2] Moutinho, H. R, Albin, D, Yan. Y, Dhere, Perkins. C., and Al-Jassim M. M., " A comparative study of CdS Thin Films Grown by Chemical-Bath Deposition and Close-Spaced Sublimation" Renewable Energy Lab., United States R. G. vol. 54, 2005.

[3] Lupan, O., Shishiyanu, S., Chow, and Shishiyanu, T., "Nanostructured zinc oxide gas sensors by successive ionic layer adsorption and reaction method and rapid photothermal processing" *Thin Solid Films,* vol. 516, pp. 3338-3345, 2008.

[4] https://en.wikipedia.org/wiki/Atomic-force -microscopy.

[5] Choudhury, M.G.M., Islam, M.R., Rahman, M. M., Hakima, M.O., Khana, M., K. R., Kaob, K. J., and Laib, G. R., "Preparation and characterization of ZeSe: Al thin films" *Acta Phys. Solv.,* vol. 54, pp. 417-425, 2004.

[6] http://www.qualitnano.eu/uploads/QNano-TA/ICN-XRay-Diffraction-%28XRD%29 pdf.

[7] http://nanoall.blogspot.in/2011/06/x-ray-technique-in-nanotechnology.html.

[8] http:/www. Intertek.com/analysis/materials/nano-research/xrd-brochure/.

[9] https://old.vscht.cz/clab/RTG/dokumenty/thermo/xrd/introduction%20to%20powder%20 diffraction.pdf.

[10] Babar, A.R., Kumbhar, S.B., Shinde. S.S., Moholkar, A.V., Kim, J. H., and Rajpur, K. Y., "Structural compositional and electrical properties of co-precipitated zinc stannate" *J. Alloy and comp*. vol. 509, pp. 7508-7514, 2011.

[11] Poole Jr. C. P., and Owens, F. J. (2003). Introduction to nanotechnology. John Wiley & Sons.

[12] Babar, A. R., Shine, S.S., Moholkar, A.V., Bhosale, C.H., Kim, J.H., and Rajpure, K. Y., "Structural and optoelectronic properties of antimony incorporated tin oxide thin films" *J. Alloy. Com.*, vol. 505, pp. 416-422, 2010.

[13] Samat., M.H., Adnan, N,. Taib, M.F.M., Hassan, O. H., Yahya, M.Z.A.,. and Ali, A.M.M., "structural, electronic and optical properties study of brookite TiO_2" *Solid state sci. and Tech.*, vol. 24, pp. 107-120, 2016.

[14] Abodurin, O.W., and Oluyamo,S. S., "Structural stability of nano-crystalline Aluminium-glass composite" IOSR-JAP, vol. 9, pp. 96-99, 2017.

[15] Sanjoy, C.D., Robert, J.G., Podder, J., Chang, Z.R., and Alexander, M., "Band gap tuning in ZnO through Ni doping via spray pyrolysis" *J. Phys. Chem. C.* vol. 117, pp.12745-12753, 2013.

[16] Motel, V.D., Purushtham, Y., and Dole, B.N., "Tuning optical properties of graphene oxide under compressive strain using wet ball milling method*" J. Ther. Appl. Phys*., vol. 6 pp. 2251-7235, 2012.

[17] https://textilestudycenter.com/x-ray-diffraction-method/

[18] Wang, Li. Y., Deng, J., Wu, Z., Sun, Yu, X., and Yang, D., "Bismuth nanotubes: a rational low-temperature synthetic route".*J. of Amer. Chem. Soc.* vol. 123, pp. 9904-9905, 2001.

[19] Anders, A. (Ed.). Handbook of plasma immersion ion implantation and deposition (Vol. 8). New York etc.: Wiley.

[20] Htttps://www.chemguide.co.uk/analysis/uvvisble/theory.html.

[21] Shimono D., Tanaka S., Torikai T., Watari T., and Murano M., " Preparation of transparent and conductive ZnO films using a Chemical Solution deposition process" *J. of Ceramic Prog. Res.,* vol. 2, pp. 184-188, 2001.

[22] Fouad El-Diasty "Application of Fizeau fringes with bending technique to determine the shear modulus of the cladding material of single-mode optical fibers through the mechanically induced change of refractive index", *optical Communication*, vol. 212, pp. 267-274, 2002.

[23] Reddy. T. S., and Kumar. M. C. S., "Co-evaporated SnS thin films for visible light photo-detector applications" *RSC Adv*., vol. 6, pp. 95680, 2016.

[24] Khan M. K. R., Rahaman M. A., Shahjahan M., Rahaman M. M., Hakim M. A., Saha D. K., and Khan J. U., " Effect of Al-doping on optical and electrical properties of spray pyrolysis nano-crystalline CdO thin films" *Current Appl. Phys.*, vol. 10, pp. 790-796, 2010.

[25] Fouad El-Diasty "Application of Fizeau fringes with bending technique to determine the shear modulus of the cladding material of single-mode optical fibers through the mechanically induced change of refractive index", *optical* Comm., vol. 212 , pp. 267-274, 2002.

CHAPTER-5

THEORETICAL STUDY

5.1 Introduction

The basic principles involved in the theoretical modeling will be discussed in this chapter, A detailed review of how such theoretical models are used for the verification of experimental results of TiO_2 based thin films will also be done.

5.2 First Principle Study at T= 0 (K)

The Latin term *ab*-initio "from the beginning" and is derived from the Latin *ab* ("from") + initio (beginning"). The most widespread method for calculating the ground state properties of periodic system is the *ab*-initio technique. In this method all results are based on solution of Schrodinger equation and the wave function used. No empirical data is used. It does not mean that we are solving the Schrodinger equation exactly. It means that we are selecting a method that in principle can lead to a reasonable a basis set that will implement that method in a reasonable way. When a given crystalline structure and chemical composition for any periodic system, the *ab*-initio method is used to calculate the physical and chemical properties of the system as accurately as possible without any need for a prior information [1]. In this method the fundamental approximation made is the expansion of the single particle wave function as a linear combination of Bloch functions defined in terms of local functions. The local functions are, in turn linear combination of Gaussian type functions (GTF) whose exponents and coefficient are defined by input [2]. The advantage of ab-initio methods is that they can be made to converge to the exact solution, when approximations are sufficiently small in magnitude. The convergence, however, is not monotonic, and sometimes the smallest calculation gives the best results for some properties. The disadvantage of *ab*-initio methods is their cost. They often take enormous amount of computer time. Memory and disk space.

5.3 Schrodinger Equation

Both density functional theory and wave function mechanics start with the formulation of the time-independent Schrödinger equation [3]

$$\hat{H}\Psi = \mathrm{E}\,\Psi \tag{5.1}$$

Where Ψ is the wave function, which contains all the information on the system described, $\widehat{H}$ is the Hamilton operator which operates on the wave function and present an output *E*, the total energy of the system, as it‟s Eigen value. There are several other operator available, for example for spin, electric dipole moments and so on. These can be used to obtain expectation values of physical observables from the wave function. The schrödinger equation appears relatively straight forward to solve but is in reality unsolved without approximations for non-hydrogenic systems. The most fundamental approximation is the Born-Oppenheimer (BO) approximation, which uncouple the motion of the nuclei in the system from the motion of the electrons [4]. The BO approximation states that any change in the position of the nuclei corresponds to an immediate restructuring of the electronic configuration, i.e. the nuclei are viewed as stationary at each geometry with respect to the motion of the electrons and the interactions between electronic configurations, i.e. the nuclei are viewed as stationary at each geometry with respect to the motion of the electrons and the interactions between electron-nucleus and the nuclear kinetic energy can more readily be evaluated.

5.4 Born Oppenheimer Approximation

The Born-Oppenheimer Approximation is the assumption that the motion of atomic nuclei approximation can be separated [5]. In mathematical terms, it allows the wave-function of a molecules to be broken into it‟s electronic and nuclear (vibrational, rotational) components. Computation of the energy and the wave function of an average size molecule is simplified by the approximation. Since, the motion of the nuclei and electron can be separated; the electronic and nuclear problems can be solved with independent wave functions. When the nuclei assumed as stationary then the Coulomb interaction between the nuclei is constant. Therefore, the final terms can be omitted. In solving the Schrodinger equation and added later as a constant to the total energy. This separation of electronic and nuclei problems is known as the Born Oppenheimer Approximation.

5.5 Hartree and Haree-Fock (HF) Methods

In computational physics, the Hartee-Fock method is an approximation method for the determination of the ground states wave function and ground-state energy of a quantum many-body system. The Hartree-Fock method is also called, especially in the order literature, the self-consistent field method (SCF). The goal of this method is similar to

that of the vibrational method. Since there are no known solutions for many-electron systems, then the problem is solved numerically. This method treats the problem of many electron system in which the wave function for the system is represented as the product of Z single electron wave function. Each one of these wave functions is determined as a solution of Schrodinger equation (SE) in the field of the nucleus and the average electron distribution of the electrons in the other wave functions must be the same as the field used in evaluating these wave functions. This aspect led to the term "SCF" for the atomic field so determined. The Hartree-Fock method finds its typical application in the solution of the Schrödinger equation for atoms, molecules, nanostructures [6] and solid but it has also found widespread used in nuclear physics. In atomic structure theory, calculations may be for a spectrum with many excited energy levels and consequently the Hartree-Fock method for atoms assume the wave function is a single configuration state function with well-defined quantum numbers and that the energy level is not necessarily the ground state [6].

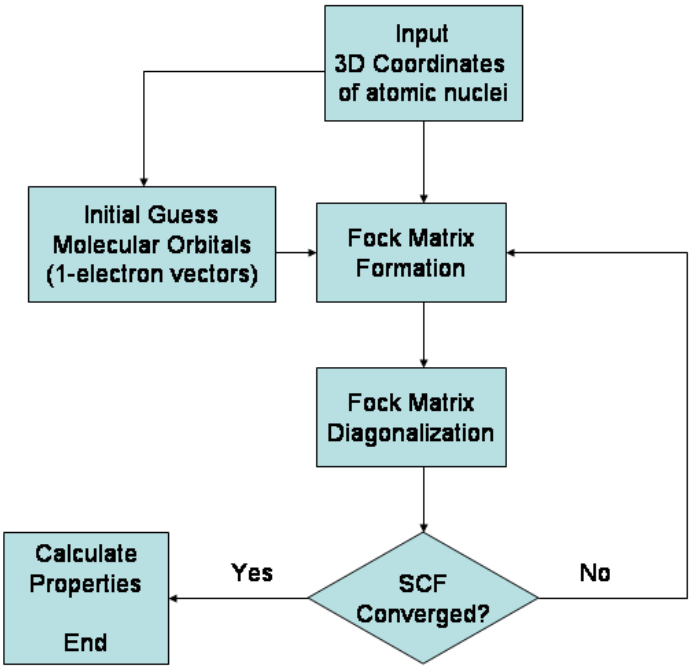

Fig. 5.1: Algorithmic flowchart illustrating the Hartree-Fock method [4].

5.6 Density Functional Theory

Density functional theory (DFT) is an alternating type of *ab-inito* method. In physics and chemistry, this method is a quantum mechanical theory used to investigate the electronic structure (principle the ground state) of many body systems, particularly atoms, molecules and the condensed phases and which is the spatially dependent electron density. The success of density functional theory not only encompasses standard bulk materials but also complex materials such as proteins. The main idea of density functional theory is to describe an interacting system of fermions via its density and not via its many-body wave function. For N electrons in a solid, which obey the Pauli principle and repulse each other via Coulomb potential, this means that the basic variable of the system depends only on the three spatial coordinates x, y, and z rather than $3N$ degrees of freedom. Density Functional (DF) techniques are based on two theorems, proved by Hohenberg and Kohn in 1964 [7], and on a computational scheme proposed by Kohn and Sham (KS) the following years [8]. They showed that the total energy is a functional of the electron density. This means that one does not need to know the complicated many-electron wave function; but only the electron density, which is the key quantity in density functional theory.

5.7 Local density of Approximation (LDA)

The local density approximation (LDA) is a simple physical approximation of the exchange-correlation energy, which does not require any empirical parameter, being based on the exact quantum Monte Carlo calculation of the exchange-correlation energy terms, and it has to be approximated. One widely used approximation is the local density is slowly varying, the exchange correlation energy at that point can be considered the same as that for a locally uniform electron gas of the same charge density in the case we can write E_{xc} as

$$E_{xc}^{LDA}[\rho] = \int \rho\,(\mathrm{r})\,\varepsilon_{xc}\,[\rho\,(\mathrm{r})]\,\mathrm{dr} \tag{5.2}$$

Khon and Sham [9] gives this expression of exchange correlation energy. They also introduced the local spin density approximation (LSDA) where the spin polarization is allowed and the exchange correlation energy becomes a functional of the local electron-spin densities.

LDA depends only upon the value of electron density but not on the gradient of electron density. Although this approximation is extremely simple, it is surprisingly accurate,

and forms the core of most modern DFT code. It even works reasonably well in systems where the charge density is rapidly varying.

5.8 Generalized Gradient Approximation (GGA)

Many modern codes using DFT now use more advanced approximations to improve accuracy for certain physical properties. The DFT calculations in this study have been made using the generalized gradient approximation (GGA). The generalized gradient approximation is more efficient than local density approximation. The exchange-correlation energy for the uniform electron gas at every point in the same system is not regarded to the homogeneity of the real charge density by using LDA. For non-uniform charge densities the exchange-correlation energy can deviate significantly from the uniform result. This deviation can be expressed in terms of the gradient and higher spatial derivatives of the total charge density. The GGA uses the gradient and higher spatial derivatives of the total charge density. The GGA uses the gradient of the charge density to correct for this deviation. Thus it is able to yield the more appropriate results and the exchange-correlation energy E_{xc} is a function of the spin density and their gradient [10]:

$$E_{xc}^{GGA}[\rho\uparrow, \rho\downarrow] = \int \rho\,(\mathrm{r})\, \varepsilon_{xc}\,[\rho\uparrow(\mathrm{r}), \rho\downarrow(r), \nabla_{\rho}\uparrow(r), \nabla_{\rho}\downarrow(r)]\,\mathrm{dr} \tag{5.3}$$

The purpose of introduction of GGA is to improve the quality of LDA results significantly.

5.9 Pseudo potential

In physics, a Pseudo potential or effective potential is used as an approximation for the simplified description of complex systems including especially atomic physics and neutron scattering. The Pseudo potential approximation was first introduced by Hans Hellmann in the 1930s. The Pseudo potential is an attempt to replace the complicated effect of the motion of the core electron of an atom and its nucleus with an effective potential or Pseudo potential so that the Schrödinger equation contains a modified effective potential term instead of the Columbic potential term for core electron normally found in the Schrödinger equation. The Pseudo potential is constructed to replace the atomic all-electron potential such that core states are eliminated and the valance electrons are described by modeless pseudo-wave functions.

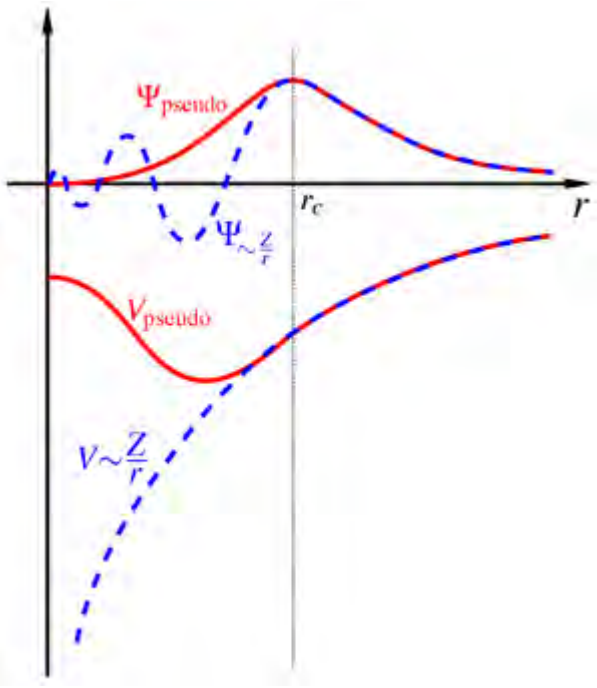

Fig. 5.2: A schematic illustration of the all-electron and pseudized wavefunction and potentials [11]

5.1.0 K-points and Cut off Energy Sampling

In reciprocal space, the phases are nodes or points in the unit cell, which are described by sampling the Brillouin zone (BZ). The BZ describes the unique region of space closest to the G=0 point onto which all other points can be mapped by periodicity, therefore by sampling the BZ, the entirety of the bulk sampled. The change in energy when sampling k-points determines how many of them need to be sampled, that is an energy convergence test is carried out using an increasing number of k-points, in a similar method to the cut-off energy convergence test. In a crystal of high symmetry, the number of k-point is reduced by symmetry operations where girds of sampling points such as the Monkhurst-pack gird, are formulated by the generation of periodic function based on point group symmetries. Efficient k points sampling reduces the computational time required as it reduces the number computations, there is highly beneficial to determine the symmetry of the unit cell to produce a primitive cell and thus the smallest number of k-points. The basis set, as defined by the energy cut off value, is one of the most important parameters that determine the accuracy of CASTEP calculation [12].

5.11 CASTEP Code

CASTEP is a commercial software package which uses density functional theory with a plane wave basic set to calculate electronic properties of solids, surfaces, molecules, liquids and amorphous material from first principles. CASTEP permits geometry optimization and finite temperature molecular dynamics with implicit symmetry and geometry constraints, as well as calculation of a wide variety of derived properties of the electronic configuration. CASTEP has been completely written for use on parallel computer by research at the University of York, durham, St. Andrews, Cambridge and Rutherford Labs. “CASTEP” (Cambridge Serial Total Energy Package), originally written in the late 1980‟s and early 1990‟s [13] by Mike Payne and co-workers at Cambridge University. The CASTEP program [15, 13] is a first-principles quantum mechanical code for performing electronic structure calculations. It is based on density function theory (DFT), density-Functional Perturbation Theory (DFPT), plane wave basis set and Pseudo potentials (both norm-conserving and ultra-soft). Within density functional formalism it can be used to simulate a wide range of materials including crystalline solid, surface, molecules, liquids and amorphous materials; the properties of any material that can be thought of as an assembly of nuclei and electrons can be calculated with the only limitation being the finite speed and memory of the computers being used.

5.12 Ground State Energy

The ground state of a quantum-mechanical system is its lowest energy states; the energy of the ground state is known as the zero-point energy of the system. An excited is any state with energy greater than the ground state. In the quantum field theory, the ground state is usually called the vacuum state. If more than one ground state exists, they are said to be degenerate. Many systems have degenerate ground states. Degeneracy occurs whenever there exists a unitary operator that acts non-trivially on a ground state and commutes with the Hamiltonian of the system. For obtaining a stable structure of a 3D periodic system the CASTEP Geometry Optimization task allows one to refine the geometry [11]. An iterative process is used to perform this task in which the cell parameters and the coordinates of the atoms are adjusted provided that the total energy of the system is minimized. This minimized total energy is the ground states energy of the system [11]. In the field of computational chemistry, energy minimization (Also

called energy optimization or geometry optimization) is the process of finding an arrangement in space of a collection of atoms where, according to some computational model of chemical bonding, the net inter-atomic force on each atom is acceptably close to zero and the position on the potential energy surface is a stationary point [11]. The collection of atoms might be an ions, a single molecules, a transition states, a condensed phase or even a collection of any these. In this case, quantum mechanics might be the computation model of chemical bonding. The geometry of set atoms can be described by a vector of the atoms position [16]. This could be the set of Cartesian coordinates of the atoms. When considering molecules, this might be so called internal coordinates formed from a set of bond length, bond angle and dihedral angles [11].

5.13 Computation at Different Properties

Cambridge Serial Total energy Package (CASTEP) code [17] based on the plane-wave Pseudo potential density functional theory (DFT) [18–20] is used to investigate the ground state physical properties, namely structural parameters, electronic and mechanical properties of Al doped and (Al, Co) co-doped TiO_2 thin films samples. The interactions between the ion cores and valence electrons are described by Vanderbilt-type ultra-soft pseudo-potential [21]. The energy due to electronic exchange and correlation has been estimated using the generalized gradient approximation with the Perdew-Burkey-Ernzerhof functional [22]. The crystal structure is completely optimized through minimizing the total energy, internal forces and external stresses varying both the lattice parameters and internal coordinates concurrently using Broyden-Fletcher-Goldfarb-Shanno (BFGS) algorithm [22]. The theoretical calculations of the transition metal Al doped and (Al, Co) TiO_2 thin films were simulated using first-principles calculation the supercell approach. For putting impurities in TiO_2 a super-cell having size 8 times the unit cell of the pristine sample is constructed as shown figure 1. The impurities are inserted in pure TiO_2 by Al and (Al, Co) atoms (Substitution doping) which corresponds to doped and co-doped. As a result, the new chemical formula of TiO_2 can be written as Ti_{1-x} Al $_x$ O_2 in mono-doping structure. Another, the chemical formula can be written as $Ti_{1-x}Al_xCo_yO_2$ as co-doped structure.

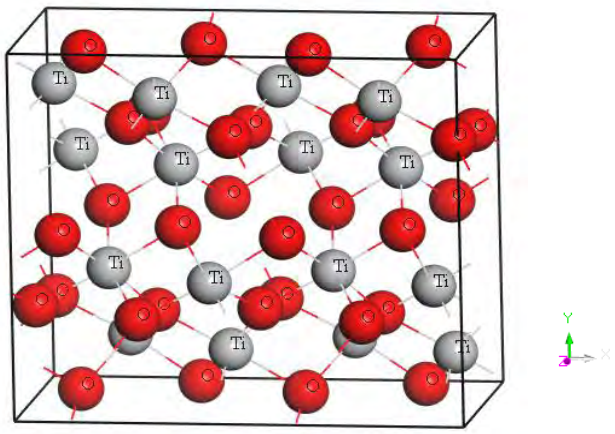

Fig. 5.3: The crystal structure of pristine (2× 1 × 1) supercell of TiO_2 thin film samples

Firstly, the unit cell is modeled using VCA method within the code for adding Al in TiO_2 (mono-doping) and another (Al, Co) in TiO_2 (co-doped) [22]. This method allows us to mix different atoms, isotopes and oxidation states for a particular atomic position to be occupied randomly. The VCA method has already become successful for describing the disorder in some silicates and perovskites [22]. Any possible short range order is not considered in this approach. Every potentially disordered site is assumed to be occupied with a virtual atom, which interrupts between the behaviors of the actual components. The VCA method overlooks the local distortions around the atoms and consequently, no finer details of the disordered structures can be expected to reproduce with sufficient precision**.**

Within the CASTEP code**,** the elastic constants C_{ij} are determined by using the finite-strain theory [23, 24]. In which a given set of homogeneous strains (deformations) is applied to the conventional unit cell tolerating the atomic degrees of freedoms to relax. Then the resultant external stresses are evaluated. Stress tensor has six stress components σ_{ij} for each strain δ_j applied to the unit cell. The elastic tensors C_{ij} are then obtained by solving a set of linear equations as follows [25]

$$\sigma_{ij} = \sum_{ij} C_{ij}\delta_j \tag{5.4}$$

The bulk modulus B and shear modulus G are then determined from C_{ij} using the well-established Voigt–Reuss–Hill (VRH) approximations [26–28]. The Young's modulus E and Poisson's ratio v are also calculated from the following equations [29]

$$E = \frac{9BG}{3B + G} \tag{5.5}$$

$$v = \frac{3B - 2G}{6B + 2G} \tag{5.6}$$

The bulk modulus and shear modulus are reduced to [29]

$$B = \frac{1}{3}(C_{11} + 2\,C_{12}) = \frac{5}{9}C_{11} \tag{5.7}$$

and

$$G = \frac{1}{3}C_{11} \tag{5.8}$$

For specific case of orthorhombic lattices, the Voigt shear modulus G_V and Voigt bulk modulus (B_V) are

$$G_V = \frac{1}{15}(C_{11} + C_{22} + C_{33} - C_{12} - C_{13} - C_{23}) + \frac{1}{5}(C_{44} + C_{55} + C_{66}) \tag{5.9}$$

$$B_V = \frac{1}{9}(C_{11} + C_{22} + C_{33}) + \frac{2}{9}(C_{12} + C_{13} + C_{23}) \tag{5.10}$$

Using energy considerations Hill proved that the Voigt and Reuss equations represent upper and lower limits of true polycrystalline constants, and recommended that a practical estimate of the bulk and shear moduli were the arithmetic means of extremes.

References

[1] Islam, F.N., Ph.D thesis. Department of physics, University of Rajshahi, Rajshahi, Bangladesh (2002).

[2] Saunders, V.R., Dovesi, R., Roetti. C., Causa, M., Hartsion, N.M., Orlando, R., Zicovich, C.M., CRYSTAL98 user‟s Manual, 1998.

[3] Schrödinger, E., "Quantisierung als eigenwertproblem," *Annalen der physic*, Vol. 385, pp. 13 1962.

[4] Born, M., Oppenheimer, R., "The genesis of the quantum theory and chemical bonding" *Annalen der physic* 1927.

[5] "Born-oppenheimer Approximation," Wikipedia, Wikimedia Foundation, 15 Jan.2019.

[6] "Hartree-Fock Method."Wikipedia, Wikimedia Foundation, 28 June 2018. En.wikipedia.org/wiki/Hatree%E2%80%93Fock-method.

[7] Hohenberg, P., Kohn, W., "Density functional theory study of exohedral carbon atoms effect on electrophilicity of nicotine: comparative analysis" *Phys. Rev. B*, Vol. 136, pp. 864 (1964).

[8] Kohn, W., Sham, L.J., "Self-consistent equation of including exchange and correlation effects" *Phys. Rev. A*, Vol. 140, pp. 1133, (1965).

[9] http://en.wikipedia.org/wiki/pseudopotential.

[10] Pisani, C., "Lecture Notes In Chemistry (Quantum-Mechanical *Ab-inito* Calculation of the Properties of Crystalline Materials) Springer-Verlag, Heidelberg, Vol. 67 (1996).

[11] Hadi, M.A., "First-principles study of superconducting Max phase, M. Phi. Thesis, Department of Physics, University of Rajshahi, 2015.

[12] http://cmt.dur.ac.uk/sjc/thesis_dlg/node26.html

[13] Hohenberg, P., Kohn, w., "Inhomogeneous electron gas" *Phys. Rev. B*, Vol. 136, pp. 864, 1964.

[14] Kohn, W., "Density functional and density matrix method scaling linearly with the number of atoms", *Phys. Rev. Lett*. Vol. 76, pp. 3168, 1965.

[15] http://en. Wikipedia.org/wiki/pseudo-potential.

[16] Islam, M.N., "Physical properties of Mn_2CoX (X= Al, Si, Sb) (Structural properties, Electronic properties, Elastic properties, Perovskite properties, Charge

density, Fermi surface, Debye temperature and optical properties" Department of Physics, Pabna University of Science and Technology, Pabna, Bangladesh.

[17] Clark S J, Segall M D, Pickard C J, Hasnip P J, Probert M I J, Refson K and Payne M C 2005 *Z. Kristallogr*. 220 567

[18] Martin R 2004 *Electronic Structure: Basic Theory and Practical Methods* (Cambridge, Cambridge University Press).

[19] Nasir, M.T., Hadi, M.A., Naquib, S.H., Farvin, F., Zirconium metal-based Max phses Zr_2AC (A=Al, Si, P and S): *A frist principle calculation*" Vol. 29, pp. 1550022, 2015.

[20] Kholil, M.I., Ali, M.S., Aftabuzzaman, M., "Structural, elastic, electronic and vibrational properties of $BaRh_2P_2$ and $SrLr_2As_2$ superconductors: DFT study" *J. alloy and coms.* Vol. 740, pp. 754-765, 2018.

[21] Hadi, M.A., Rayhan, M.A., Naqib, S.H., Chroneos, A., Islam, A.K.M.A., "Structural, elastic, thermal and lattice dynamic properties of new 21 Max phases" *Com. Mater. Sci.* 2019.

[22] Roknuzzaman, M., Jose, A. A., Hongxia, W., Aijun, A., Tuquabo, T., "*Ab* initio atomistic insights into lead-free formamidinium based hydrid perovskites for photovoltaic and optoelectronic" *Com. Mater. Sci.* Vol. 169, pp. 109118, 2019.

[23] Winkler, B., Pickard, C.J., Milman, V., "Applicability of a quantum mechanical virtual crystal approximation to study Al/Si-disorder" *Chem. Phys. Lett*. Vol. 362, P. 266, 2002.

[24] Ramer, N.J, Rappe, A.M., "Virtual-crystal approximation that works: locating a compositional phase boundary in Pb $(Zr_{1-x}\,Ti_x)O_3$" *Phys. Rev. B, Vol.* 62, pp. 743, 2000.

[25] Murnaghan F D 1951 *Finite Deformation of an Elastic Solid* (New York, Wiley).

[26] Voigt W 1928 *Lehrbuchder Kristallphysik* (Leipzigund Berlin, Teubner).

[27] Reuss A 1929 *Z. Angew. Math. Mech*. 9 49.

[28] Hill, R., "Elastic behaviour of a crystalline aggregate" *Proc. Phys. Soc. A*, Vol. 65, pp.349, 1952.

[29] Hadi, M. A., "New ternary nanolaminated carbide Mo_2Ga_2C: Frist principle comparison with the Max phase counterpart Mo_2GaC" *Comp. Mater. Sci*., Vol. 117, pp. 422, 2016.

[30] behavior of a crystalline aggregate" phys. Soc. London, Vol. 65, pp. 350, 1952.

CHAPTER-6
RESULTS AND DISCUSSION

6.1 Introduction

The results obtained from different experimental measurements of the Al doped and (Al, Co) co-doped TiO_2 thin films have been provided in this chapter. The possible explanations and discussion of the results of studied samples have been given in this section.

6.2 Sample Preparation Procedure for Characterization

- Cutting the glass substrate 2.5 cm × 2.5 cm.
- Cleaning the glass substrate by acetone and de-ionized water in ultrasonic bath and drying.
- A suitable mask was put on the substrate at a particular temperature 450 $^{\circ}$ C, controlled by variac.
- The distance between the tip nozzle and the substarte was kept 25 cm.
- Passing the compressed air at constant pressure through pipe and at the same time pass the liquid solution through the spray nozzle.
- A fine aerosol was produced and finally desired film was deposited on the heated substrate.
- Finally crack free uniform films is used at different characterization.

6.3 Scanning Electron Microscopy

Scanning electron microscopy is a convenient technique widely used to obtained surface morphological information of the thin films. Surface morphology of pristine, Al doped and (Al, Co) co-doped TiO_2 thin films on glass substrate were studied by scanning electron microscopy (SEM). Figure (6.1 and 6.2) shows the surface morphology of as deposited TiO_2, Al doped and (Al, Co) co-doped TiO_2 thin films 10,0000X magnifications respectively. The films were found uniform and well covered on the glass substrate. The pure TiO_2 thin films SEM image have clustered collapsed particle shape [1].

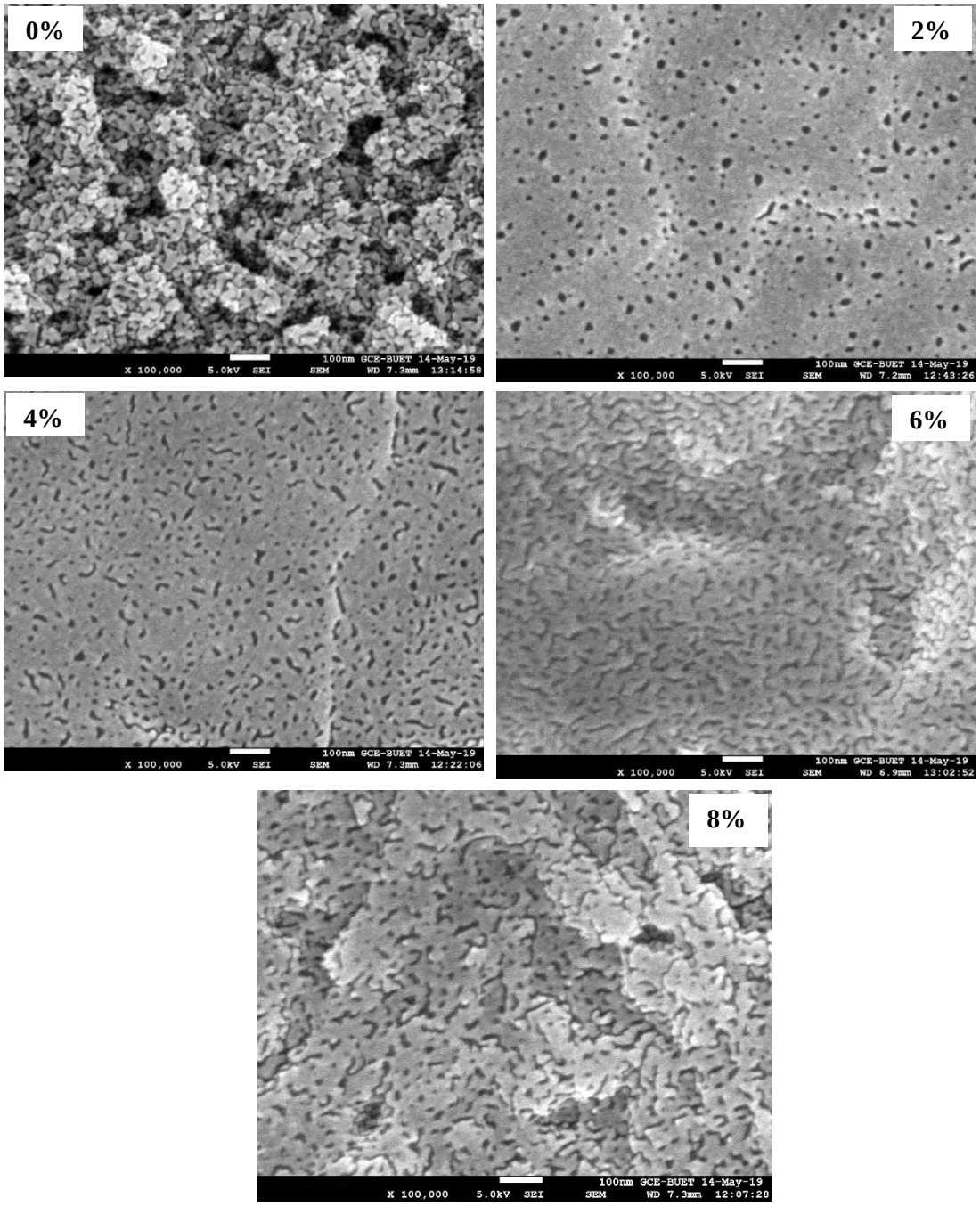

Fig. 6.1: Scanning electron microscopy (SEM) image of pristine and Al doped TiO_2 thin film samples.

Table 6.1: The pore classification by the IUPAC according to the size [3].

Pore width (nm)	Types of pore	This experimental
≤ 2	Micropores	
2-50	Mesopores	Mesopores
>50	Macropores	

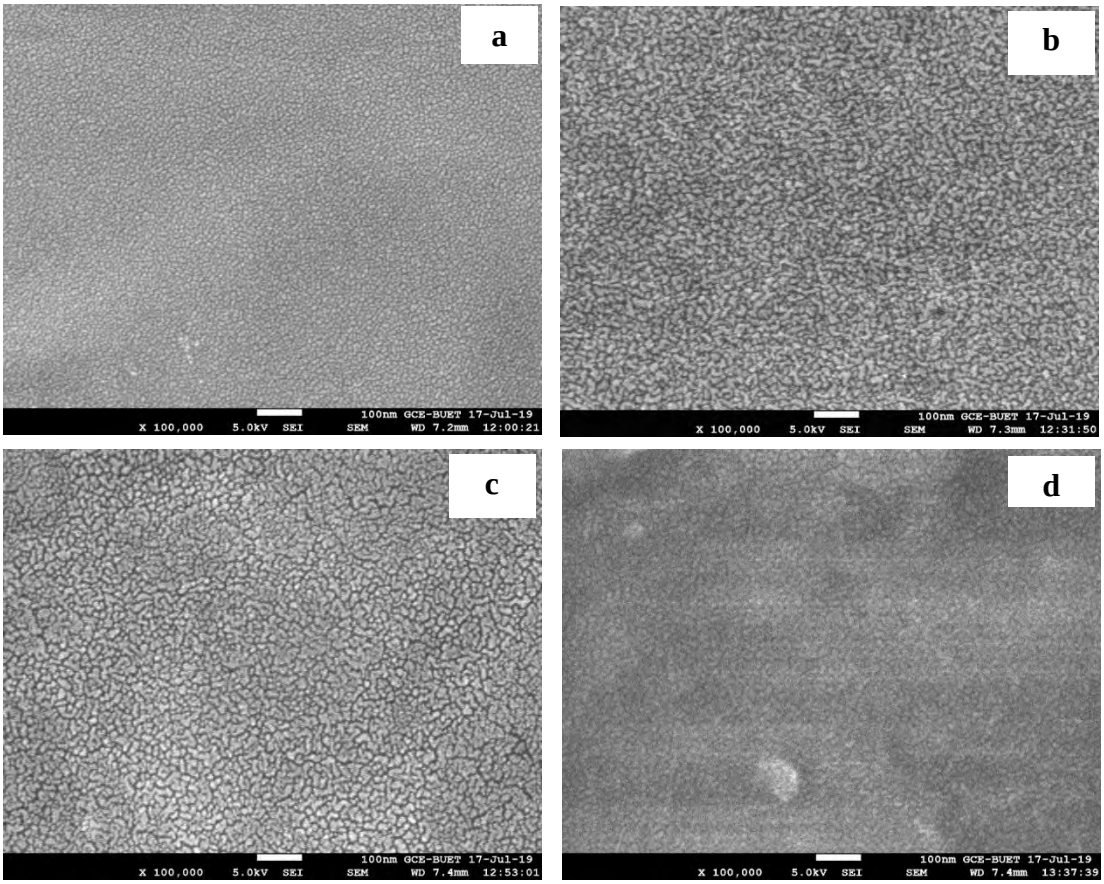

Fig. 6.2: Scanning electron microscopy image of (a) 1% Co, 6% Al, (b) 2% Co, 6% Al, (c) 3% Co, 6% Al and (d) 4% Co, 6% Al co-doped TiO_2 thin film samples.

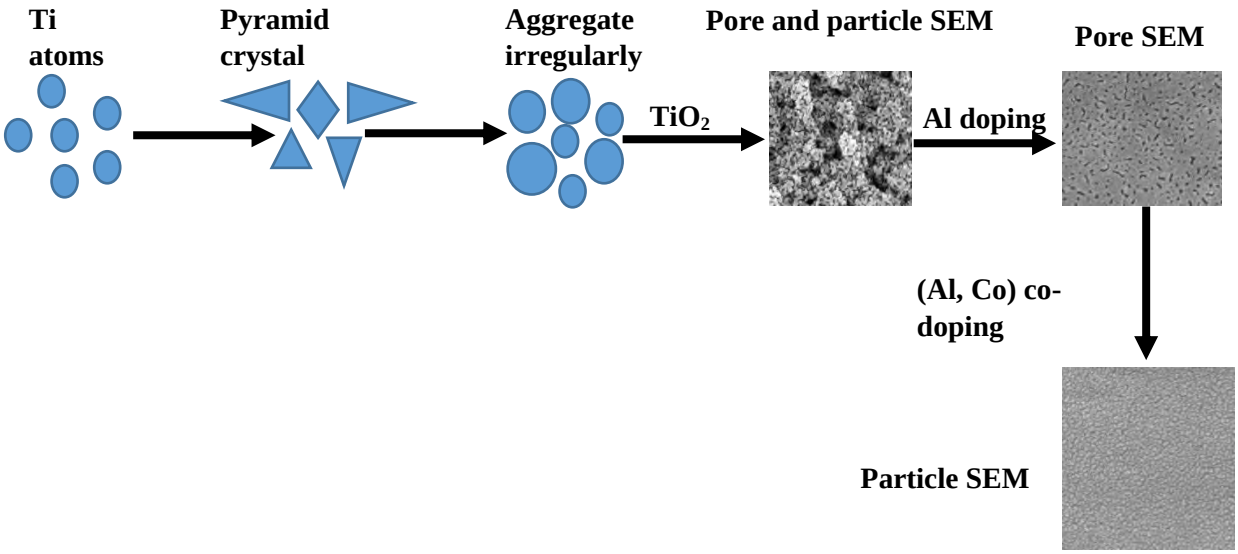

Fig. 6.3: A schematic diagrams of formation pore and particle shaped.

The particles shape distribution are non-uniform and diameters of a particle around 42 nm. The average primary particle size of the bimodal distribution at the films surface

around 42 nm to 50 nm. Al doped samples are pore structure with diameter around 6 nm to 9 nm. Particle and pore diameters were measured by image J software. After Al doping all of the samples reduces particle shaped owing to incorporation of dopants the TiO_2 lattice networks. Al is a low melting metal compare to TiO_2 nanoparticles, in the case Al is melted after doping. Non-uniform pyramidal particle filled by melted Al nanoparticle, obtain to porous structure in studied samples. It is seen in the SEM images that the pore diameter decreases with increasing doping concentration compared to a pristine sample. The pore shape image, indicating that the samples are absorbed in different types of gas molecules. As a consequence, we assume that our samples may be suitable for gas sensing purposes [2].

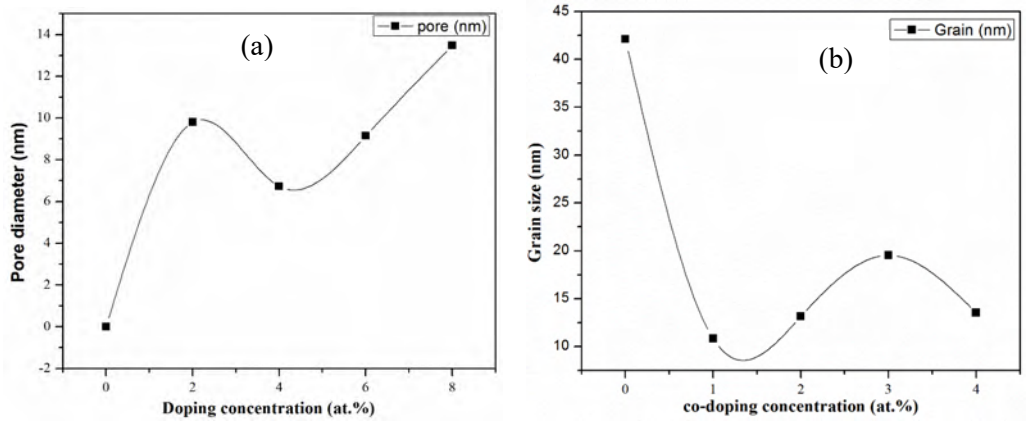

Fig. 6.4: Variation of (a) pore size and (b) grain size as a function of doping and co-doping content.

Al doped TiO_2 has shown the porous morphology, which is mostly important of physical adsorption of gas molecules. The crystalline, crystal size and porosity are three most important parts that affect the gas sensitivity of metal oxide thin films device. The pristine and (Co, Al) co-doped samples have nano-particle shapes images. The co-doped all samples are uniform and grain boundary range 10∼19 nm.The grain boundary are listed in figure 6.3. In the case of co-doped samples, the grain boundary gradually increases with the dopant concentrations. The 1% co-doped samples have minimum grain 10 nm, implies that the films enable more controllable carrier densities.

6.4 Compositional Studies

The element composition and chemical states of Al doped and (Al, Co) co-doped TiO_2 thin films samples under study was analyzed by energy-dispersion analysis x-ray spectroscopy (EDAX). The presence of Ti, O, Al and Co can be observed from fig. 6.5, 6.6 and 6.5. The atomic percentage of Al increase from 0 to 8 as for Al doped TiO_2 thin films samples respectively In the case of co-doped TiO_2 samples Al is fixed 6% which is the optimize percentage and Co is change 1 to 4 percentage. The results obtained in this research shows that the films of Al doped and (Al, Co) co-doped TiO_2 samples are stoichiometric. The presence of Si and other elements are present may come from the glass slide used but we are omitted the Si in the EDAX spectra [4]. The O_2 peak detected from the EDAX spectra is unavoidable in any chemical deposited thin films. The incorporation of the dopants in the TiO_2 lattice and their compositional homogeneity have been confirmed by means of EDAX spectra.

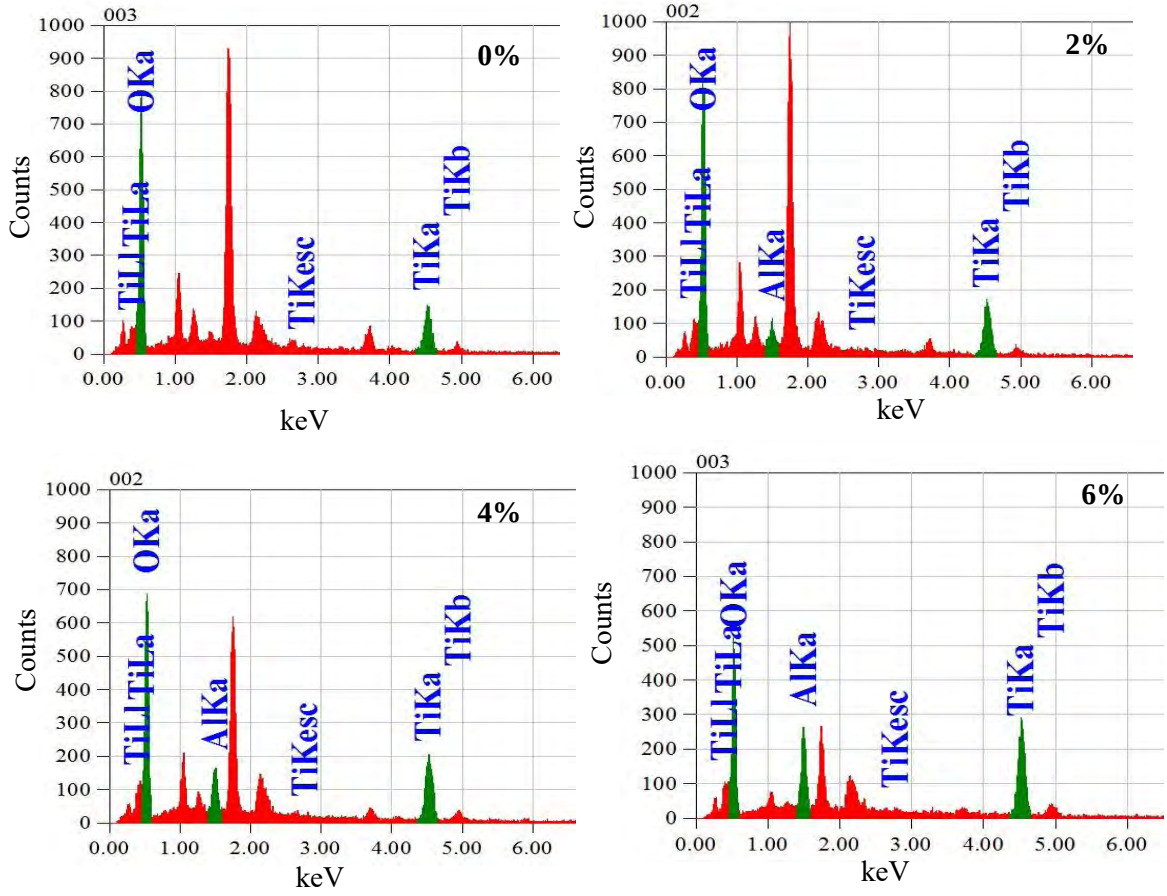

Fig. 6.5: Energy-Dispersion Analysis spectra of Al doped TiO_2 thin film samples at different concentration.

The element analysis atomic percentages are tabulated in table 6.2. The EDX spectra are good agreements in the previous EDX spectra [5]. No trace we are found in our samples.

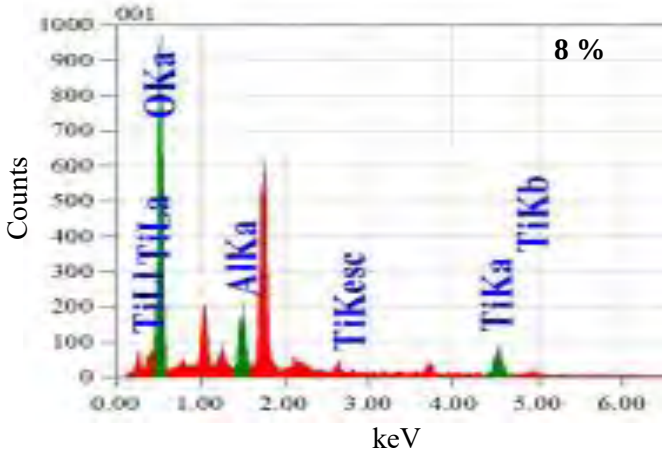

Fig. 6.6: Energy-Dispersion Analysis spectra of 8% Al doped TiO_2 thin film sample.

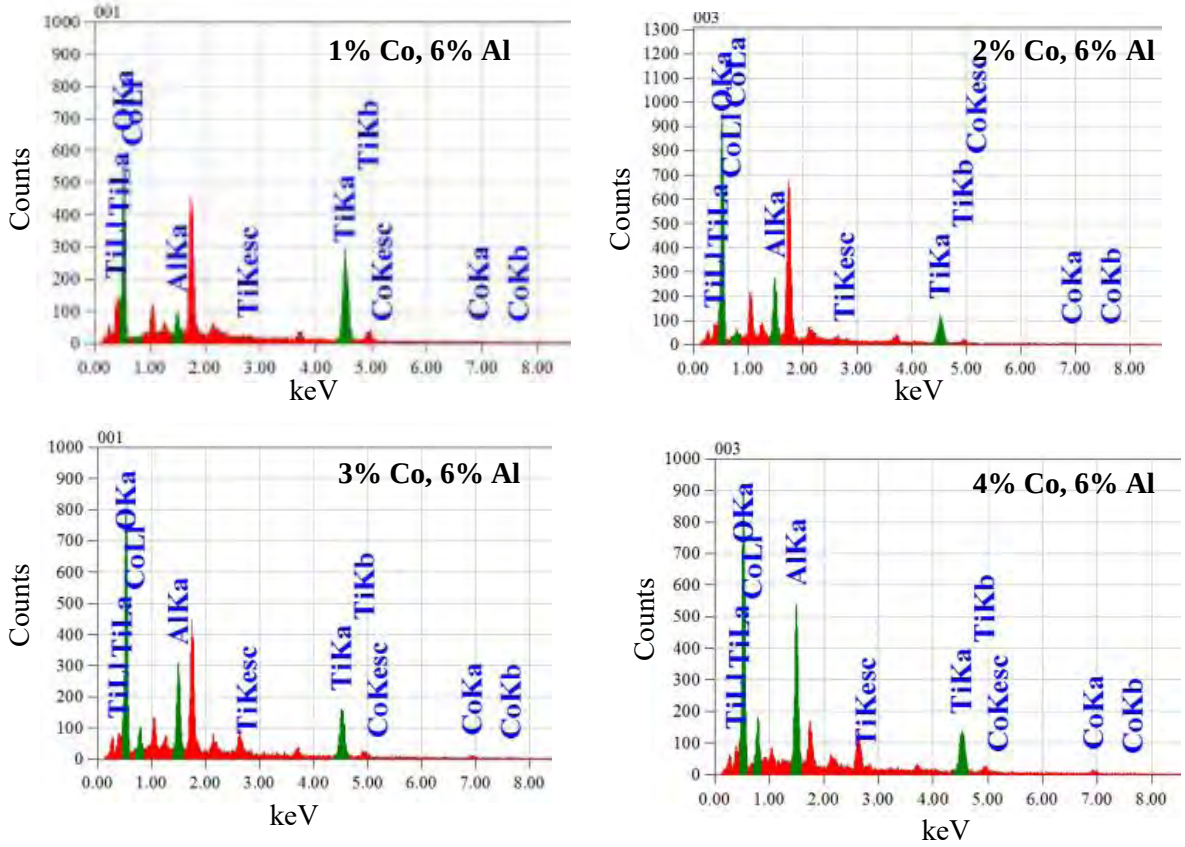

Fig. 6.7: Energy-Dispersion Analysis spectra of (Al, Co) co-doped TiO_2 thin film samples at different concentration.

Table 6.2: Elemental analysis of pristine, Al doped and (Al, Co) co-doped TiO_2 thin films.

Sample	Elements	Mass%	Atom%
Pristine	Ti	66.53	14.39
	O	33.47	85.41
2% Al; TiO_2	Ti	32.65	13.54
	O	66.32	84.92
	Al	2.03	1.54
4% Al; TiO_2	Ti	38.63	17.33
	O	57.26	78.88
	Al	4.10	3.35
6% Al; TiO_2	Ti	47.93	24.45
	O	45.68	69.77
	Al	6.39	5.78
8% Al; TiO_2	Ti	18.99	7.50
	O	74.03	87.60
	Al	6.98	4.90
(6% Al, 1% Co); TiO_2	Ti	45.43	22.46
	O	51.49	75.55
	Al	1.95	1.69
	Co	0.73	0.29
(6% Al, 2% Co); TiO_2	Ti	22.33	9.56
	O	64.44	82.60
	Al	7.86	5.97
	Co	5.36	1.87
(6% Al, 3% Co); TiO_2	Ti	25.81	12.65
	O	50.62	74.31
	Al	7.72	6.72
	Co	15.86	6.32
(6% Al, 4% Co); TiO_2	Ti	19.71	10.16
	O	44.78	69.08
	Al	11.85	10.85
	Co	23.66	9.91

6.5 Atomic Force Microscopy

Atomic force microscopy is a convenient technique widely used to obtained surface information of the thin films. Surface roughness of pristine, Al doped and (Al, Co) co-doped TiO_2 thin films on glass substrate were studies by Atomic force microscopy (AFM). The surface properties of the Al doped and (Al, Co) co-doped TiO_2 thin films samples deposited at various concentration onto glass substrate was measured using AFM; the results are shown in table 6.4 and 6.9.1. Fig. 6.8, 6.9 and 6.11 shows two and three dimensional AFM images of spray-deposited TiO_2 thin films. The images were recorded at the scan rate of 10.17 Hz of on 1 $\mu m \times 1\ \mu m$ planar in contact mode. The Atomic force microscopy images were analyzed by Gwyddion software. Uniform distributed spherical grain are seen in pristine samples. Comparing the entire Al dopant image, increasing doping concentration, the fiber size decreasing compare to 2% Al doped TiO_2 thin films samples.

At 6% Al doped TiO_2 sample, surface roughness is maximum, which identifies the 6% is the optimize percentage. In the co-doping purpose, 6% Al was fixed and cobalt was varying 1%, 2%, 3% and 4%. The surface root mean square (RMS) values of the roughness amounted to 43 nm to 115 nm for Al doped and (Al, Co) co-doped TiO_2 thin films are 43 to 245 nm. The pristine sample AFM image are good agreement with SEM image, which indicating that samples are used in dye sensitized solar cell. The (Al, co) samples image shows the truncated trapezoidal terraces and island are clearly observed, in good with the previous AFM image [6, 7]. The non-uniform particle shape are excellent application in gas sensing. The thickness of pure, doped and co-doped samples is listed in table 6.4. The thickness range is about 280 nm to 320 nm for doped and 280 nm to 340 nm for co-doped samples. The thickness was measured by Fizeau fringes method. The slight change of surface roughness might results from two factors such as the limited surface diffraction caused by relatively low thermal energy and crystalline effects; nevertheless, our studied samples have same surface roughness [8]. The irregular shape are absorbs in gas molecules, our studied samples may be used in gas sensing device.

Table 6.3: The fiber classification by the IUPAC according to the size [9, 10].

Fiber diameter	Types of pore	This experimental
< 500 nm	Nano-fiber	
$0.9\ \mu m$	Micro-fiber	Nano-fiber
$12 - 24\ \mu m$	Macro-fiber	

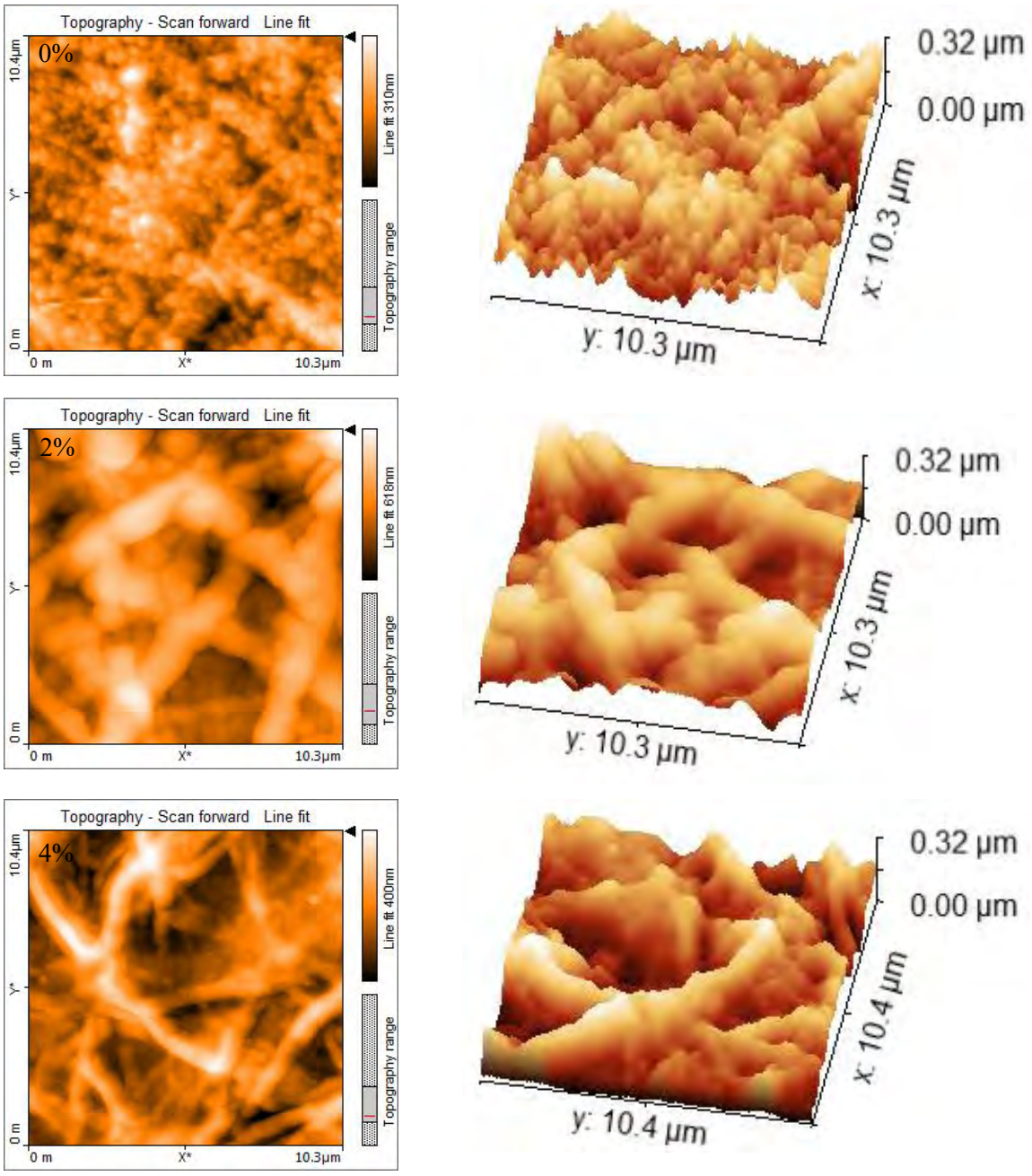

Fig. 6.8: Atomic Force Microscopy image (left 2D) and (right 3D) of Al doped TiO_2 thin films.

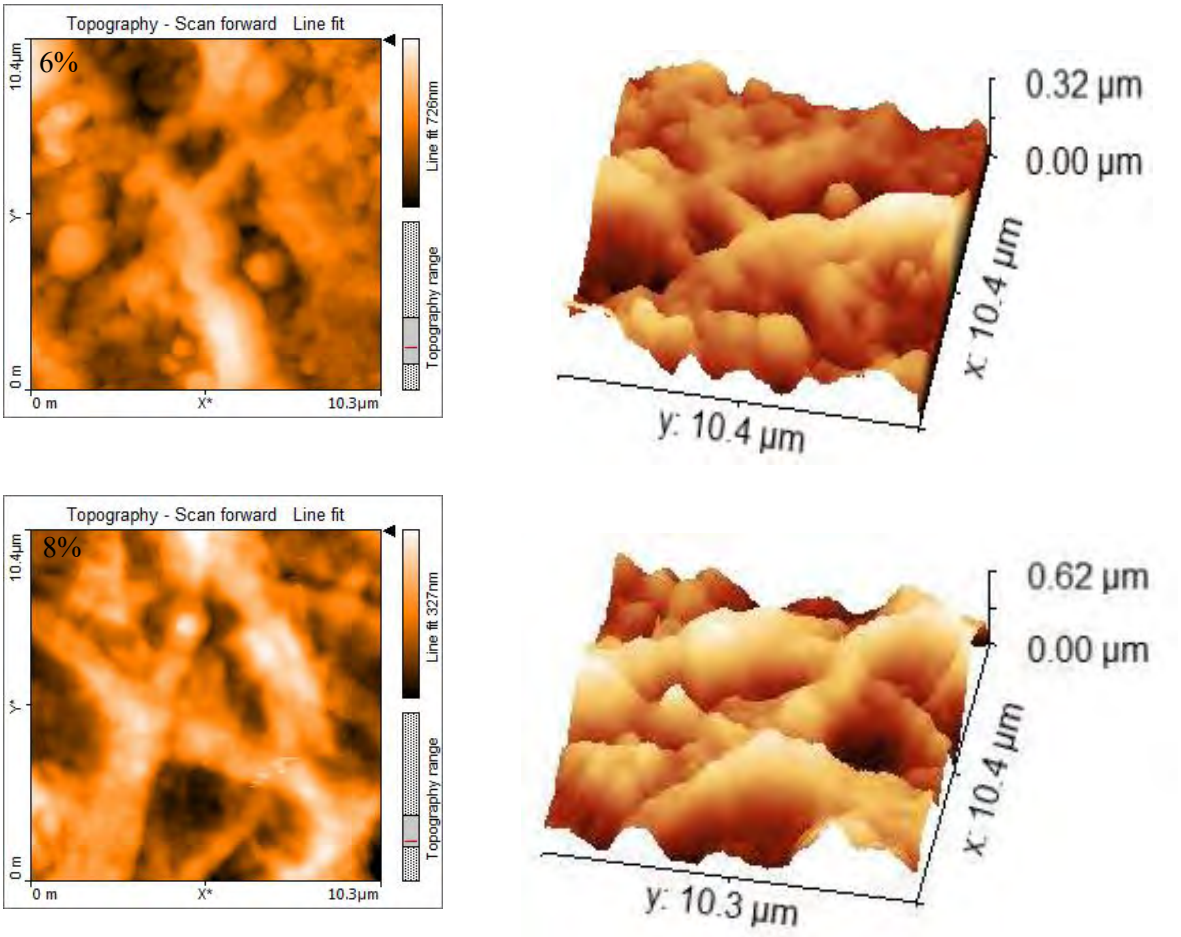

Fig. 6.9: Atomic Force Microscopy image (left 2D) and (right 3D) of Al doped TiO_2 thin films.

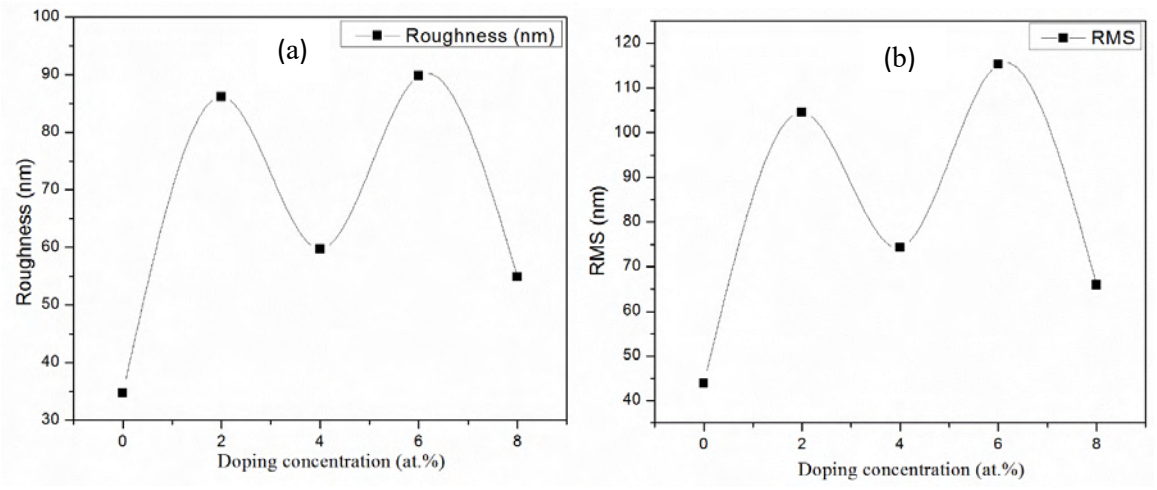

Fig. 6.10: Variation of (a) roughness and (b) RMS as a function of Al doped TiO_2 thin films.

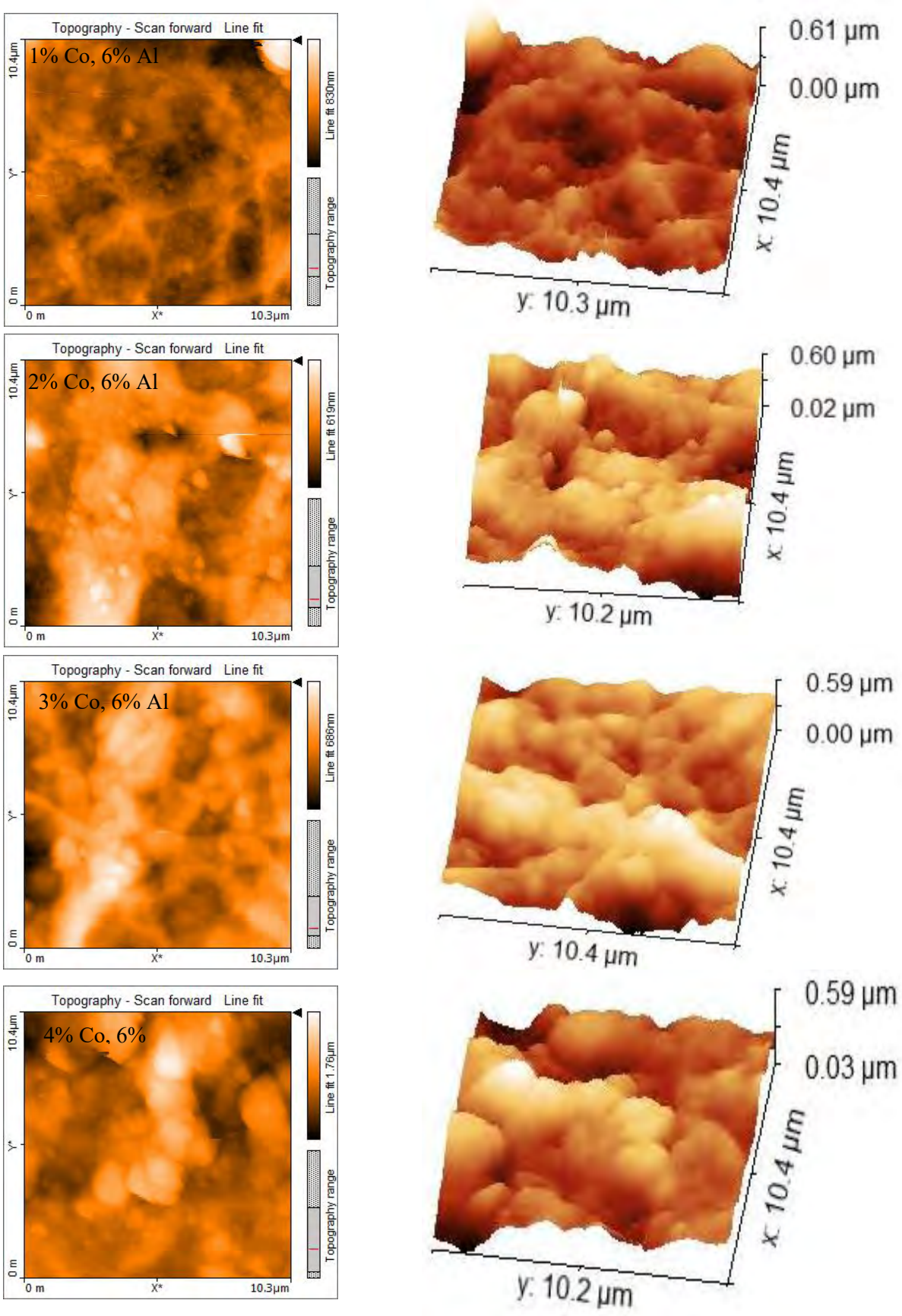

Fig. 6.11: Atomic Force Microscopy image (left 2D) and (right 3D) of (Al, Co) co-doped TiO_2 thin films.

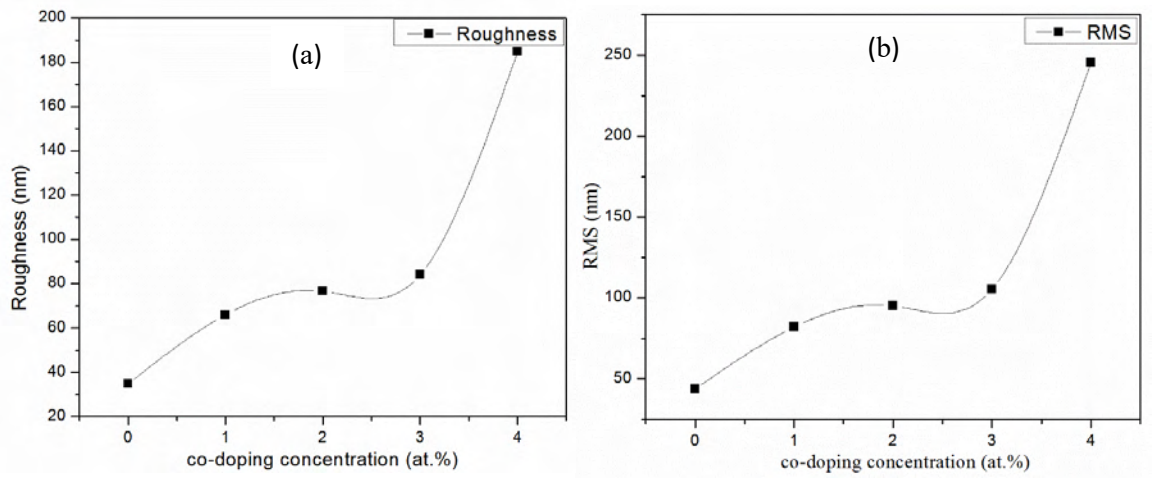

Fig. 6.12: Variation of (a) roughness and (b) RMS as a function of (Al, Co) co-doping content.

Table 6.4: Thickness, grain size (D), surface roughness, root means square velocity of the Al doped and (Al, Co) co-doped TiO_2 thin film samples.

Samples	Films thickness (nm)	Roughness (nm)	RMS (nm)
Pristine	280	34.72	43.84
2% Al; TiO_2	282	86.17	104.54
4% Al; TiO_2	288	59.77	74.28
6% Al; TiO_2	290	89.83	115.32
8% Al; TiO_2	321	54.89	125.41
(Al 6%, Co 1%); TiO_2	310	66.01	82.10
(Al 6%, Co 2%); TiO_2	325	76.64	95.25
(Al 6%, Co 3%); TiO_2	295	84.04	105.4
(Al 6%, Co 4%); TiO_2	340	59.00	118

6.6 Structural Analysis

The structural properties of Al doped and (Al, Co) co-doped TiO_2 thin films samples are analyzed thoroughly by using X-ray diffraction (XRD) technique. The crystal structure and phase purity of the powdered samples were analyzed by X-ray powder diffraction (XRD) technique using Cu K_α source of wavelength 1.5404 Å and scan size of 0.01^0 from 10^0 to 70^0. All measurement were carried out at room temperature. From figure 6.13 shows the XRD pattern of Al doped and (Al, Co) TiO_2 thin films samples deposited onto the glass substrates. The identified peak are mainly dominate brookite phase.

The average crystalline size was estimated by Debye-Scherrer formula [11, 12] as follows:

$$<D>= \frac{0.9\,\lambda}{\beta \cos\theta} \qquad (6.1)$$

Where D is the average crystalline size in angstroms (Å), shape factor taken as 0.9, λ is the wavelength of X-ray radiation, β is the full width half maximum (FWHM) after making appropriate base correction and θ is the diffraction angle at the position of the peak maximum

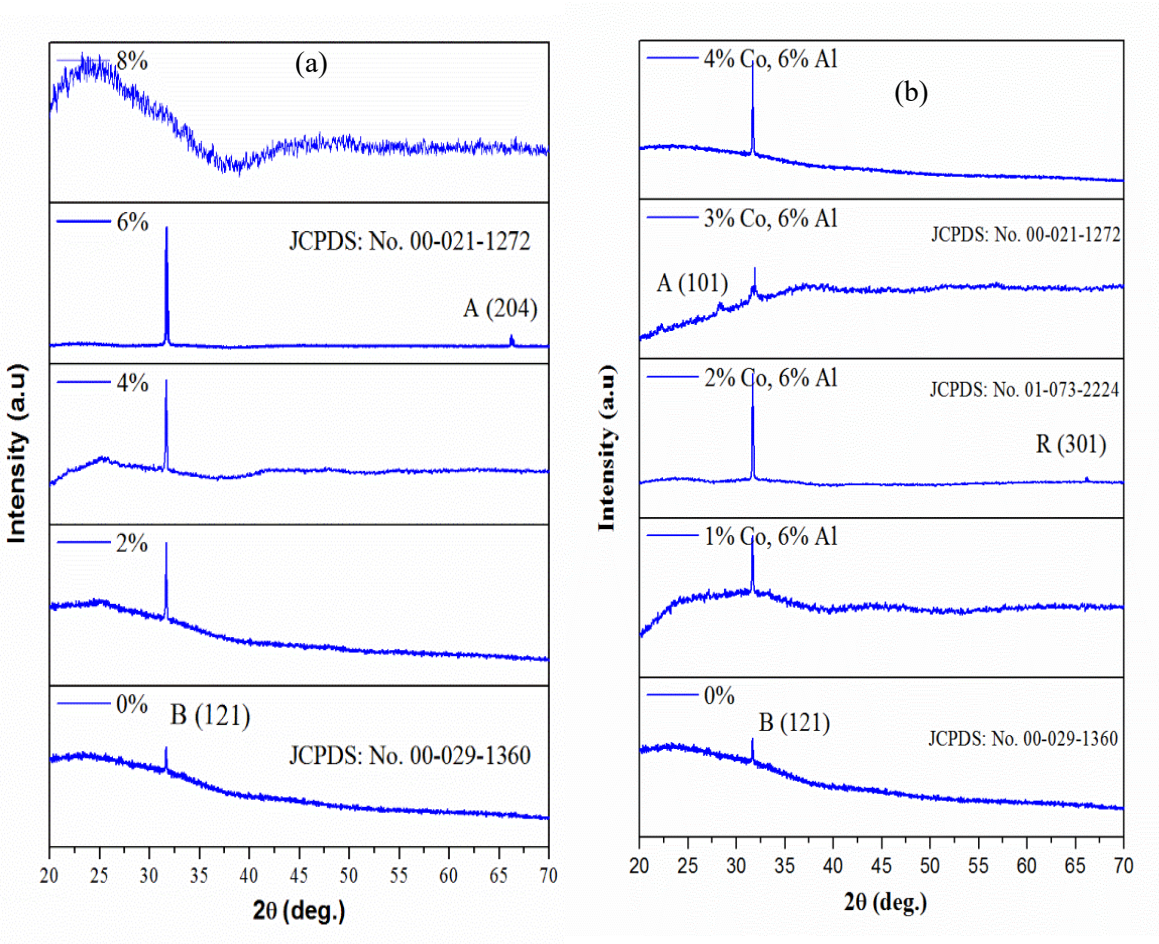

Fig. 6.13: XRD pattern of (a) Al doped and (b) (Al, Co) co-doped TiO_2 thin films.

We notice that the crystalline size changes by increasing the number of concentration because of the size of ionic radii of Al^{+3} (0.54 Å), Co^{+2} (0.70 Å) and Ti^{+4} (0.61 Å). The decrease of crystalline size can be attributed to the nucleation process, due to the difference in the density of nucleation centers in the films with different thickness. An increased density of nucleation centers leads to the formation crystallite size with smaller size.

The average crystalline size was estimated based on the value of full width half maximum of the most dominate peak which is associated to (121) of the brookite phase. The brookite phase was identified by the JCPDS card no. 00-029-1360 [13]. The identified peak are mainly dominated brookite phase TiO_2 which in ensured by the MATCH XRD software and finally the Riveted refinement. Subsequently, there are no secondary phases observed in the pure samples. At 6% Al doped TiO_2 samples has rutile phase which is the tetragonal phase. Moreover, it can also be observed that the main diffraction peak shifted towards the higher angle, after Al doped and (Al, Co) co-doped samples.

Al doped and (Al, Co) co-doped samples changes Strain and dislocation density compares to the pristine of TiO_2 thin films samples. These changing behaviors can be explained as the Quantum size effect owing to accumulation of Al or Co causes a significant change in the crystalline size as shown in table 6.5. At the Al doped TiO_2 thin films samples became amorphous when a higher Al concentration was applied. At 8% Al doped TiO_2 thin films, it can be seen that the films are mainly amorphous (neither brookite, rutile, anatase could be detected) nature [14].

Table 6.5: X-ray diffraction studies data at pristine, Al doped and (Al, Co) doped TiO_2 thin films samples.

Samples	Crystallite size (nm)	Strain × 10^{-4} (m^2)	Dislocation density× 10^{-4} (lines/m^2)
Pristine	66.00	2.29	5.24
2% Al; TiO_2	82.00	1.48	4.22
4% Al; TiO_2	63.87	2.45	5.42
6% Al; TiO_2	66.63	2.25	5.19
8% Al; TiO_2	Amorphous	-	-
(Al 6%, Co 1%); TiO_2	62.71	2.54	5.52
Al 6%, Co 2%); TiO_2	72.56	1.94	4.77
(Al 6%, Co 3%); TiO_2	42.02	3.12	5.07
(Al 6%, Co 4%); TiO_2	85.50	5.42	2.50

Strain is defined as the fractional change in length and the dislocation density as the length of dislocation lines per unit volume of the crystal, and it is measured from the following equation [15, 16]

$$\varepsilon = \frac{\beta \cos\theta}{4} \tag{6.2}$$

$$\delta = \frac{1}{D^2} \tag{6.3}$$

The strain and dislocation density increase with the increase in doping concentration and was attributed to the combination of the atoms in TiO_2 in the substitution.

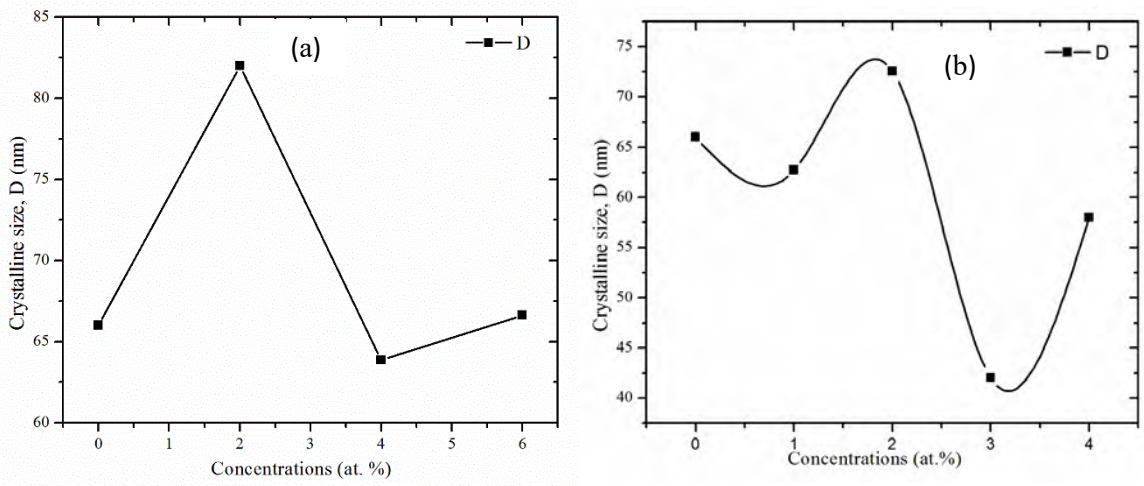

Fig. 6.14: The crystallite size Vs Concentration of (a) Al doped TiO_2 thin films and (b) (Al, Co) co-doped TiO_2 thin films.

Table 6.6: Refined crystallographic data of Al doped and (Al, Co) co-doped TiO_2 thin films samples.

Parameters	pristine	Al doped TiO_2	(Al, Co) co-doped TiO_2
Crystal system		orthorhombic	
Space group		P b c a (61)	
a (Å)	5.23494	4.74420	5.23730
b (Å)	9.03553	10.14030	8.93150
c (Å)	5.50438	5.23980	5.53130
α, β, γ (deg.)	90	90	90
V (Å^3)	260.35	252.07	258.73
χ^2	2.22	2.57	1.80
R_p (%)	2.66	2.69	3.10
R_{WP} (%)	10.0	9.19	9.56

For further quantitative analysis of the structural parameters Rietveld refinement of the observed X-ray diffraction patterns has been carried out by using FULLPROF package [15]. The refinement X-rad diffraction data of Al doped and (Al, Co) co-doped TiO_2 thin films samples are listed in table 6.7. Negligible difference has been found between the experimental and theoretical results. The refinement crystallography parameters are tabulated in table 6.4 with the corresponding fitting parameters. The negligible difference has been found between the experimental and theoretical results. The major phases of the studies samples are observed to be orthorhombic structured TiO_2 with space group P b c a (61). The obtained lattice parameters are good agreement with published data [17].

Table 6.7: Fractional atomic coordinates of pristine TiO_2 thin films.

Sample	Atom	x	Y	z	Wyckoff site
Pristine	Ti	0.36280	0.12900	0.09990	8c
	O1	0.03660	0.23220	0.11170	8c
	O2	0.18310	0.00980	0.35160	8c
$Ti_{0.96}Al_{0.4}O_2$	Ti	0.36280	0.12900	0.09990	8c
	O1	0.03660	0.23220	0.11170	8c
	O2	0.18310	0.00980	0.35160	8c
$Ti_{0.1}Al_{0.6}Co_{0.3}O_2$	Ti	0.36280	0.12900	0.09990	8c
	O1	0.16100	0.16900	0.03600	8c
	O2	0.18310	0.00980	0.35160	8c

6.7 UV-Vis Spectroscopy

The optical transmission and absorbance spectra are shown in fig.6.9.2 with wavelength range 300 nm to 1000 nm. Fig. 6.9.2 shows the variation of transmittance and absorbance with the different doping concentration Al and (Al, Co) TiO_2 thin film samples. In the visible region Al doped TiO_2 films shows good transparent and have maximum transmit ant of pure samples. After increasing doping concentration, the transmittance decreases compare to pristine samples. At 8% Al doped samples have 83.49% transmittance, owing to increase the charge carrier concentration of Al^{+3} and Ti^{+4}. From these spectra we can observe that the increasing doping concentration

increase charge carrier recombination rate and shift the transmittance spectra. The behavior of absorption spectra is completely reverse of transmittance spectra as shown in fig. 6.9.2. The absorption spectra for Al doped TiO_2 exhibit strong absorption below 450 nm which was attributed to the charge transfer transition (O^{2-} to Ti^{+4}) from ligand to metal. The increase in absorption before 400 nm is due to intrinsic band gap energy of TiO_2 (3.2 eV) [18]. The higher atomic % of Al in the photo-anodes achieved the larger absorption value exhibits the red shift in-the absorption spectrum. The doping of Al influenced the charge transfer transition on titanium dioxide conduction band [19].

Glass were used as a substrate in this experiment to prevent the influence of the absorption edge of the substrate. The spectra of Al doped TiO_2 films with different Al doping concentration were also compare in the figure 6.9.2. The optimum TiO_2 thin films samples spectra exhibited high visible transmittance as high as 90.01% for pristine TiO_2 thin films. At high doping concentration the transmittance decreases, which may be due to the increased scattering photon by crystal defect and also due to free carrier absorption of photons created by doping. The optical gap shifting is occurred by two competing effects, Burstein-Moss band filling effect and band gap narrowing effect. The well-known optical band gap blue or red shift in heavily doped semiconductor occurs because the lower states in the conduction band are blocked. Conversely, band gap narrowing is caused by exchange interactions in the free electron gas and electrostatic interaction between free electrons and ionized impurities.

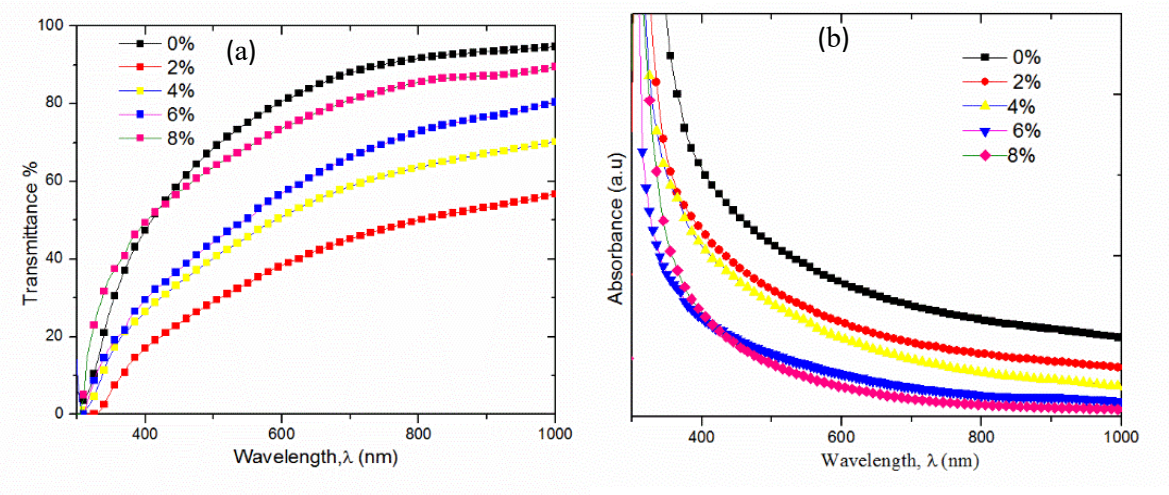

Fig. 6.15: The plot of (a) transmittance and (b) absorbance for Al doped TiO_2 thin films having different concentration.

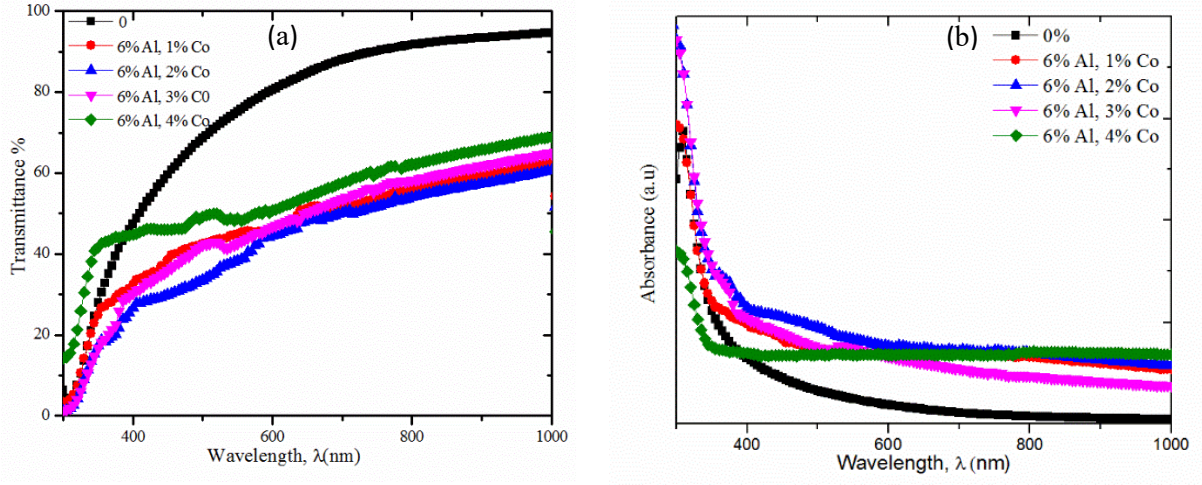

Fig. 6.16: The plot of (a) transmittance and (b) absorbance for (Al, Co) co-doped TiO_2 thin films having different concentration.

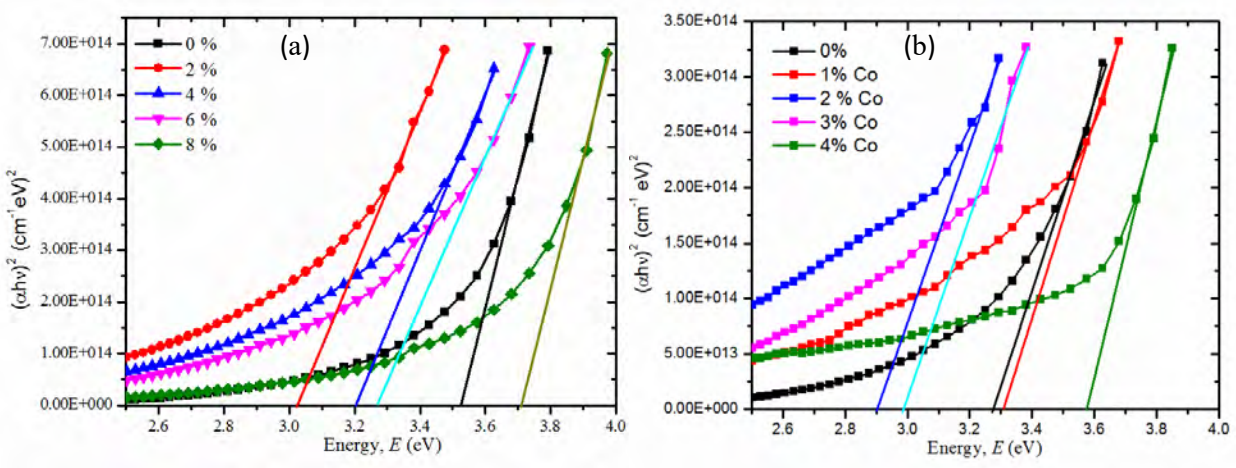

Fig. 6.17: Optical band gap energy of (a) Al doped and (b) (Al, Co) (at constant 6% Al) co-doped TiO_2 thin films.

The linear nature of the plots at the absorption edge ensures that films are a semiconductor. The optical band gap decrease with increasing doping and co-doping concentrations in direct band gap. The optical band gaps of doped and co-doped samples are listed in table 6.9. With an increase in the amount of doping, the band gap energy decrease due to Al and (Al, Co) dopants can occupy the new energy states. Our results are in good agreement with the previous reported band gap values [22].

The optical band gap E_g can be estimated from the following relation which is known as the Tauc plot [20, 21] for direct band gap

$$(\alpha h\vartheta)^2 = A\ (h\nu - Eg)^n \quad (6.4)$$

Where, A is a constant value, $h\nu$ is the photonic energy, n is a constant which depends on probability of the transition, n= 2 correspond to direct allowed and direct forbidden transmissions and α is the absorption co-efficient. Our results are in good agreement with the previous reported band gap values [22]. The optical band gap does not followed any trend due to the metastable phase of TiO_2 nanoparticles. The Co 3d and Ti 3d hybridization is occurred in TiO_2 lattice network which is strongly attributed to band gap tailoring. With an increase in the amount of doping, the band gap energy decrease due to Al and Co dopants can occupy the new energy states.

Table 6.8: The optical parameter values of pristine, Al doped and (Al, Co) co-doped TiO_2 thin films.

Samples	Transmittance, T %		
	550 nm	650 nm	750 nm
Pristine	75.23	84.72	90.10
2% Al; TiO_2	33.82	42.07	47.76
4% Al; TiO_2	45.75	55.28	61.49
6% Al; TiO_2	50.54	61.86	69.75
8% Al; TiO_2	68.83	77.62	83.49
(Al 6%, Co 1%); TiO_2	39.10	42.80	45.80
(Al 6%, Co 2%); TiO_2	32.4	38.30	43.30
(Al 6%, Co 3%); TiO_2	42.7	50.20	56.20
(Al 6%, Co 4%); TiO_2	45.40	45.70	45.90

Table 6.9: Optical band gap measurement pristine, Al doped and (Al, Co) co-doped TiO_2 thin films samples.

Samples	Optical band gap (eV)
Pristine	3.52
2% Al; TiO_2	3.02
4% Al; TiO_2	3.20
6% Al; TiO_2	3.26
8% Al; TiO_2	3.70
(Al 6%, Co 1%); TiO_2	3.30
(Al 6%, Co 2%); TiO_2	2.90
(Al 6%, Co 3%); TiO_2	2.98
(Al 6%, Co 4%); TiO_2	3.57

6.8 Electrical Properties

Resistivity of the pristine, Al doped and (Al, Co) TiO_2 thin films samples have been measured by Four Probe method. The resistivity measurement has been performed over a range from room temperature to 100 K. During the measurement, the temperature increased slowly as a consequence, the whole film is heated with uniform temperature. The variation of resistivity with temperature for films is shown in fig. 6.19. The figure shows that the resistivity gradually decrease with increase of temperature, which ensure that the samples are semiconducting behavior [23, 24]. This results indicating that when Al dopant substitutes the Ti site in the TiO_2 lattice network, a free hole is produced and this free hole compensates the electrons of n-type TiO_2 network.

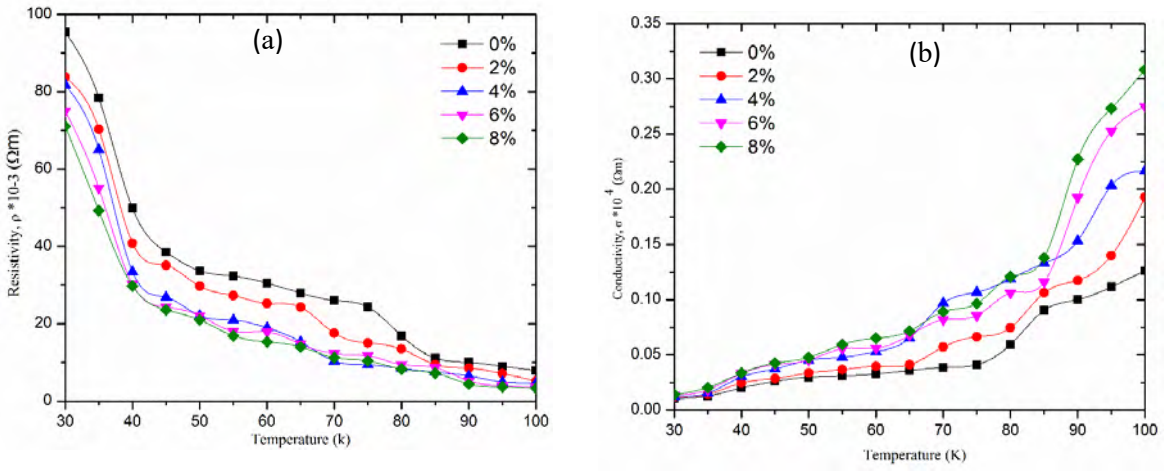

Fig. 6.18: Variation of resistivity with respect to temperature for (a) Al doped and (b) (Al, Co) co-doped TiO_2 thin films samples.

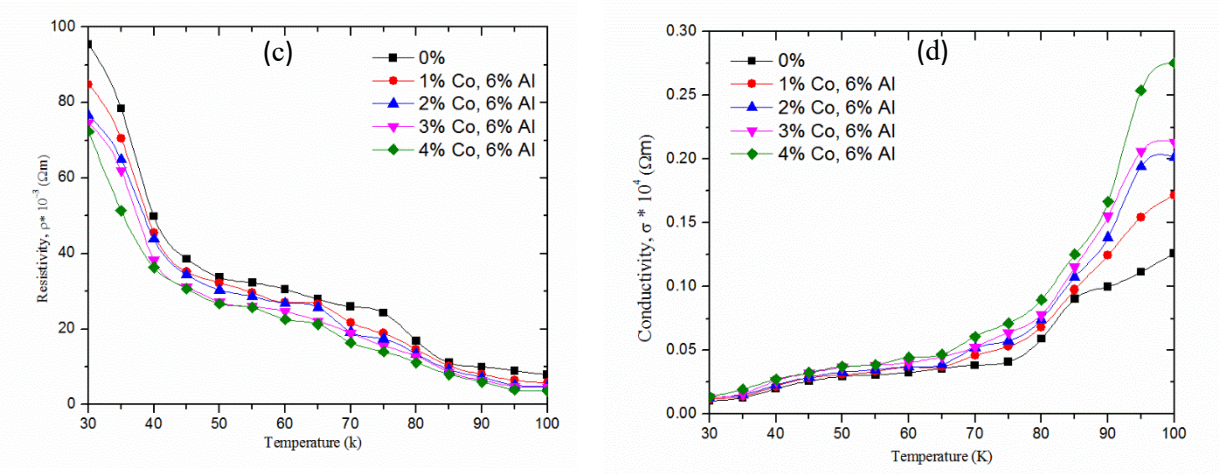

Fig. 6.19: Variation of electrical conductivity with respect to temperature for (c) Al doped and (d) (Al, Co) co-doped TiO_2 thin films samples.

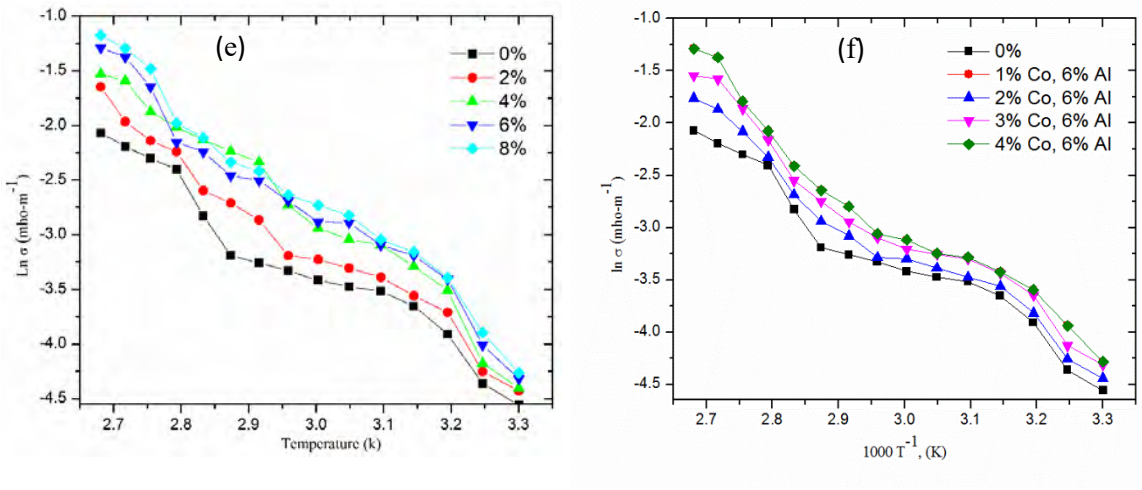

Fig. 6.20: Variation of lnσ with 1/T to for (e) Al doped and (f) (Al, Co) co-doped TiO_2 thin films samples.

In the case of co-doped samples Co and Al dopants are interact with the n-types TiO_2 network, electron hole migration would be occurred in the samples this migration ensure that those samples is used in photo-catalytic activity. Al is a p-types and TiO_2 is a n-types semiconductors, which is used in hetero-junction and homo-junctions [25]. The decrease in resistivity is mainly owing to the free electron is escape to the conduction band. Therefore, higher concentration of Al^{+3} can completely replace Ti^{+4} in the TiO_2 lattice networks, in the case increasing the carrier concentration to drastically decrease the resistivity of samples [26].

6.9 Theoretical Analysis

6.9.1 Structural Properties

The orthorhombic structure of TiO_2 has space group P b c a [27]. The unit cell of material contains 12 atoms. In the unit cell, Ti atoms located on the body centered position with 8*c* Wyckoff site and (0.36280 0.12900 0.09990) fractional coordinates, the O atoms occupy the face centered position with 8c Wyckoff site and fractional coordinates O1 (0.03660 0.23220 0.11170) and O2 (0.18310 0.00980 0.35160) and the optimize lattice constants a, b and axial ratio a_0/b_0 and c_0/b_0 are tabulated in table 6.10 and 6.11. The calculated equilibrium lattice parameter *a, b, c* and *V* unit cell volume in super-cell structures are good agreement with experimental as well as theoretical results

shown in Table. We have also found that transition metal Al doped and (Al, Co) co-doped TiO_2 materials increase the lattice parameters and unit cell volume.

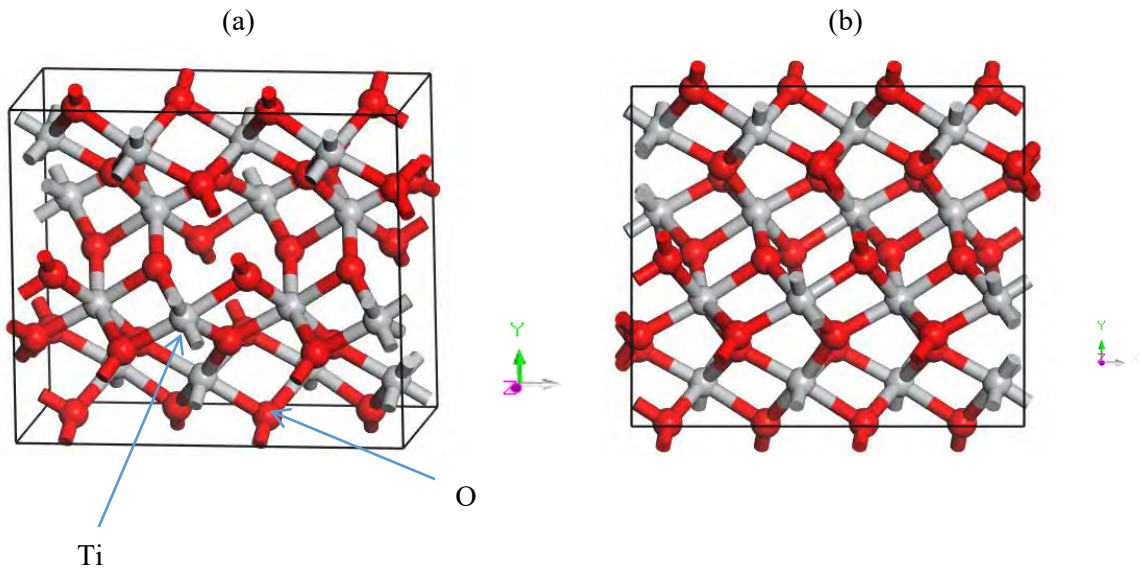

Fig. 6.21: The crystal structure of pristine (2× 1 × 1) supercell (*a*) Three dimensional (*b*) Two dimensional view of TiO_2 thin films. (Drawing for CASTEP calculations)

Table. 6.10: The theoretical and experimental unit cell parameters of pristine and Al doped TiO_2 thin films.

Properties	Experimental	0% Cal.	2% Cal.	4% Cal.	6% Cal.	8% Cal.
a_o (Å)	5.234	5.185	5.215	5.265	5.312	5.35
b_0 (Å)	9.035	9.297	9.308	9.387	9.475	9.55
c_0 (Å)	5.504	5.504	5.635	5.646	5.644	5.73
a_0/b_0	0.57	0.55	0.56	0.56	0.56	0.56
c_0/b_0	0.60	0.59	0.69	0.60	0.59	0.60
V_0 (Å^3)	260.5	265.3	273.5	279.1	284.1	293.2

Table. 6.11: The theoretical and experimental unit cell parameters of pristine and (Al, Co) co-doped TiO_2 thin films.

Properties	Experimental	0% Cal.	1% Cal.	2% Cal.	3% Cal.	4% Cal.
a_o (Å)	5.234	5.185	5.318	5.320	5.368	5.986
b_0 (Å)	9.035	9.297	9.516	9.592	9.604	10.974
c_0 (Å)	5.504	5.504	5.659	5.683	5.773	4.487
a_0/b_0	0.57	0.55	0.59	0.55	0.56	0.54
c_0/b_0	0.60	0.59	0.59	0.59	0.60	0.41
V_0 (Å^3)	260.5	265.3	286.4	290.0	297.6	320.1

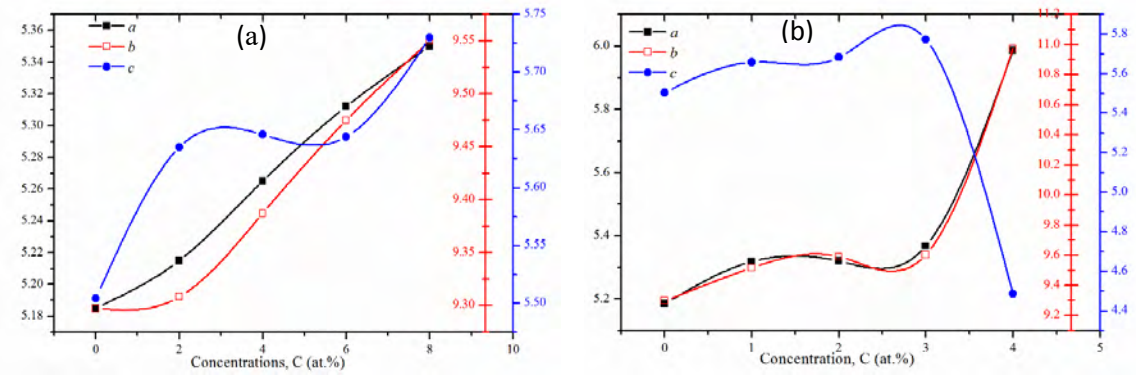

Fig. 6.22: Lattice constant, *a*, *b*, *c* Vas *C* (a) Al doped TiO_2 thin films and (b) (Al, Co) co-doped TiO_2 thin films.

6.9.2 Mechanical Properties

The elastic property is essential parameters which are related to many physical properties of materials. Some mechanical properties and dynamical behaviors of the materials can be obtained by its elastic constants. For orthorhombic structures, there are nine elastic constants C_{11}, C_{22}, C_{33}, C_{44}, C_{55}, C_{66}, C_{12}, C_{13}, C_{23} .In table 6.9.6 to 6.9.9 we represented the elastic constant and its increasing rate with different concentration rate of pristine, mono-doped and co-doped.

The mechanical unstable of orthorhombic crystal depends on the fulfillment of the conditions derived from the independent elastic constants:

$$C_{11} > 0;\ C_{44} > 0;\ C_{55} > 0;\ C_{66} > 0,\ C_{11}\ C_{22} - C_{12}^{\ 2} > 0,$$

$$C_{11}C_{22}C_{33} + 2\ C_{12}C_{13}C_{23} - \ C_{11}\ C_{23}^{\ 2} - C_{22}\ C_{13}^{\ 2} - C_{33}\ C_{12}^{\ 2} > 0\ [28]$$

The deference (C_{12} - C_{44}) is known as the Cauchy pressure, which is frequently used to assess the nature of chemical bonding in a solid crystal [29]. It negative value corresponds to the directional covalent bonding with angular character, whereas its positive value is a sign of metallic bonding.

The increasing rate of pugh‟s and poisons ratio with different dopant concentration is derived from the slope of the corresponding linear fitted curve, as shown in fig 6.23. According to calculated elastic constants and mentioned formula in reference [28] we have calculated the mechanical properties of Al doped and (Al, Co) co-doped TiO_2 under variation dopant concentration. The bulk modulus *B*, shear modulus *G*, Young‟s

modulus *E*, and poisson‟s ratio *v*, which are listed with other theoretical data in table 6.14 and 6.15. On the other hand, the bulk modulus *B* and shear modulus *G* can implies that the resistance to volume change and shape change respectively. The Young‟s modulus is related to the stiffness of the materials. From table we have found that bulk modulus *B*, shear modulus *G* and Young modulus *E* decreasing with different dopants, indicating that the decrease of resistance ability to volume and shape and the stiffness constant of TiO_2 is getting soft. Pugh ratio used to the bulk to shear modulus ratio (B/G) to predict the failure mode (brittle/ductile) of solids. In conformity with, a material has ductile behavior if its B/G ratio is greater (or brittle if lower) than a critical value of 1.75, which serves as the border line between the brittle and ductile behaviors of crystalline solids. From table elastic constant table and figure, it is seen that the all of the samples are brittle nature materials [30].

Poisson‟s ratio *v* is also used successfully in engineering science. Poisson‟s ratio separate crystalline solids as ductile or brittle with a critical value of *v* = 0.26 [31, 32]. Poisson‟s ratio *v* can be used to estimate the ductility and brittleness of the material.

Table 6.12: The evaluated elastic constants C_{ij} (GPa) of pristine and Al doped TiO_2 thin films.

Samples	C_{11}	C_{22}	C_{33}	C_{44}	C_{55}	C_{66}	C_{12}	C_{13}	C_{23}
Pristine	358	294	309	80	98	88	161	151	169
2%	254	257	262	54	85	91	123	122	148
4%	211	234	312	84	80	70	117	135	159
6%	219	222	256	93	79	75	121	124	167
8%	243	184	236	123	66	64	111	113	159

Table 6.13: The evaluated elastic constants C_{ij} (GPa) of pristine and (Al, Co) co-doped TiO_2 thin films.

Samples	C_{11}	C_{22}	C_{33}	C_{44}	C_{55}	C_{66}	C_{12}	C_{13}	C_{23}
Pristine	358	294	309	80	98	88	161	151	169
1% Co	209	201	270	82	67	51	111	126	145
2% Co	213	177	233	106	56	59	110	105	134
3% Co	157	173	156	79	53	43	98	84	114
4% Co	208	183	232	104	53	59	110	102	137

Table 6.14: The evaluated mechanical parameters of pristine and Al doped TiO_2.

Samples	*B*	*G*	*B/G*	*Y*	*E*	*v*	B_V	G_V
Pristine	198	119	1.66	253	297	0.24	213	85
2%	173	71	2.43	180	187	0.31	171	68
4%	166	70	2.37	138	184	0.31	173	67
6%	121	73	1.65	169	182	0.25	168	68
8%	156	69	2.26	172	180	0.30	157	65

Table 6.15: The evaluated mechanical parameters of pristine and (Al, Co) co-doped TiO_2.

Samples	B	G	B/G	Y	E	v	B_V	G_V
Pristine	198	119	1.66	253	297	0.24	213	85
1% Co	155	60	2.58	134	159	0.32	158	57
2% Co	145	62	2.33	141	162	0.31	145	60
3% Co	118	48	2.45	97	126	0.32	119	46
4% Co	115	70	1.64	138	160	0.31	147	61

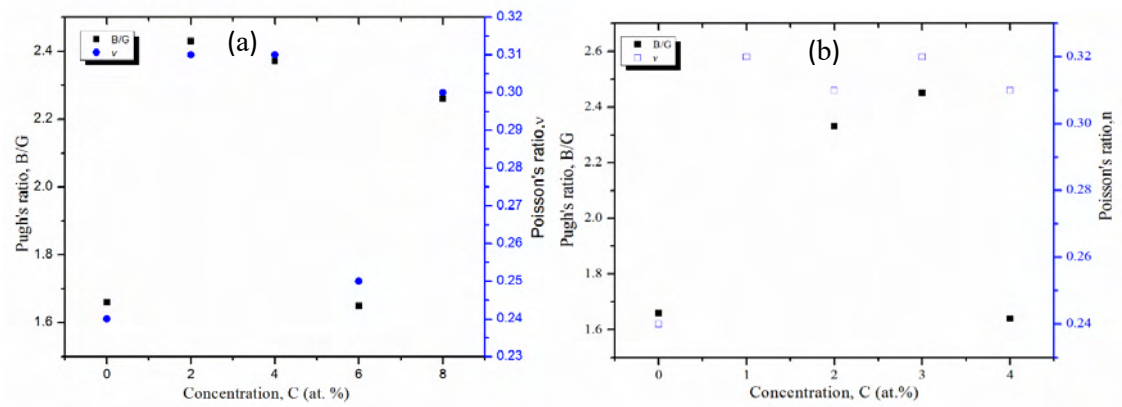

Fig. 6.23: Pugh"s and poisson"s ratios (a) Al doped TiO_2 thin films and (b) (Al, Co) co-doped TiO_2 thin films.

6.9.3 Electronic Properties

6.9.3.1 Electronic band structure

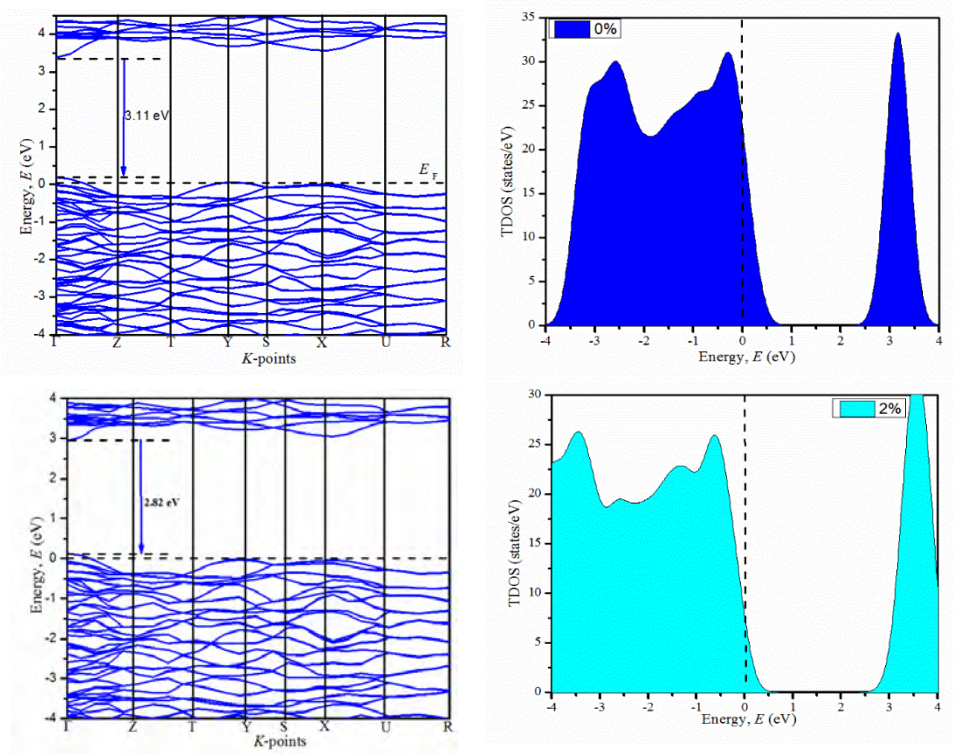

Fig. 6.24: Electronic band structure (left) and total dos (right) of pristine and 2% Al doped TiO_2 thin films.

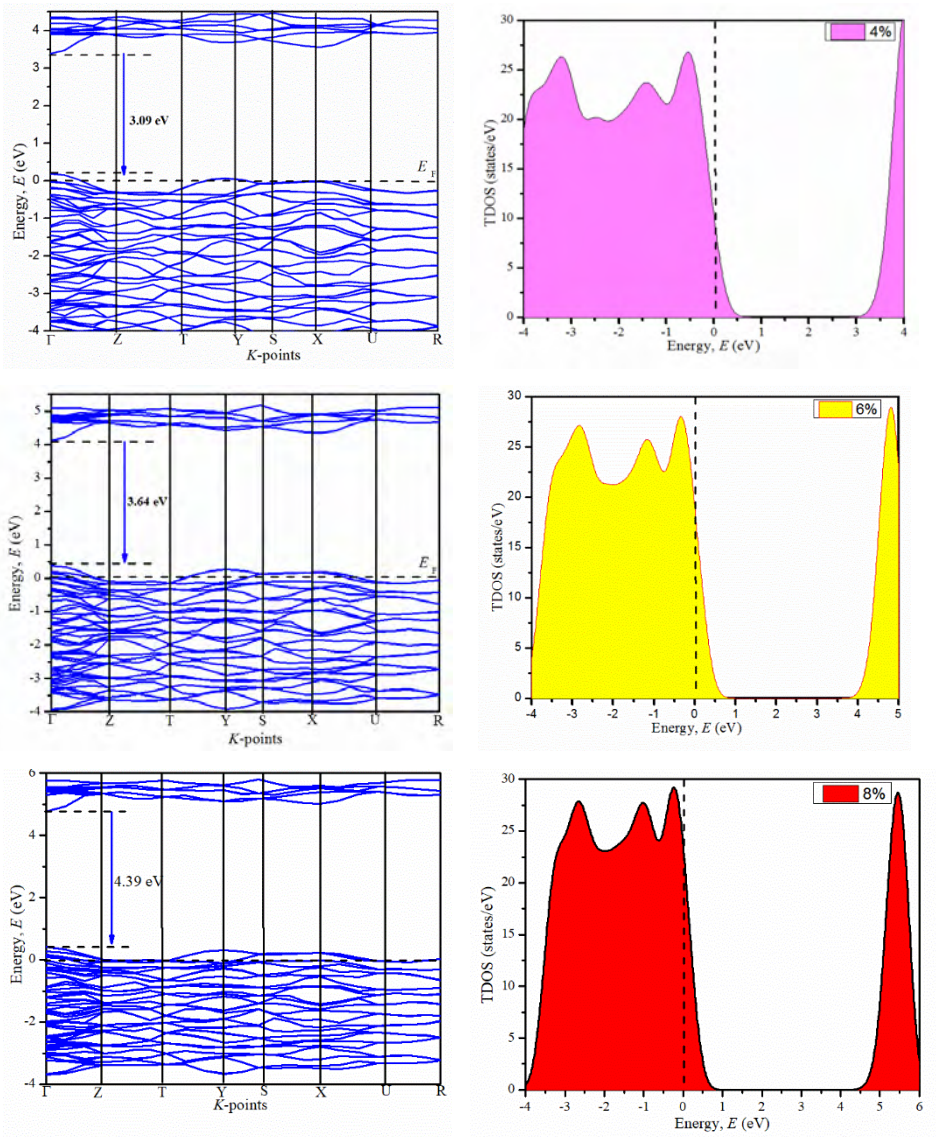

Fig. 6.25: Electronic band structure (left) and total dos (right) of 4%, 6% and 8% Al doped TiO_2 thin films.

.

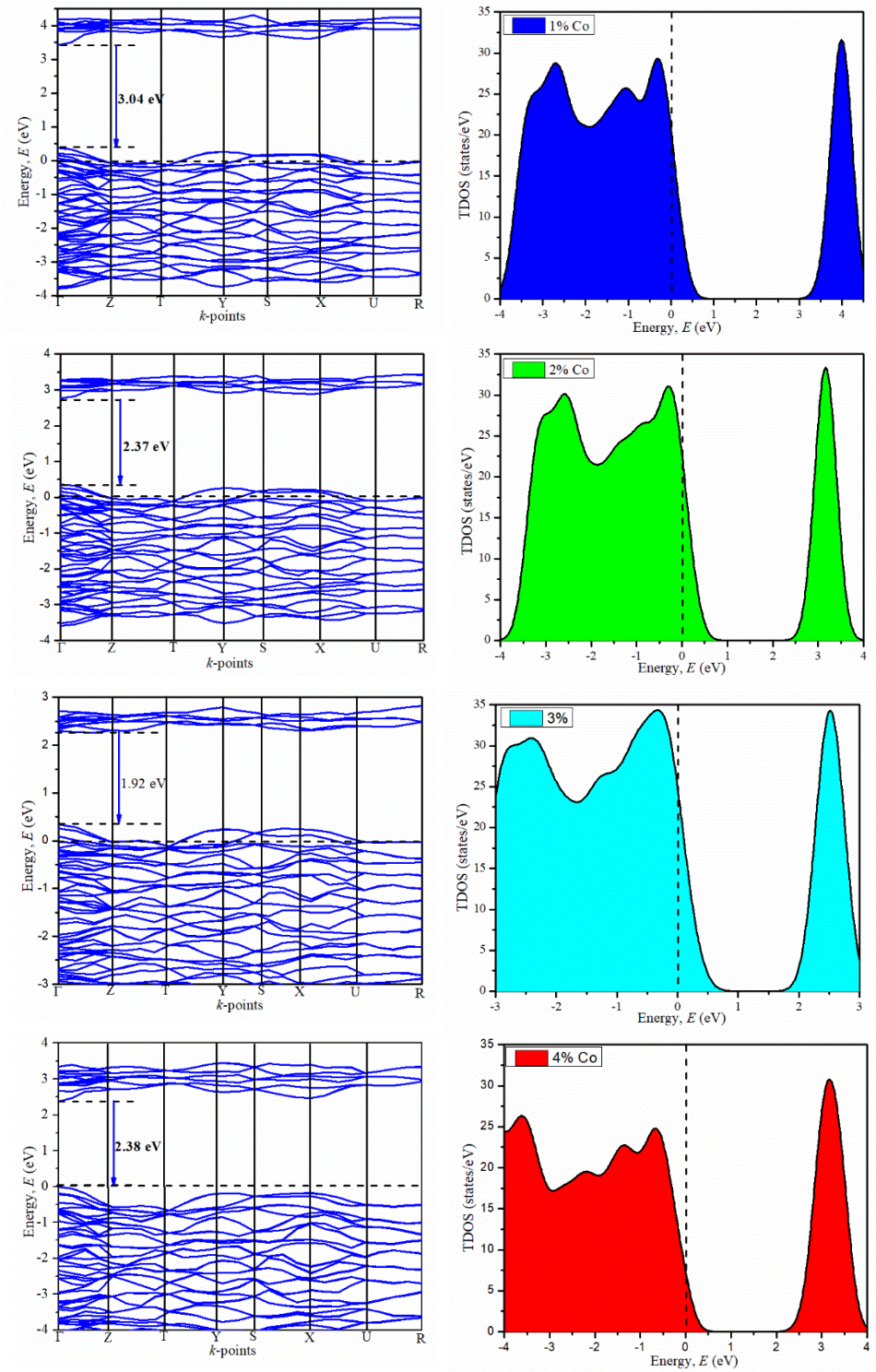

Fig. 6.26: Electronic band structure (left) and total dos (right) (Al, Co) co-doped TiO_2 thin films.

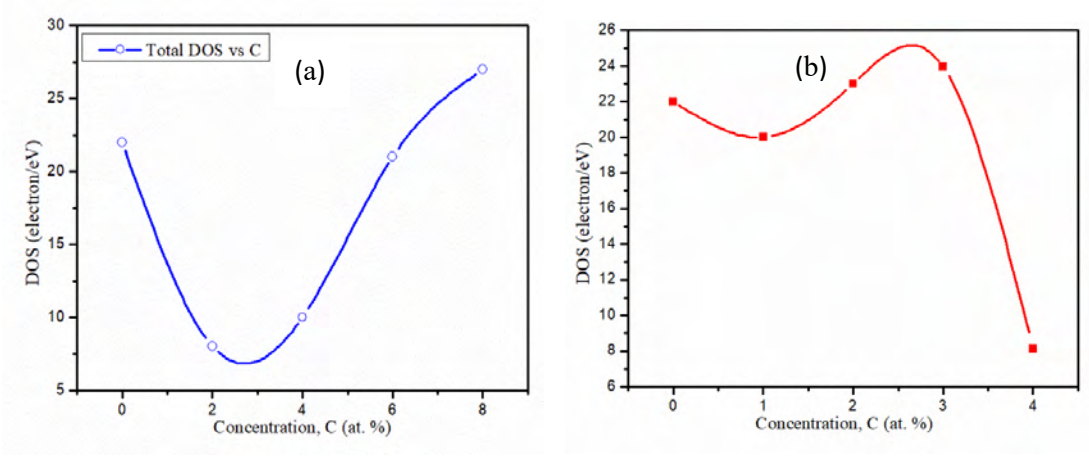

Fig. 6.27: The Concentration vs DOS (a) Al doped TiO_2 thin films (b) (Al, Co) co-doped TiO_2 thin films.

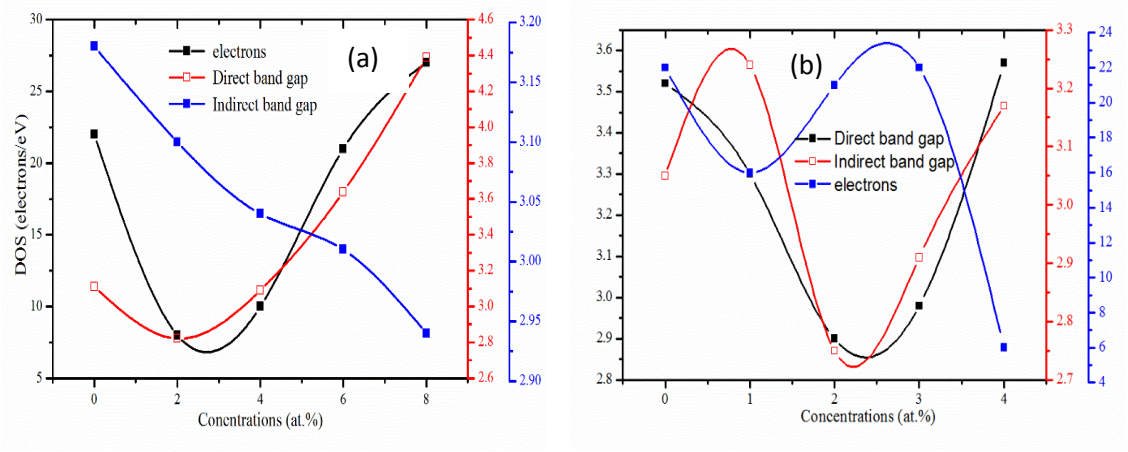

Fig. 6.28: Experimental and theoretical results variations (a) Al doped TiO_2 thin films and (b) (Al, Co) co-doped TiO_2 thin films.

We have studied the electronic band structure for our considered material, to know its band gap values, which gives insight about the optical behavior of the materials. In order to investigate the electronic band structures of transition metal Al doped and (Al, co) co-doped TiO_2 thin films, we set the general gradient approximation for all samples. The simulated electronic band gap values are found good agreements with the available theoretical results in literature using the same theory while some diversity has been found with other results [33]. For band gap measurement, like HSE method may give better estimation owing to band gap value close to the experiment value but it is not valid for all of the materials [34]. The results of calculated band gap values for pure and doped and co-doped are plotted in figures 6.24, 6.25 and 6.26 respectively. It is clear from figure, the Fermi level is fixed at 0 eV on energy scale. The conduction band

minima (CBM) and valance band maxima (VBM) are separated in the energy gap in each case of the corresponding material. As shown in figures the conduction band gap minimum and valance band maximum lies at Γ (*k*-points) indicating the-indirect band gap nature of all samples. The calculated band gap is found indirect band gap in the range of 3.11 eV to 4.39 eV for Al doped samples and 3.11 eV to 1.92 eV for (Al, Co) co-doped samples. As shown in the band gap data of experimental and theoretical data are dissimilar due to the limitation of the generalized-gradient approximation (GGA). The calculated band structure suggests that the pattern of the band gap is affected with Al doped and band gap shifted towards the higher energy region (blue shift). In addition, (Al, Co) co-doped TiO_2 thin films the band gap value shift towards the lower energy region (red shift). It is investigated that the band gap is about the pristine TiO_2 thin films 3.11 eV which is less than the experimental results 3.52 eV it is familiar that the underestimated band gap can due to the choice of exchange-correlation energy. The top of the valance band approximately locates near Γ k-points and the bottom of the conduction band located at the same *k*-points, which means that TiO_2 band structure is indirect-gap materials. The valance band maxima occur at Γ point and the conduction band minima is at same point. The orbital projected band structure analysis shows that the bottom of the most valance band at Γ_{vb} point is characterized by a strong admixture of Ti $d_{z,}$ and O P_z .while the top most conduction band at the Γ point (Γ_{cb}) is characterized by Ti $p_{y/x}$, some O $P_{y/x}$ characterized mixed with Al p states. One obvious approach to lowering the band gap of TiO_2 is to add trace impurity atoms or ions resulting in the incorporation of donor or acceptor states between the valance and conduction band. Several studies have shown that the properties of metal-doped titanium depend substantially on the metal ion incorporated dopant concentration and the structure and binding mode of dopant metal ions within the host lattice. Various Density Functional Theory (DFT) calculations have investigated the structural and electronic consequence of inclusion of dopants into TiO_2. These calculations confirms that the presence of metal or non-metal atoms within the bulk lattice of TiO_2 is responsible for the modification of band gap and optical properties, by creating hole or electron states. An expected, however, the higher HOMO- LUMO energy separation in these molecules compared to that between the bonding and anti-bonding states in the lattice of titanium oxide leads to considerably higher measurement band gap [9]. Interestingly, although the HOMO-LUMO/band gap of particular POT cage is highly

dependent on the precise structure, there is a general decrease in the band gap with increase TiO_2 core size.

6.9.3.2 Partial Density of States

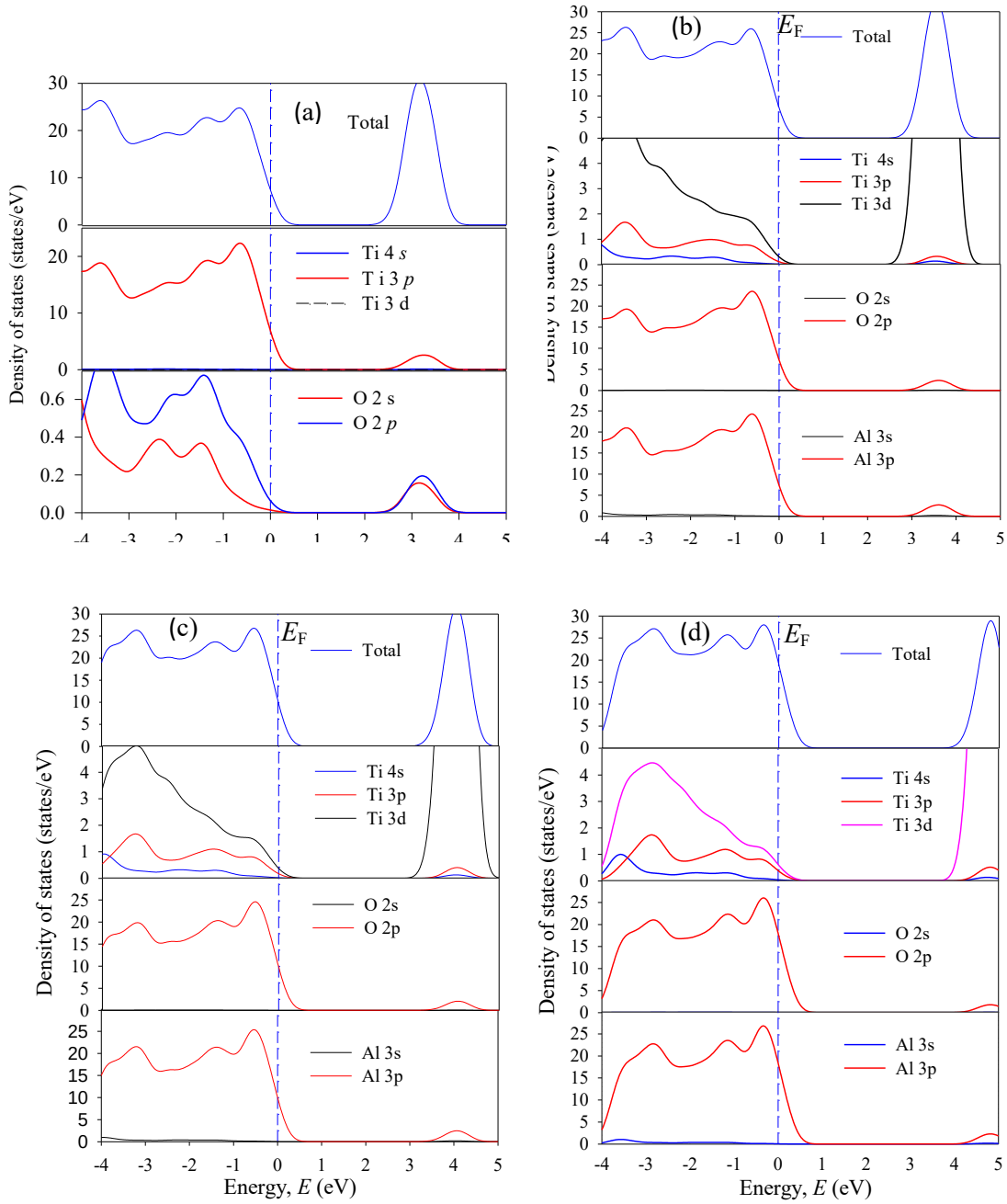

Fig. 6.29: The partial density of states (a) Pristine, (b) 2%, (c) 4%, (d) 6% Al doped TiO_2 thin films.

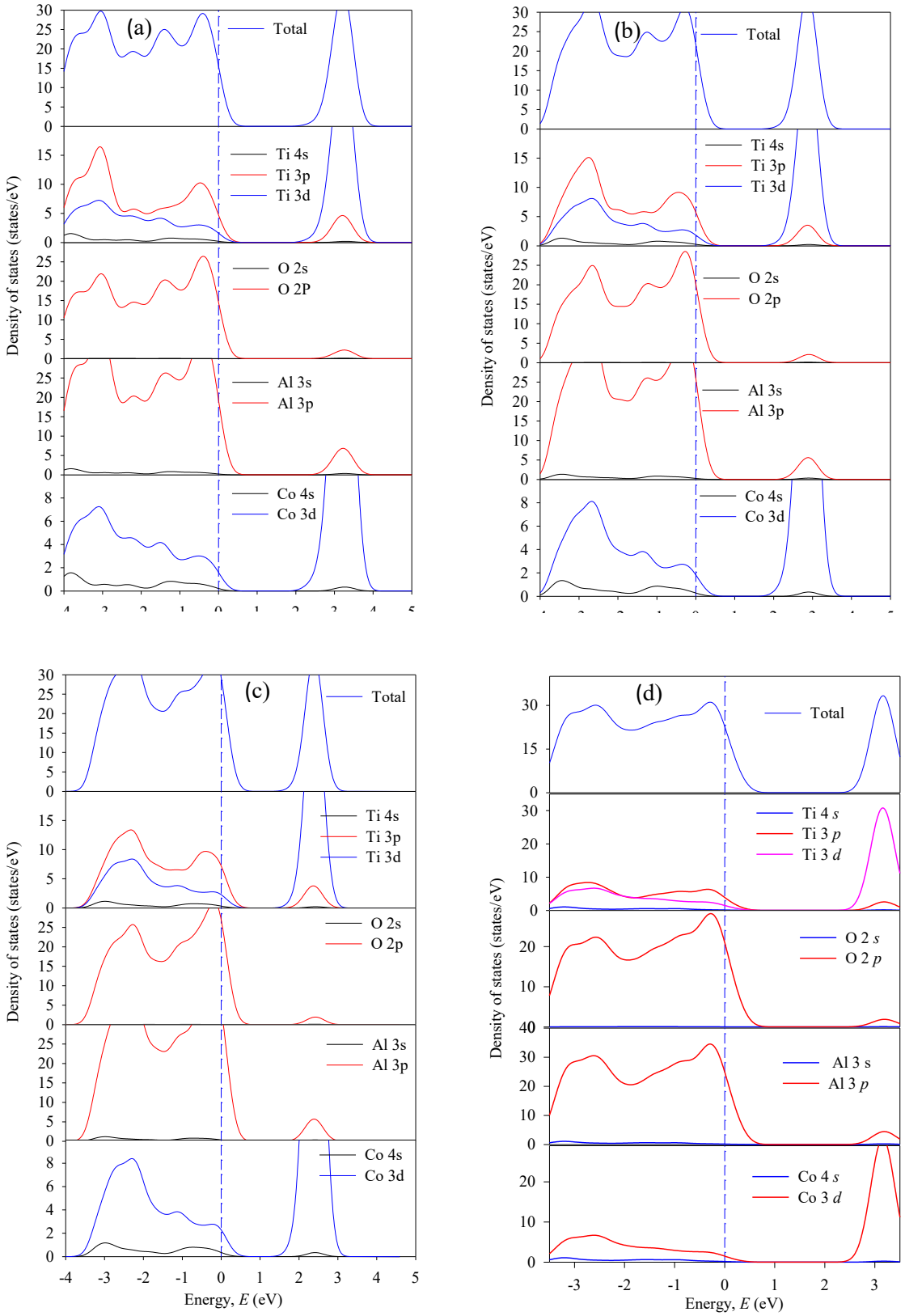

Fig. 6.30: The partial density of states (a) 1% Co, 6% Al, (b) 2% Co, 6% Al, (c) 3% Co, 6% Al, 4% Co, 6% Al co-doped TiO_2 thin films.

Figure shows the calculated total density of states (DOS) and site projected density of states (PDOS) for Al doped and (Al, Co) co-doped TiO_2 obtained from the general gradient approximation using optimized structural parameters in the PBE level. The Fermi level is set to 0 eV to have meaningful comparison. In both DOS graphs Al states appear at the bottom of the conduction band and hence not significantly contribute to the valance band region. From figure of the total dos of Al doped and (Al, Co) co-doped TiO_2 thin films. Because of Al and (Al, Co) co-doping introduce the n-types carriers into TiO_2 network, the Fermi-level shift into the conduction band, which is agreement with the experimental results that Al ion fully acts as electron donor in the TiO_2 system and TiO_2 sample is an n-type degenerate semiconductor. The same tendency is found (Al, Co) co-doped TiO_2 samples. However, it is interesting that Al doped TiO_2 shows a further movement of the Fermi-level into the conduction band compared to TiO_2. In particular, the DOS of the two compounds shift significantly toward the higher energies region and optical band gap broadened after Al doping compared with the DOS reported in figure 6.16. On the other hand, interaction among electron charges results in a many body effect, which causes the optical band gap to become narrowing. In addition, it should be noticed that although the Fermi level shifts upwards into the original CBs, there are no changes of the topmost of the VBs and the bottom of CBs of pristine, doped and co-doped samples.

6.9.3 Charge Density

The charge density diagram is very useful for analyzing the chemicals bonding nature within samples. In order to get a clear insight about the total electronic charge distribution and bonding properties, the total electronic charge density map of pristine, doped and co-doped is illustrated in figure 6.31, 6.32 and 6.33. For representing the intensity of charge (electron) density, a scale has been shown at the head of the counter plots where the yellow and red color indicates the light and high density of electron, respectively.

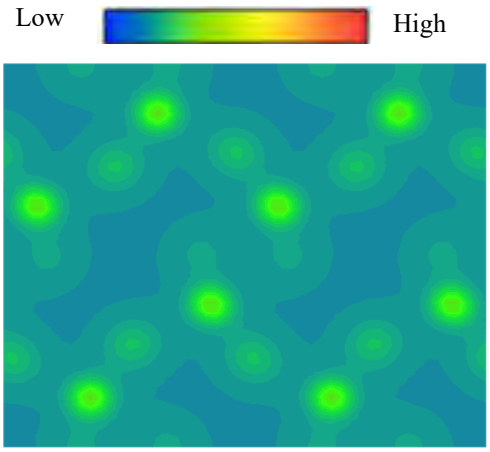

Fig. 6.31: The charge density and for difference charge density for different configuration pure TiO_2 thin film.

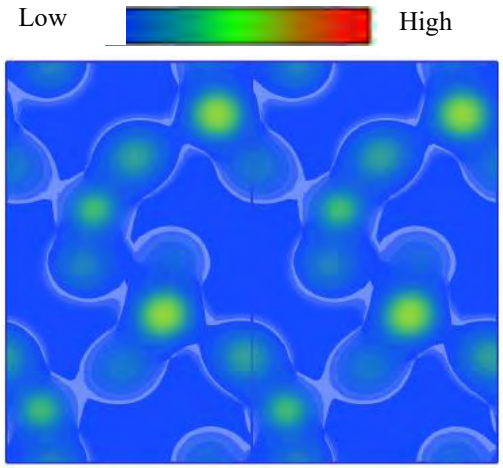

Fig. 6.32: The charge density and for difference charge density for different configuration Al doped TiO_2 thin film.

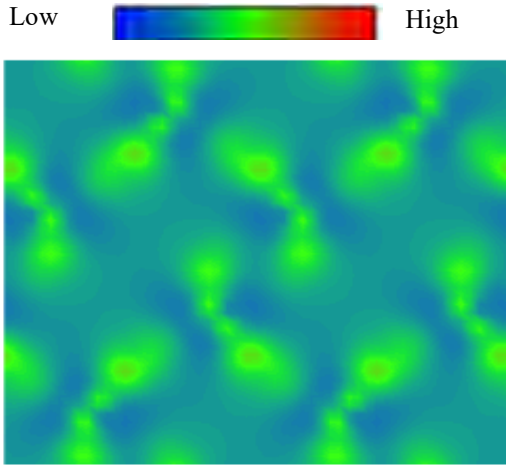

Fig. 6.33: The charge density and for difference charge density for different configuration (Al, Co) co-doped TiO_2 thin film samples.

From figure charge density it is evident that there is overlapping charge distribution of all the samples. It is evident from fig. all of the samples consists the covalent bond. The charge density shows that electrons moves from V_0 to the neighboring Ti and O atoms in TiO_2 lattice networks [35].

6.10 Conclusions

In this thesis, we have fabricated Al doped and (Al, Co) co-doped TiO_2 thin films by using the thermal spray pyrolysis method. The effect of Al and Co alloying was investigated by X-ray diffraction (XRD), scanning electron microscopy, atomic force microscopy, ultraviolet-visible spectroscopy, four-probe method and density functional theory. The lattice constant decreased linearly with increasing Al dopants, which is proved by experimental and theoretical results. The crystallite size is varying from 66 nm to 82 nm indicating that the samples have nanostructured nature. The pore diameters are increased with increasing dopants concentration investigated by scanning electron microscope images. The particle nature is found in co-doped samples. Resistivity decrease with increases in temperature, indicating that the samples are semiconductor behaviors. The transmittance decrease with increasing doping concentration, due to the ionic radius of Al^{+3} and Ti^{+4} easily incorporated in the TiO_2 lattice network. The optical and electrical band gap energies were found to decrease compared to a pristine one. The charge density indicates that the overlapping charge distribution is found in all samples. Our reported results suggested that the Al-doped and (Al, Co) co-doped TiO_2 nanoparticle with tunable optical and electrical band gap energy would be suitable for gas sensing and optoelectronic device application.

References

[1] Ramezani., M., Hosseinpour., S.M., Nasab., A.S., and Estarki., H.G., "Synthesis, Characterization, and morphological controls of $ZnMoO_4$ nanostructures through precipitation method and its photo-catalyst application" *J. mater. Sci.: Mater. Electro.* vol. 26, pp. 7588-7594, 2015.

[2] Ravidhas., C., and Anitha., B., "Tunable morphology with selective faceted growth of visible light active TiO_2 thin films by facile hydrothermal method: Structural, optical and photo-catalytic properties" *J. mater. Sci.: Mater. Electro.* vol. 27, pp. 5020-5032, 2016.

[3] Stetsovych., O., Milica., T., K. S. Tomoko, "Atomic specifies identification at the anatase (101) surface by simultaneous scanning electron tunnelling and atomic force microscopy" *Nature comun.,* vol. 6, P. 7256, 2015.

[4] Godbert., N., Mastropietro., T. F., and Poerio., T., " Meso-porous TiO_2 thin films: state of art" DOI: 10.5772/intechopen.74244.

[5] Wang., F., Min., S., Han., Y., and Feng., L., "Visible-light-induced photo-catalytic degradation of methylene blue with poly-aniline-sensitized TiO_2 composite photo-catalysts" *Super. Lattic and Micro.* Vol. 48, P. 376, 2010.

[6] Sad., N.D.M., and Sahdan., M.Z., "Difference in structural and chemical properties of sol-gel spin coated Al doped TiO_2 , Y doped TiO_2 and Gd doped TiO_2 based on trivalent dopants" *RSC ADV.*, Vol. 8, P. 29686, 2018.

[7] Babu., M., Dev., C.B., Podder., J., and Islam. N., "Influence of Fe^{2+}/Fe^{3+} ions in tuning the optical band gap of SnO_2 nanoparticle synthesized by TSP method: Surface morphology, structural and optical studies" *Matt. Sci. proc*., vol. 89, pp. 223-233, 2018.

[8] Samat., M.H., Adnan., N., Taib., M.F.M., Hassan., O.H., Yahya., M.Z.A., and Ali., A.M.M. "structural, electronic and optical properties study of brokite TiO_2" *Solid state sci. and Tech*., vol. 24., pp. 107-120, 2016.

[9] Hanini., Faouzi, and Bouachiba., Y. "Characteristic of Al-doped TiO_2 thin films grown by pulse laser deposition" *Int. J. nanoparticles*, vol. 6, pp. 2-3, 2013.

[10] Nam., S.H., Cho., S.J., and Boo., J.H., "Growth behavior of titanium dioxide thin films at different precursor temperatures" *Nano. scale resea. Let.,* vol. 7, P. 89, 2012.

[11] Chimupala., Y., Hyett., G., Simpson., R., Mitchell., R., Douthwaite., R., and Brydson., "Synthesis and characterization of mixed phase anatase TiO_2 and sodium-doped TiO_2 (B) thin films by low pressure chemical vapor deposition (LPCVD)" *RSC, Adv,* vol. 4, pp. 48507-48515, 2015.

[12] Galstyan., V., "Porous TiO_2-based gas sensors for cyber chemical systems to provide security and medical diagnosis" *Sensor,* Vol. 17, P. 2947, 2017.

[13] Zhang, Q., Wang., X., Hu., X., Miao., X., and Chaker., M., Ma., D., "Advance fabrication of chemically bonded grapheme/TiO_2 continuous fibers with enhance broadband photocatalytic properties of involved mechanisms exploration" *Scientific reports,* vol. 6, P. 38066, 2016.

[14] https://www.elmarco.com/

[15] Rydosz., A., "The use of copper oxide thin films in gas sensing applications" *Coating.,* vol. 12, P. 425, 2018.

[16] Moslah., C., Kandyla., M., Mousdis., G.A., and Ksibi., M., "Photo-catalytic properties of titanium dioxide thin films doped with noble metals (Ag, Au, Pd and Pt) *Phys. status solidi A*, Vol. 215, pp. 25143-25157, 2018.

[17] Hanini., Faouzi, and Bouachiba., Y. "Characteristic of Al-doped TiO_2 thin films grown by pulse laser deposition" *Int. J. nanoparticles*, vol. 6, pp. 2-3, 2013.

[18] Reddy., K. M., Manorama., S.V., and Reddy., A.R., " Band gap studies on anatase titanium dioxide nanoparticles" *Mater. Chem. And Phys.,* vol. 78, pp. 239-245, 2002.

[19] Song., Y.S., Kim., B. Y., Cho., N.L., and Lee., D.Y., " Effect of Al doping on optical band gap energy of Al-TiO_2 thin films" *J. Nano. and Nanotec.,* vol. 15, pp. 5228-5231, 2015.

[20] Babu., M., Dev., C.B., Podder., J., and Islam. N., "Influence of $Fe^{2+/}Fe^{3+}$ ions in tuning the optical band gap of SnO_2 nanoparticle synthesized by TSP method: Surface morphology, structural and optical studies" *Matt. Sci. proc.*, vol. 89, pp. 223-233, 2018.

[21] Salha., N, Habib., S.S., Khan., Z.H., Alarfaj., E., and Khan., S.A., "Synthesis and characterization of Se35Te65-xGex nanoparticle films and their optical properties" *J.of nanometer*. Vol. 2012, P. 9, 2011.

[22] Tsai., C,Y., Kuo., T.H., and His., H.C., "Fabrication of Al doped TiO2 visible-light photo-catalyst for low-concentration mercury removal" *Int. J. photo. energy*, Vol. 2012, pp. 8-10, 2011.

[23] Yildiz, A., Lisesivdin., S.B., Kasap., M., and Mardare., D., "Electrical properties of TiO_2" *J. of non-crystalline solids*, vol. 354, pp. 4944-4947, 2008.

[24] Das., S.C., Green., R.J., Podder., J., T. Z, Regier., "Band gap tuning in ZnO through Ni doping via spray pyrolysis" *J. phy. Chem. C*, vol. 117, pp. 12745-12753, 2012.

[25] https://www.researchgate.net/post/What_is_the_difference_between_Homojunction_and_Heterojunction

[26] Ghamdi., A., Omar., A., OKI., M.E., Gazzar., S.E. et. al "Semiconducting properties of Al doped ZnO thin films" *Spectrochimica acta part A: Mole. Bio. Spec.,* vol. 131, pp. 512-517, 2014.

[27] Shojaee, E., Abbasnejan, M., Mohammadizadeh, M.R., "First-principles study of lattice dynamics of TiO_2 in brookite and contunnite structures" *Phys*. *Rev*. B, vol. 83, P. 174302, 2011.

[28] Music, D., Schneider, J.M., "Effect of transition metal additives on electronic structure and elastic properties of TiAl and Ti_3Al. *Phys*. *Rev*. *B*., Vol. 74, p. 174110, 2006.

[29] Hadi, M.A., Islam, M.N., Babu, M.H., "Cubic perovskite (Pb(Mg1/3, Nb2/3)O_3: A damage tolerant, mechinable, and thermal barrier coating material" *Z. Naturforsch.*, vol. 74, P. 71, 2018.

[30] Lackey, W.J., Stinton, D.P., Cerny, G. A., Schaffhauser, A.C., Fehrenbacher, L.L., "Monolithic material fabrication by chemical vapor deposition" *Adv. Cerm. Mater*., vol. 2, P. 24, 1987.

[31] Pugh, S.F., "Relation between the elastic moduli and the plastic properties of polycrystalline pure material" *Phillos. Mag.,* Vol. 45, p. 823, 1954.

[32] Hadi, M.A., Rayhan, M.A., Naqib. S.H., Chroneos, A., and Islam, A.K.M.A., "Structural, elastic, thermal and lattice dynamics properties of new 321 max phases" *Com. Mater. Sci.,* Vol.170, 2019.

[33] Mazmira, M., Bakhtiar U.H., Ahmed. R., Shaari, A., Ali, N., "A density functional study of structural, electronic and optical properties of titanium dioxide : Characterization of rutile, anatase and brookite polymorphs" *Mater. Sci. semi. Proce.,* vol. 31, pp. 405-414, 2015.

[34] Roknuzzaman, M., Kostya, O., Warg, H., "Insight into lead-free organic-inorganic hybrid perovskites for photo-voltaics and optoelectronic: A first principles study" *organic electro.,* vol. 59, PP. 99-106, 2018.

[35] Li-Bin, M., Wang, Yu., Yang, B., et all., "Hydrogen impurity defects in rutile TiO_2" *Scientifics reports,* vol. 5, P. 176, 2015.

CHAPTER-7
CONCLUSIONS AND SUGGESTION FOR FUTURE WORK

7.1 Summary

Transparent conducting (TC) titanium dioxide (TiO_2) thin films were prepared by a low-cost thermal spray pyrolysis technique. In our present study, the effect of Al and Co doping on the structural, morphological, optical and electronic properties of TiO_2 thin films were studied. The crystallite sizes are varying from 66 nm to 82 nm. The cell parameters are found in good agreement with experimental and theoretical results. The pore diameters are found to be in between 6 nm to 9 nm confirmed by the Scanning Electron Microscopy images. The EDX spectra show that all samples are stoichiometric. AFM images show that the surface roughness are varying from 34.72 nm to 89.83 nm. The study of optical properties shows that the absorption edge of Al-doped and (Al, Co) co-doped TiO_2 samples are shifted toward the lower energy region compare to the pristine one. The electrical band gap values are very closed to the results of optical band gap. The charge density map indicating that the covalent bonds are present in our samples.

7.2 Conclusions

In the present study, Al doped and (Al, Co) co-doped TiO_2 thin films were prepared by an inexpensive low cost thermal spray pyrolysis method. Films are made of different doping (Al: TiO_2) and co-doping (Al, Co: TiO_2) concentrations were deposited onto a glass at substrate temperature 450 ^{0}C. Different physical properties have been studied such as structural, optical and electrical properties. A DFT analysis based theoretical investigation has been carried out to study the mechanical, electronic and bonding properties of studied samples.

The basic outcome are summarized are follows,

- From SEM image confirmed that pure samples have pore and particle shaped images. SEM micrographs of Al doped TiO_2 shows pore diameters vary from 6 to 9 nm. In the case of co-doped SEM micrographs shows particle size grain varies from 42 to 50 nm.

- The EDX analysis corresponding to Ti and O peaks of the spectrum, which ensure the TiO_2 samples. For the different concentrations of Al, Co in the film, there is also Al and Co peaks in the spectra. EDX results reveal that the element compositions are stoichiometry.

- The XRD patterns confirmed that the formation of orthorhombic type titanium dioxide having space group P b c a.

- Atomic force microscopy image shows that pristine samples have particle shape surface morphology, Al doped TiO_2 thin films have fiber, increasing the Al doping concentration decreased the fiber size. In the case of Al, Co: TiO_2 thin film samples have particle shaped. The root means square values of mono-doped are higher than co-doped samples.

- The optical measurements show the optical band gap varies from 3.52 eV to 3.70 eV for direct semiconductor of Al doped TiO_2 thin films and 3.52 eV to 3.57 eV for direct band gap semiconductor of (Al, Co) co-doped TiO_2 thin films. The observed value of band gap is found to be in good agreement with the value of reported by others. The transmittance decreased with increasing the Al, Co dopants compare to pristine samples.
- The electrical resistivity measurements were made on a number of films from room temperature up to 100K. The figure shows that the resistivity gradually decreased with the increase of temperature, indicating the materials have semiconducting nature.
- The theoretical calculation of mechanical properties ensured that the studied samples are mechanical stability.
- The electrical band structure shows that the studied samples have indirect band gap. The band gap values are varying from 3.11 eV to 4.39 eV for Al doped and 1.92 eV to 3.11 eV for co-doped samples.
- The charge density map shows that all studied samples have a covalent bond.

7.3 Future Work

This is the first time that (Al, Co) co-doped TiO_2 thin films have been prepared in our laboratory. We have deposited at temperature 450 ^{0}C and studied some of their structural, electrical, optical and DFT analysis. Further investigations on different aspects are possible for fundamental interest and potential applications of the studied thin films. Following recommendation are made for further extension of the present work.

- Neutron diffraction analysis may be performed for the compositions to determine the distribution of substituted ions.
- X-ray photoelectron spectroscopy (XPS) studies may be carried out to determine the oxidation states of the substituted elements.
- Transmission electron microscopy (TEM) may be taken for proper under-standing of the domains.
- Gas sensing efficiency measurement for purpose of gas sensing device applications.
- Study of magnetic properties.
- Study of temperature dependent Hall effect.
- Study of electrical properties of low temperature.

LIST OF PUBLICATIONS

Relevant Publications

1. The role of Aluminum, Cobalt co-doping on the band gap tuning of TiO_2 thin film deposited by spray pyrolysis.
2. Band gap tuning of p-type Al doped TiO_2 thin films for application in gas sensing device.

Other Publications

1. Majibul Haque, D. Bidhen Chandra, P. Jiban, Nurul Islam and Z. Abdullah "Influence of Fe^{2+} /Fe^{3+} ions in tuning the optical band gap of SnO_2 nanoparticles synthesized by TSP method: Surface morphology, structural and optical studies" *Materials Science in Semiconductor Processing* 89 (2019) 223-233.